# Physics and Applications of Quantum Hall Effect

Klaus von Klitzing, Patricia Haremski, and Jürgen Weis

*Max-Planck-Institut für Festkörperforschung, Heisenbergstr.1,*
*D-70569 Stuttgart, Germany,*

The quantized Hall resistance plays a crucial role for the implementation of a new international system of units (SI system) since this quantum resistance can be used not only for high precision realizations of electrical standards but also for a new realization of a kilogram by comparing electrical and mechanical forces with the Watt balance. The General Conference on Weights and Measures at his last meeting in November 2014 published a resolution with the recommendation to replace the present SI units by invariants of nature; the new definitions will be based on fixed numerical values of the Planck constant (h), the elementary charge (e), the Boltzmann constant (k), and the Avogadro constant ($N_A$), respectively. A prerequisite for such a change (expected for 2018) is the precise experimental realization of practical standards on the basis of natural constants.

The talk summarizes the recent developments in this field and will discuss new experimental results related to the current distribution in quantum Hall devices and the electrical breakdown of the quantum Hall effect.

# Topological Transport Phenomena in Graphene and Related Systems

Tsuneya Ando
*Department of Physics, Tokyo Institute of Technology*
*2–12–1 Ookayama, Meguro-ku, Tokyo 152-8551, Japan*

The electron motion in monolayer graphene is governed by Weyl's equation for a neutrino or the Dirac equation in the relativistic limit. The pseudo-spin is quantized into the direction of the electron motion and the wave function exhibits a sign change due to Berry's phase when the wave vector is rotated around the origin (which should be called the Weyl point) and therefore has a topological singularity. This singularity is the origin of the peculiar behavior in transport properties of graphene, such as the minimum conductivity at the Dirac point, the half-integer quantum Hall effect, the dynamical conductivity, crossover between weak- and anti-localization, and a very singular diamagnetic response [1, 2, 3]. Quite recently, the singularity was studied also in the weak-field Hall conductivity [4].

When the graphene is placed on an appropriate substrate, a gap can open up, causing nonzero orbital magnetic moment perpendicular to the system [5, 6]. The Hall conductivity becomes nonzero and quantized into the half of $\pm e^2/2h$ in the gap, although being opposite between the two valleys K and K'. The valley Hall conductivity in the clean limit, where the strength of scatterers is assumed to be much smaller than the gap, has shown to be strongly enhanced over the simple result obtained by assuming no scattering [7].

Explicit numerical results are obtained for scatterers with Gaussian potential and the Coulomb potential. The gap easily disappears in the presence of disorder, but the valley Hall conductivity there remains almost unaffected although it is no longer quantized. Similar calculations have also been performed for bilayer graphene, where a band gap can be opened by external gate field perpendicular to the system and similar valley Hall conductivity appears with quantized value $\pm e^2/h$ within the gap. The valley Hall conductivity is shown to be strongly enhanced over that obtained in ideal systems [8].

A Weyl point appears also in a two-dimensional system with strong Rashba-type spin-orbit interaction. In usual semiconductor heterostructures, this spin splitting is small and the presence of a Weyl point is easily obscured by inherent disorder. Recently, the giant spin splitting has been realized in the bulk of a polar semiconductor BiTeI [9] and the two-dimensional electronic system on its surface is shown to exist [10]. The weak-field Hall effect due to orbital motion and the anomalous topological Hall effect due to spin-Zeeman contribution near the Weyl point have also been studied [11].

References

[1] T. Ando, Physica E **40**, 213 (2007).
[2] A. H. Castro Neto, F. Guinea, N. M. Peres, K. S. Novoselov, and A. K. Geim, Rev. Mod. Phys. **81**, 109 (2009).
[3] D. S. L. Abergel, V. Apalkov, J. Berashevich, K. Ziegler, and T. Chakraborty, Adv. Phys. **59**, 261 (2010).
[4] M. Noro and T. Ando, J. Phys. Soc. Jpn. (submitted for publication).
[5] M. Koshino and T. Ando, Phys. Rev. B **81**, 195431 (2010).
[6] D. Xiao, M.-C. Chang, and Q. Niu, Rev. Mod. Phys. **82**, 1959 (2010).
[7] T. Ando, J. Phys. Soc. Jpn. **84**, No. 11 (2015).
[8] T. Ando, J. Phys. Soc. Jpn. **84**, No. 11 (2015).
[9] K. Ishizaka, M. S. Bahramy, H. Murakawa, M. Sakano, T. Shimojima, T. Sonobe, K. Koizumi, S. Shin, H. Miyahara, A. Kimura, K. Miyamoto, T. Okuda, H. Namatame, M. Taniguchi, R. Arita, N. Nagaosa, K. Kobayashi, Y. Murakami, R. Kumai, Y. Kaneko, Y. Onose, and Y. Tokura, Nat. Phys. **10**, 521 (2011)
[10] M. Sakano, M. S. Bahramy, A. Katayama, T. Shimojima, H. Murakawa, Y. Kaneko, W. Malaeb, S. Shin, K. Ono, H. Kumigashira, R. Arita, N. Nagaosa, H. Y. Hwang, Y. Tokura, and K. Ishizaka, Phys. Rev. Lett. **110**, 107204 (2013).
[11] H. Suzuura and T. Ando, in preparation.

# Kondo Effect in the Quantum Hall Regime: A New Probe for the Electronic Structure of the Edge?

Rolf J. Haug
*Institut für Festkörperphysik, Leibniz Universität Hannover, Germany*

*e-mail: haug@nano.uni-hannover.de*

The influence of the edge in the quantum Hall effect (QHE) is under discussion almost since the discovery of the QHE [1]. Bert Halperin discussed in detail the role of edge states being localized within a cyclotron radius [2]. Due to the chiral nature of such edge states many features of the quantum Hall effect observed in experiments could be explained invoking such simple edge states (see e.g. [3]). But it was realized that screening leads to a reconstruction of the quantum Hall edge and a more complicated structure at the edge involving compressible and incompressible regions [4,5].

Several years ago it was shown that Kondo effect in transport through quantum dots exists also in the quantum Hall regime [6,7]. The influence of the chirality of the edge structure on the Kondo effect was observed for a system with two quantum dots connected via a quantum Hall system [8]. Recently measurements of the Zeeman splitting in the Kondo effect showed an unexpected dependence on magnetic field which hints towards an intricate competition between Kondo screening and the reconstruction of the quantum Hall edge [9]. In the talk such probing of the edge structure via the Kondo effect will be discussed.

[1] K. v. Klitzing, G. Dorda, M. Pepper, Phys. Rev. Lett. 45, 494 (1980).
[2] B. I. Halperin, Phys. Rev. B 25, 2185 (1982).
[3] R. J. Haug, Semicond. Sci. Technol. 8, 131 (1993).
[4] D.B. Chklovskii, B.I. Shklovskii, L.I. Glazman, Phys. Rev. B 46, 4026 (1992).
[5] K. Lier, R.R. Gerhardts, Phys. Rev. B 50, 7757 (1994).
[6] M. Keller, U. Wilhelm, J. Schmid, J. Weis, K. v. Klitzing, K. Eberl, Phys. Rev. B 64, 033302 (2001).
[7] C. Fühner, U.F. Keyser, R.J. Haug, D. Reuter, A.D. Wieck, Phys. Rev. B 66, 161305 (2002).
[8] D. Tutuc, B. Popescu, D. Schuh, W. Wegscheider, R.J. Haug, Phys. Rev. B.83, 241308 (2011) .
[9] A.W. Heine, D. Tutuc, G. Zwicknagl, R.J. Haug, arXiv 1510.05805

# ATLAS-TFET: Toward Green Transistors and Sensors

Kaustav Banerjee
*Nanoelectronics Research Lab, Department of Electrical and Computer Engineering*
*University of California, Santa Barbara, CA 93106, USA*
*e-mail: kaustav@ece.ucsb.edu*

MOSFETs have been the workhorse of the worldwide semiconductor industry and the primary building blocks of most electronic products of everyday use since the 1970's. However, continuous miniaturization of MOSFETs, well beyond 100 nanometers, to sustain the ever growing need for increased transistor densities has given rise to a daunting power dissipation challenge during the past decade due to increasing leakage power arising from a fundamental limitation of their turn-on characteristics [1]. This talk will examine the genesis of this challenge, and provide an overview of the recently demonstrated atomically-thin and layered semiconducting channel tunnel-FET or ATLAS-TFET [2] that overcomes this challenge and is a fundamentally different transistor employing several innovations. The ATLAS-TFET is the only planar architecture TFET to achieve subthermionic subthreshold swing (~30 millivolts/decade at room temperature) over four decades of drain current, satisfying ITRS requirements for the first time, and the only one in any architecture that can be switched ON using an ultra-low drain–source voltage of 0.1 V, and at present is the thinnest-channel subthermionic transistor ever made.

The ATLAS-TFET operates with high ON/OFF ratio, and lowers power dissipation by over 90% compared to the state-of-the-art MOSFETs. Moreover, $MoS_2$ channel based conventional FET has been proven to provide an excellent platform for biosensing [3], since the atomically thin nature of $MoS_2$ with their pristine surfaces lead to excellent electrostatic control and the presence of a finite bandgap helps in suppressing the leakage currents, both of which in combination are instrumental in increasing the sensitivity and reducing the minimum detection limit of the $MoS_2$-FET based sensors. Hence, ATLAS-TFETs that combine the advantages of an atomically-thin $MoS_2$ channel and the unprecedented sensitivity of a tunnel-FET (owing to their steep turn-on characteristics) [4], can be employed for building a revolutionary new class of sensors.

References:

[1] Y. Khatami and K. Banerjee, *IEEE Trans. Electron Dev*. **56**, 2752-2761, (2009).

[2] D. Sarkar et al., *Nature*, **526**, 91-95 (2015).

[3] D. Sarkar, et al., *ACS Nano*, **8**, 3992–4003 (2014).

[4] D. Sarkar and K. Banerjee, *Appl. Phys. Lett.*, **100**, 143108 (2012).

# Electronic Structure, Magneto-excitons and Valley Polarized Electron Gas in 2D Semiconductors MoS2 and WS2

Isil Ozfidan[1], Marek Korkusinski[2], Pawel Potasz[3] and Pawel Hawrylak[1]

[1] *Department of Physics, University of Ottawa, Ottawa,K1N6N5, Canada*
[2] *Emerging and Disruptive Technologies Portfolio, National Research Council Canada, Ottawa, K1A0R6,Canada*
[3] *Department of Theoretical Physics, Faculty of Fundamental Problems of technology, Wroclaw University of Technology, Wroclaw, Poland*
*e-mail: pawel.hawrylak@uottawa.ca*

We discuss our recent theory of the electronic and optical properties of single monolayer 2D hexagonal semiconductors MoS2 and WS2. The ab-initio calculations [1,2] establish these materials as direct gap single monolayer semiconductors with strong spin orbit coupling. The SO coupling and broken sublattice symmetry leads to locking of spin and valley quantum numbers and valley selective interband circularly polarized transitions. The optical selection rules are however different for both materials and these difference are discussed. Based on ab-initio input a tight binding model involving Mo and W d-orbitals and S2 p orbitals is established. The effective tight binding model is further reduced to the massive Dirac model which allows to introduce magnetic field and develop a theory of the magneto-exciton and charged exciton spectra. In the presence of high density electron gas we predict the existence of a Valley Polarized Electron Gas as a ground state of WS2. The Valley Polarized state leads to spontaneous circular polarization of the emitted light, an effect which has been recently observed[2]. Our theory is discussed in comparison with recent experiments[3].

In collaboration with A. Petrou, G. Kioseoglou, M. Potemski, A. Stier, J.Kono and S. Crooker.

[1] Eugene S. Kadantsev and Pawel Hawrylak, Solid State Comm.152, 909 (2012).

[2] T. Scrace, Y. Tsai, B. Barman, L. Schweidenback, A. Petrou, G. Kioseoglou, I. Ozfidan, M. Korkusinski, and P. Hawrylak, Nature Nanotechnology 10, 603 (2015) .

[3] A. Stier, J. Kono, S. Crooker, et al. (to be published)

# Scanning gate imaging of $MoS_2$ transistors

Masahiro Matsunaga[1], Ayaka Higuchi[1], Guanchen He[2], Yuichi Ochiai[1],
Jonathan P. Bird[2], and Nobuyuki Aoki[1,3]

[1] *Graduate School of Advanced Integration Science, Chiba University, Chiba, Japan*
[2] *Department of Electrical Engineering, University at Buffalo, SUNY, Buffalo, New York, USA*
[3] *Japan Science and Technology Agency-PRESTO, Kawaguchi, Saitama, Japan*
*e-mail: n-aoki@faculty.chiba-u.jp*

Recently, single-layer transition-metal di-chalcogenides have attracted much attention as an ideal material for applications of two dimensional (2-d) electronics [1]. Significant interest in particular has focused on the properties of molybdenum disulfide, $MoS_2$, in which two different crystal structures are possible, dependent upon the arrangement of sulfur atoms. These are the 2H and 1T phases, and are semiconducting and metallic, respectively. Since the 2H structure is usually more stable than the 1T one, a thin layer of $MoS_2$ may be used as a transistor channel with *n*-type characteristics. However, recent reports have suggested the possibility of inducing a transition of the structure, from 2H to 1T, by several ways; most notably by Li intercalation [2] and high energy electron beam irradiation at high temperature [3]. If approaches can be developed to realize the 1T phase selectively within an $MoS_2$ crystal, then this could open the way to the realization of a new class of 2-d crystal electronics.

Recently, we found that is possible to observe the existence of a 1T-structured region within a $MoS_2$ FET channel, using a combination of scanning probe techniques. In this study, we used scanning gate microscopy (SGM) to investigate the local gate response within the channel of $MoS_2$ transistors. The single layer $MoS_2$ crystals used in this work were directly grown on $SiO_2$/Si substrates by chemical vapor deposition, and supplied by the Ajayan group at Rice University [4]. Source and drain electrodes (Cr/Au) were patterned by electron beam lithography [5]. SGM observation was performed under atmospheric conditions. In some samples, we found that SGM response was observed, not at the boundary between the $MoS_2$ and the metal electrodes, but well inside the $MoS_2$ channel, away from the electrode. In addition, we simultaneously obtained electrostatic force microscopy (EFM) images. In these images, a huge potential drop was observed at the same position where the SGM response appeared. Combining these data, we can infer the existence of a Schottky-like potential barrier formed at semiconducting/metallic boundary within the channel. It suggests that a possibility of a partial-structural transition from 2H to 1T occurred during the fabrication process. Photo luminescence mapping furthermore supports these conclusions.

[1] B. Radisavljevic *et al*., Nature Nanotech. **6**, 147 (2011).
[2] R. Kappera *et al*., Nature Mater. **13**, 1128 (2014).
[3] Y. C. Lin *et al*., Nature Nanotech. 9, 391 (2014).
[4] Y. Zhan *et al*., Small **8**, 966 (2012).
[5] G. He *et al*., Nano Lett. **15**, 5052 (2015).

# High room temperature optical polarization due to spin-valley coupling in monolayer $WS_2$

B.T. Jonker[1*], A.T. Hanbicki[1], G. Kioseoglou[2], M. Currie[1], C.S. Hellberg[1], K.M. McCreary[1], and A.L. Friedman[1]

[1]*Naval Research Laboratory, Washington, DC 20375*
[2]*University of Crete, Heraklion Crete, 71003, Greece*
** email: jonker@nrl.navy.mil*

Single monolayer transition metal dichalcogenides (TMDs) such as MoS2 or WS2 are semiconductors with degenerate, inequivalent *k*-points labeled *K* and *K'* that define the direct gap. The valence band maximum in each valley has only one spin state of opposite orientation for *K* and *K'*. Consequently, one can selectively populate one valley or the other with circularly polarized light, and determine the valley populations via the polarization of emitted light. Optical emission is dominated by neutral and charged exciton (trion) features, and changes in emitted polarization provide insight into intervalley scattering. We prepare $WS_2$ monolayers such that the photoluminescence is from either the neutral exciton or the negative trion. In most TMDs, the optical polarization is small at 300K, and we find that the neutral exciton emission indeed has zero polarization. However, we observe a record high optical polarization of 28% for the trion at 300K. The trion polarization always exceeds that of the exciton, and exhibits a pronounced, non-monotonic temperature dependence – the polarization nearly doubles as the temperature increases. The increase observed in optical polarization directly correlates with a decrease in emission intensity between 125-175K (figure panels *a* and *b*). We determine the dependence of the optical polarization on temperature and laser excitation energy, and expand a rate equation model [1] to incorporate intervalley scattering, electron-hole radiative recombination, and Auger processes. The model shows that these behaviors are due to the onset of nonradiative Auger processes [2]. In this three-particle process, an electron and hole recombine non-radiatively, transferring energy to a third electron, which moves to a higher energy level. This process produces both a decrease in emission intensity and an increase in optical polarization, and is more readily available to a trion than to the neutral exciton.

[1] G. Kioseoglou *et al*., *Appl. Phys. Lett.* **101**, 221907 (2012).
[2] A.T. Hanbicki *et al*, under review.

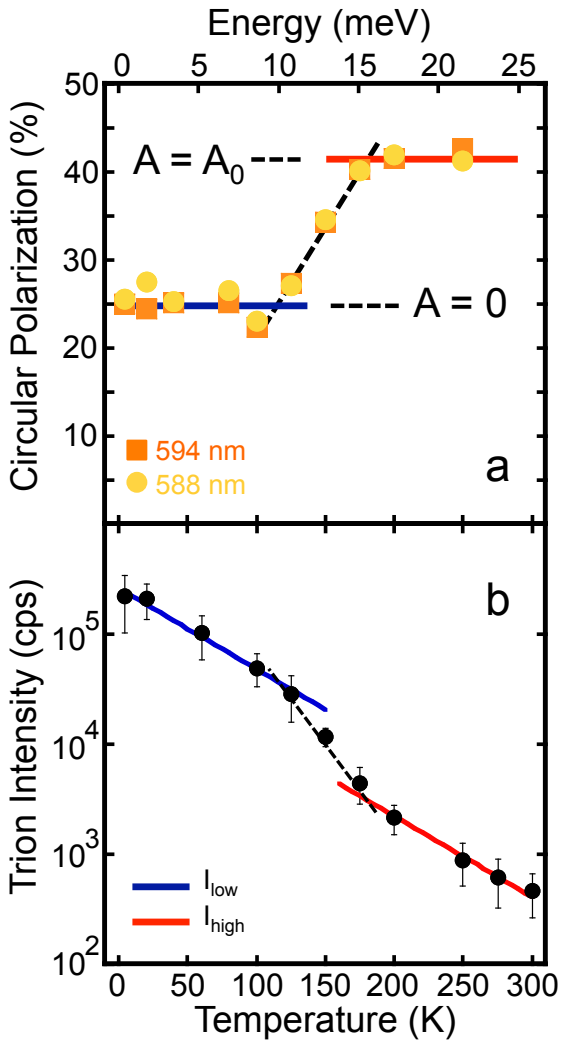


Figure 1. a) the trion polarization exhibits a pronounced increase from 125 K to 175 K that correlates with b) a corresponding decrease in emission intensity.

# Plasmon mediated energy relaxation in graphene

D. K. Ferry

*School of Electrical, Computer, and Energy Engineering,*
*Arizona State University, Tempe, AZ 85287-5706*
*e-mail: ferry@asu.edu*

The study of "hot" carriers in semiconductors, driven out of equilibrium by an applied electric field, has been pursued for many decades. With the emergence of graphene as a promising material for future nanoelectronics, there has consequently been significant interest in the processes governing its hot carrier dynamics. One aspect of graphene is the very high energy of its optical phonons, which ensures that these are ineffective at cooling electrons and holes except at higher temperatures, above room temperature. In spite of significant experimental and theoretical investigation, the mechanism of carrier cooling at low temperatures in graphene remains poorly understood. In this talk, we discuss the possibility of carrier cooling via the plasmon-mediated scattering of hot carriers. The situation for plasmon-mediated cooling involves an interaction between carriers in the streaming part of the distribution and those in the symmetric part. That is, the plasmon interaction transfers net energy *from* the streaming terms, thus serving to relax that part of the distribution that is measured by transport. The allowed plasmon emission process corresponds to almost direct back-scatting of the carriers, which accounts for the cooling. The scattering process is evaluated via the use of a momentum dependent extension of the plasmon-pole approximation which allows the determination of the imaginary part of the inverse dielectric function. We find excellent agreement with the experimental data of Ref. 1, *without the need to introduce any adjustable parameters*.

[1] Somphonsane R.; Ramamoorthy, H.; Bohra, G.; Ferry, D. K.; Ochiai, Y.; Aoki, N.; Bird, J. P.; *Nano Lett.* **2013**, *13*, 4305.

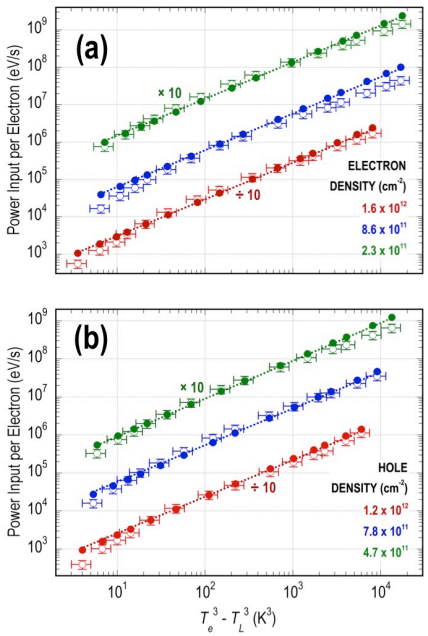


The energy loss rate per carrier for (a) electrons and (b) holes. In each case, the solid symbols are the theory and the open symbols are the data from ref. 1.

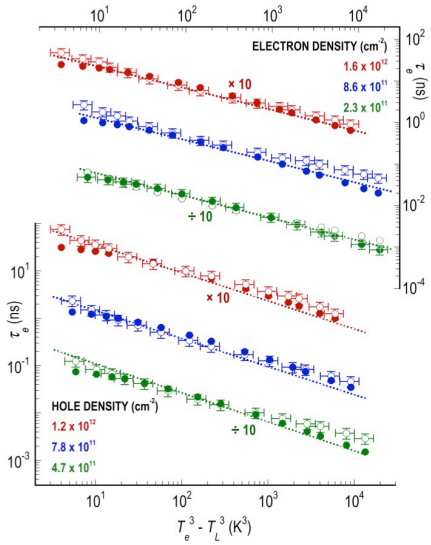


The energy relaxation time for several values of the electron and hole density. The experimental values are the open symbols and the theoretical values are the closed symbols.

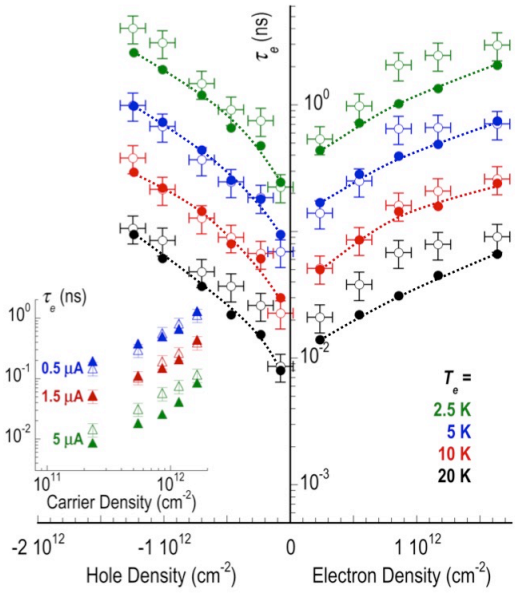


The energy relaxation time as a function of the carrier density with the electron temperature as a parameter. At the lower left, we plot the variation of the relaxation time with density for a few values of the excitation current. Dotted lines provide a guide though the theoretical data (filled symbols).

# 1/f noise in monolayer and bilayer graphene and its application to THz detection at room temperature

Yuichi Ochiai[1], Nobuyuki Aoki[1], Katsuhiko Miyamoto[1], Takashige Omatsu[1], Tomohiro Yamaguchi[2], Koji Ishibashi[2], Jonathan P. Bird[3] and David K. Ferry[4]

[1] *Graduate School of Advanced Integration Science, Chiba University, Chiba, Japan,*
[2] *Advanced Device Laboratory, Advanced Science Institute (RIKEN), Wako, Japan,*
[3] *Department of Electrical Engineering, University at Buffalo, New York, USA,*
[4] *Department of Electrical Engineering and CSSER, Arizona State University, Arizona, USA*
*e-mail: ochiai@faculty.chiba-u.jp*

There has recently been much interest in the transport properties of nano scale graphene structures. In the work presented here, monolayer and bilayer graphene devices have been fabricated with integrated antennas for application to wideband terahertz- (THz) signal detection. In these experiments, we focus specifically on the influence of THz irradiation on the noise properties of the devices. Our experiments are performed close to room temperature, where we find that the temperature coefficient of the resistance of the devices is positive (metallic) and negative (semiconducting), respectively, for monolayer and bilayer structures. In the presence of THz irradiation, we use these distinct temperature dependencies to detect a bolometric response of the devices to THz irradiation. This bolometric action is characterized via changes in the spectral density of the 1/f resistance noise the devices, induced as a function of the incident THz power. With increasing power, the spectral density was found to show opposite dependencies that are consistent with those exhibited by the opposite sign of the temperature coefficient of the resistance of the devices. These bolometric responses can be connected to a corresponding variation of the Hooge parameter[1] as a function of the THz power. We would like to discuss on the 1/f resistance noise properties in graphene films.

[1]F. N. Hooge, IEEE Trans. Electron Devices **41**, 1926 (1994)

# Molecular- and polymer-based electronic devices on flexible substrates

Takhee Lee

*Department of Physics and Astronomy, Seoul National University, Seoul 151-747, Korea*
*e-mail: tlee@snu.ac.kr*

The Idea of utilizing individual molecules as the electronic components in future ultrahigh-density electronic devices has generated tremendous attention. I will explain recently developed understanding on the electrical transport characteristics through various types of molecular junctions on flat or flexible substrates [1-3]. In particular, obtaining transistor action from molecular orbital control has been the outstanding challenge of the field of molecular electronics. In this talk, I will explain a direct electrostatic modulation of orbitals in a molecular transistor configuration in electromigration nanogap [1] and in mechanically-controllable break junction (MCBJ) [2]. I will also demonstrate functional devices such as diodes or photoswitches at the molecular-scale on both rigid and flexible substrates [3]. I will also present a brief summary on general characteristics of the materials, device structures, and switching mechanisms used in polymer-based non-volatile memory devices. Strategies for performance enhancement, integration, and advanced architectures in these devices will be presented [4].

[1] Nature 462, 1039 (2009); Adv. Mater. 23, 1583 (2011)-review

[2] Nano Lett. 13, 1822 (2013); Adv. Mater. 25, 4845 (2013)-review.

[3] Nature Nanotech. 7, 438 (2012); Adv. Funct. Mater. 24, 2472 (2014); Adv. Mater. 26, 3968 (2014), Adv. Funct. Mater. in press (2015) http://dx.doi.org/10.1002/adfm.201502312

[4] Adv. Funct. Mater. 21, 2806 (2011)-review, Org. Electron. 17, 192 (2015).

# Biological Cell Manipulation by Magnetic Nanoparticles

Frederick Gertz, and Alexander Khitun

*Electrical and Computer Engineering Department, University of California Riverside, Riverside, California, 92521, USA, email: akhitun@engr.ucr.edu*

We report a manipulation of biological cells (erythrocytes) by magnetite ($Fe_3O_4$) nanoparticles in the presence of a magnetic field. The experiment was accomplished on the top of a micro-electromagnet consisting of two magnetic field generating contours. An electric current flowing through the contour(s) produces a non-uniform magnetic field, which is about 1.4mT/μm in strength at 100mA current in the vicinity of the current-carrying wire. In responses to the magnetic field, magnetic nanoparticles move towards the systems energy minima. In turn, magnetic nanoparticles drag biological cells in the same direction. We present experimental data showing cell manipulation through the control of electric current. This technique allows us to capture and move cells located in the vicinity (10-20 microns) of the current-carrying wires. One of the most interesting results shows a periodic motion of erythrocytes between the two conducting contours, whose frequency is controlled by an electric circuit. The obtained results demonstrate the feasibility of non-destructive cell manipulation by magnetic nanoparticles with micrometer-scale precision.

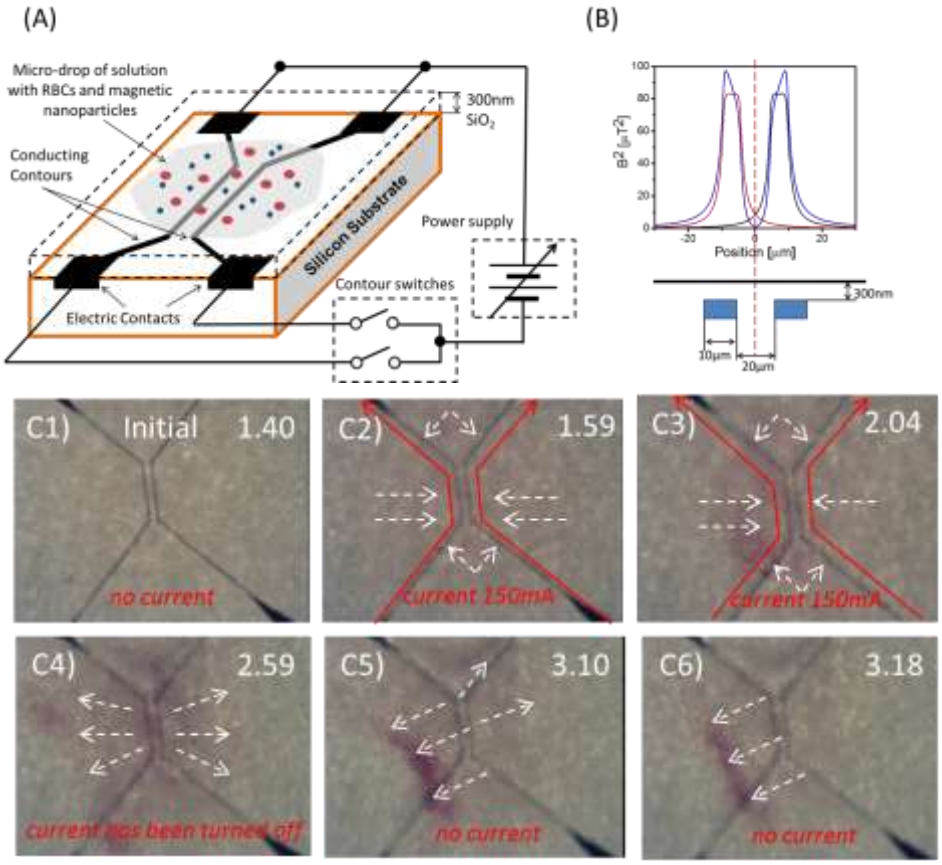


Fig.1 (A) Schematics of the micro-electromagnet and the external electric circuit. The device is fabricated on the top of a fused silica substrate. It consists of two Cu wires fabricated by optical lithography. The width of the wires is 10μm, and the height of the wires is 2μm. The wires are covered by the 300nm of silicon dioxide. The top of the structure is the working area where solution with biological cells and magnetic nanoparticles is placed. (B) Results of numerical modeling showing the surface profile of the scaled magnetic energy $B^2$ produced by the current-carrying wires. The red and the black curves show the scaled magnetic energy when 100mA electric current is flowing through the one of the contours. (C1-C6) The sequence of snapshots taken during the experiment. (C1) The beginning of the experiment: there is no electric current flowing through the contours. The blood cells of standard discoid shape are uniformly distributed over the surface. (C2-C3) 150mA current is running through the contour, the cells move towards the current-carrying wires. (C4) The current is turned off. RBCs are starting to move away from the current carrying wires. (C5-C6) The cloud of RBCs is moving away from the conducting contour as the current is turned off. The numbers in the right upper corner depict the time of the snapshot taken.

# Selective Detection of Human & Bird Influenza Virus by Sugar Chain Modified Graphene FET

Kazuhiko Matsumoto , Ryota Hayashi, and Takao Ono

*Institute of Scientific and Industrial Research, Osaka University,*
*Ibaraki-shi, Osaka 567-0047, Japan*
*e-mail:k-matsumoto@sanken.osaka-u.ac.jp*

The bird influenza virus and human influenza virus are selectively detected using the sugar chain modified graphene FET. The bird influenza virus itself is not dangerous and dose not infect to the human. However, once the bird flu get into the body of animals, such as pig, the bird flu changes the structure and get the human adaptability. This human adaptable bird influenza has the highly pathogenic and quite dangerous. So, we should know whether the virus has the human adaptability or not.

The influenza virus attached to the sugar chain of the throat of the human and of the colon of the pig. The structure of the each sugar chain is almost the similar between them, but the end of the structures is different, i.e., for the human sugar chain, sialic sugar chain is connected to the $\alpha$ 2-6 galactose, and for the bird sugar chain, sialic sugar chain is connected to the $\alpha$ 2-3 galactose. The bird and human influenza virus detect this difference and connect selectively. However, once the bird influenza virus get the human adaptability, it can connect both the bird sugar chain and the human sugar chain also as shown in Fig.1. In order to know whether the influenza virus has the human adaptability or not, the selective detection of bird & human influenza virus is indispensable.

In order to selectively detect the influenza virus, two types of the graphene FET, one is modified by the human type sugar chain, the other is modified by the birds sugar chain, are prepared as shown in Fig.2. The measurement system is shown in Fig.3. For the purpose of the safety, the pseud influenza virus, such as Lectin was used.

Figure 4 shows the selective detection of the pseud human influenza virus. SSA is the Lectin for the pseud human influenza virus, the MAM for the pseud bird influenza virus, and BSA is completely non target protein. In Fig.4, the pseud human influenza virus can be selectively caught by the human-type sugar chain and modified the current of the graphene FET, that means the selective detection of the pseud human influenza virus. Fig. 5 shows the selective detection of pseud bird influenza virus by the bird-type sugar chain modified graphene FET.

Thus, we have succeeded in the selective detection of human type and bird type influenza virus by the sugar chain modified graphene FET.

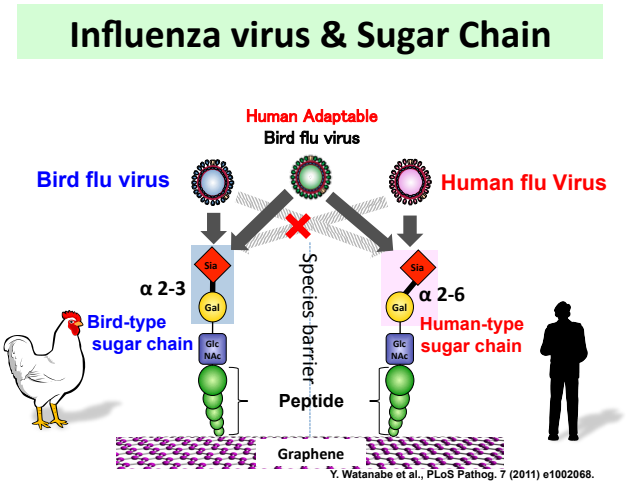


Fig.1, Relation between Birds & Human Flu virus and each sugar chains.

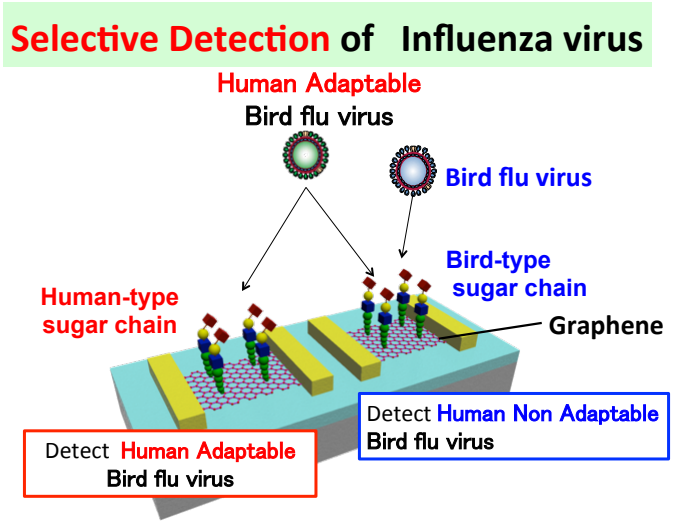


Fig.2, Sugar chain modified graphene FET for the selective detection of Bird Flu and Human Ful.

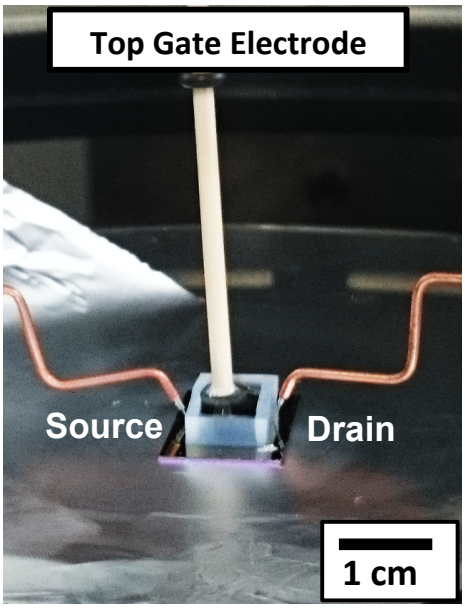


Fig.3, Measurement system.

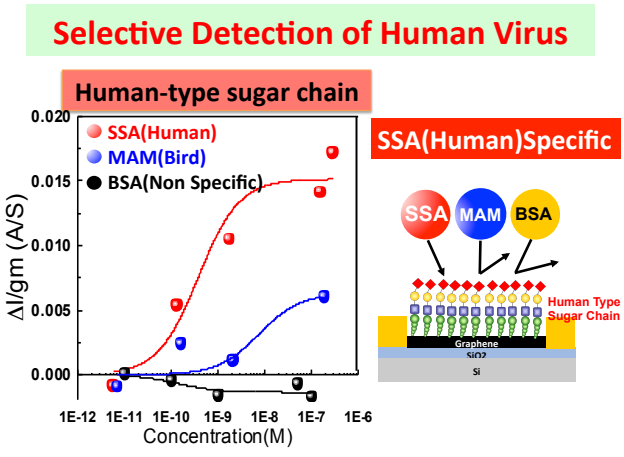


Fig.4, Selective detection of Pseudo Human Flu virus by human sugar chain.

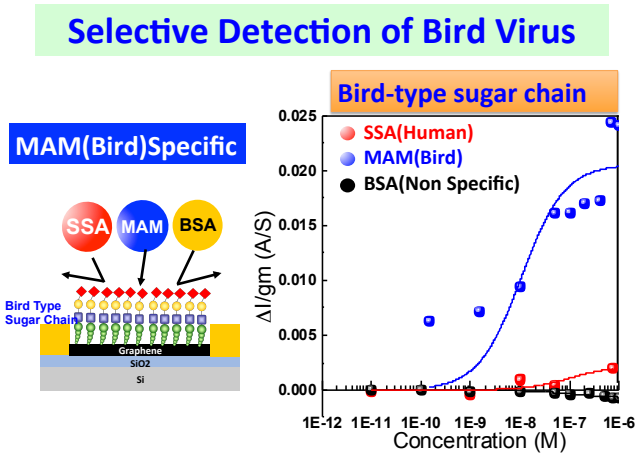


Fig.5, Selective detection of Pseudo Bird Flu virus by bird sugar chain.

# Symmetry games in driven quantum dot circuits

Stefan Ludwig

*Paul-Drude-Institut für Festkörperelektronik, Hausvogteiplatz 5-7, Berlin, Germany*
*e-mail: ludwig@pdi-berlin.de*

Quantum dots are central components of semiconductor based electronic quantum circuits and are being investigated for their potential for quantum information applications. At the same time, quantum dot circuits provide a test bed for studying more fundamental problems as they allow to control well defined single particle states embedded in the complex matrix of non-ideal crystals. Most experiments so-far have been performed close to thermal equilibrium and in setups building on a high degree of symmetry in time and space. Based on the flexibility of nanodevices such symmetry properties are usually designed by purpose as they simplify the interpretation of experiments.

Breaking the space-time symmetry, however, opens up new perspectives for studying fundamental questions and can lead to novel ideas for possible applications. Nanosystems at cryogenic temperatures are well suited for such studies as they provide particularly simple (single particle) quantum states to start with. In my talk I will present experiments, in which we purposely break the spatio-temporal symmetry in three different ways and control the symmetry properties by applying a combination of static and/or dynamic fields.

In one experiment we realized a Lissajous rocking ratchet by simultaneously driving the two tunnel barriers of a single dot and measuring a dc current induced by this driving [1]. It allows to compare and process two different rf signals and their relative phase on a chip.

In a second set of experiments we periodically drive a double quantum dot charge qubit through its avoided crossing thereby performing Landau-Zener-Stückelberg-Majorana spectroscopy [2]. We demonstrate that the straightforward extension from monochromatic to bichromatic driving opens a playground of new possibilities [3]. An interesting aspect is thereby the difference between combining commensurable versus incommensurable frequencies: compared to monochromatic driving, for two commensurable frequencies the symmetry of coherence patterns is generally reduced, while the full symmetry is always recovered for incommensurable frequencies.

Finally, I will briefly introduce an experiment in which an inhomogeneous magnetic field breaks the symmetry in regard to the electron spin [4]. This static symmetry breaking strongly influences the hyperfine interaction between electrons and nuclei and facilitates the dynamic polarization of the ~$10^6$ nuclear spins in a double quantum dot. It thereby helps us to reveal an unexpected complexity of the many body nuclear spin system which, for instance, gives rise to multistabilities in the driven system.

[1] S. Platonov, B. Kästner, H.W. Schumacher, S. Kohler, S. Ludwig, *"Lissajous Rocking Ratchet: Realization in a Semiconductor Quantum Dot"*, Phys. Rev. Lett. **115**, 106801 (2015).
[2] F. Forster, G. Petersen, S. Manus, P. Hänggi, D. Schuh, W. Wegscheider, S. Kohler, and S. Ludwig, *"Characterization of Qubit Dephasing by Landau-Zener-Stückelberg-Majorana Interferometry"*, Phys. Rev. Lett. **112**, 116803 (2014).
[3] F. Forster, M. Mühlbacher, R. Blattmann, D. Schuh, W. Wegscheider, S. Ludwig, and S. Kohler, *"Landau-Zener interference at bichromatic driving"*, arXiv:1510.01976.
[4] F. Forster, M. Mühlbacher, D. Schuh, W. Wegscheider, G. Giedke, and S. Ludwig, *"Multistability and spin diffusion enhanced lifetimes in dynamic nuclear polarization in a double quantum dot"*, arXiv:1508.06522.

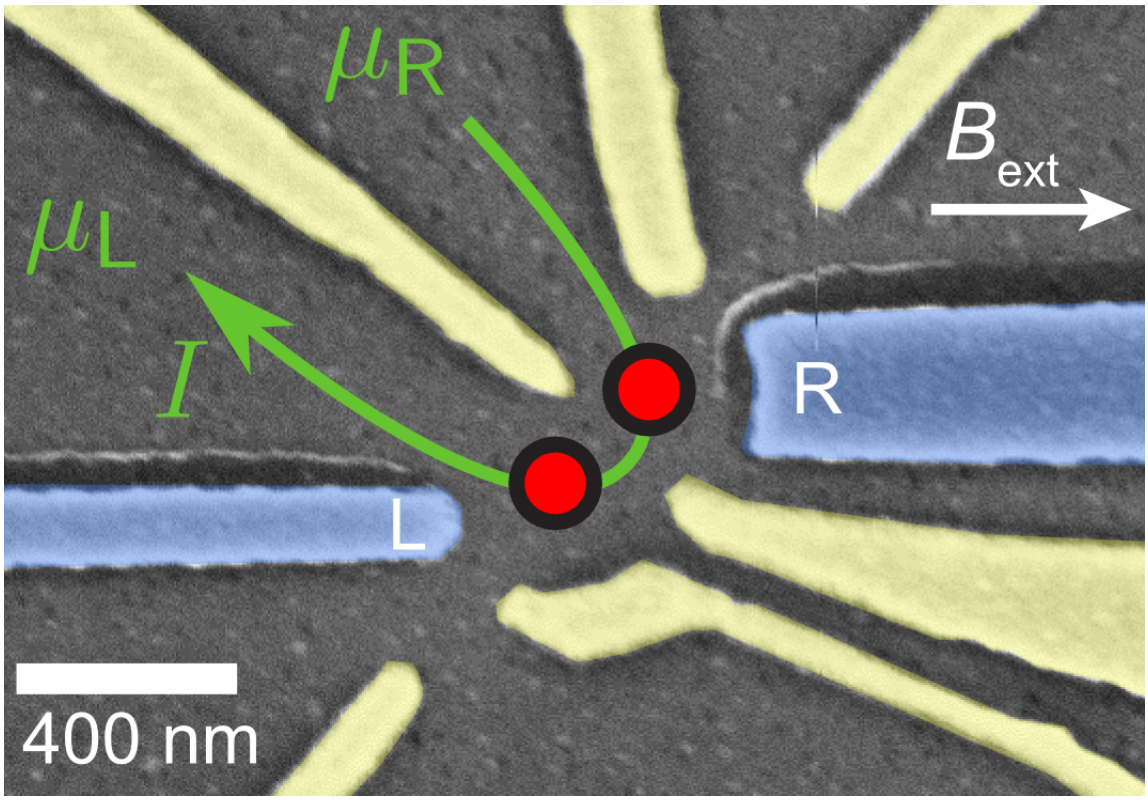


The figure displays an SEM image of one of our double quantum dot samples. It contains gold (yellow) and cobalt (blue) gates on the surface of a GaAs/AlGaAs heterostructure with a two-dimensional electron system (2DES) 85 nm beneath the surface. The gates are used to define a double quantum dot (indicated by red circles) in the 2DES by means of the electric field effect. The green arrow depicts a typical transport measurement where a tunnel current flows through the double dot and between two-dimensional leads at chemical potentials $\mu_L$ and $\mu_R$. In this device the ferromagnetic cobalt gates constitute single domain nanomagnets and generate a strongly inhomogeneous magnetic field in the region of the double dot.

# High-accuracy measurement of single-trap electron pumps in Si

Gento Yamahata[1], Stephen P. Giblin[2], Masaya Kataoka[2],
Takeshi Karasawa[1], and Akira Fujiwara[1]
[1]*NTT Basic Research Laboratories, Kanagawa, Japan*
[2]*National Physical Laboratory, Middlesex, United Kingdom*
*e-mail: yamahata.gento@lab.ntt.co.jp*

A single-electron (SE) pump controlled by a clock signal with frequency $f$ can generate an accurate electric current $ef$, where $e$ is the elementary charge. It is expected to be used for many applications: SE logic circuits [1], single-photon sources [2], quantum current standards [3], and quantum information processing [4]. Especially, current standards have recently attracted much interest because of a proposed redefinition of the SI ampere in terms of a fixed value of $e$. For practical current standards, it is desirable to generate a high-accuracy nA current ($f$ > 6.3 GHz corresponds to $ef$ > 1 nA). We have recently demonstrated 3.5-GHz SE pumping via a single-trap level in Si [5], but the accuracy has not been evaluated yet. Here, we report high-accuracy measurements [6] of such a trap-mediated SE pump at 6.5 GHz.

Our SE pump has a double-layer gate structure on an undoped Si wire [5]. An upper gate is used to induce electrons in the Si wire by applying a positive voltage. Two lower gates are used to create two potential barriers in the Si wire by applying negative voltages. In addition, we apply a high-frequency signal to one of the lower gates to pump SEs by modulating the potential barrier. We selected a device that has a single-trap level in the modulated potential barrier. When a SE is pumped via the trap level per cycle, a current $I_p = ef$ is generated.

For accurate measurements of $I_p$, we compare $I_p$ with the current generated via a 1-GOhm resistor calibrated against primary standards [6], leading to a measurement uncertainty of about 1 ppm. Using this measurement system, we measured $I_p$ at 6.5 GHz ($I_p$ ~ 1 nA), and found $I_P$ to be about 20 ppm below $ef$. In addition, we observed weak $f$ dependence of the accuracy of the trap-mediated SE pumping while the accuracy of SE pumping via a quantum dot, which has been widely studied, dramatically becomes worse with increasing $f$. This significant feature of the trap level could be due to the weak change in the potential shape during the barrier modulation. The presented precise and high-speed SE manipulation would be an important step for realizing current standards.

[1] K. Nishiguchi *et al*., Appl. Phys. Lett. **88**, 183101 (2006). [2] J. Kim *et al*., Nature **397**, 500 (1998). [3] J. P. Pekola *et al*., Rev. Mod. Phys. **85**, 1421 (2013). [4] N. Ubbelohde *et al*., Nat. Nanotech. **10**, 46 (2015). [5] G. Yamahata *et al*., Nat. Commun. **5**, 5038 (2014). [6] S. P. Giblin *et al*., Nat. Commun. **3**, 930 (2012).

# Non perturbative full counting statistics for solid state entangler with double ferromagnetic islands

Yukimi Kanai[1], Yuri Sawamura[1], Megumu Mihata[2], Takeshi Inagaki[3]
and
Shuichi Iwabuchi[1]

[1]*Department of Physics, Graduate School of Humanities and Sciences, Nara Women's University, Nara 630-8506, Japan*
[2]*Microelectronics Center, TOSHIBA Corporation, Yokohama 247-8585, Japan*
[3]*Graduate School of Material Science, Nara Institute of Science and Technology, Ikoma 630-0192, Japan*
*e-mail:iwabuchi@cc.nara-wu.ac.jp*

Recently, much interest has been shown for quantum entanglement of electrons in solid state systems. Beyond the exploration of nonlocal quantum effects through the test of Bell's inequality, a controlled generation and manipulation of electronic entanglement is of great importance for potential applications in quantum information and computation schemes. As a parallel research stream, spin polarized quantum transport has also focused an important interest. There are several preceding experimental[1] and theoretical[2] studies concerning crossed conductance which results from the competition between normal transmission and Andreev reflection (AR) channels in ferromagnet/superconductor/ferromagnet (FSF) structures. Since ferromagnetic exchange splitting is one of the most promising key set-ups for controlling quantum entanglement, it is worth considering currents and cross correlations of noises in the solid state entangler (SSE) which contains FSF junction.

We present the non perturbative theory of full counting statistics for ultra-small SSE depicted in FIG.1, which is the coupled C-SETs consisting of a common superconductor/double ferromagnetic islands (with gates)/normal metals with environmental impedances. Ferromagnetic islands are Stoner metals and/or half metals. Since, in this system, charging and energy dissipation effects are crucial to effective extraction and decoherence of quantum entanglement, the theory takes account of both effects properly in the spirit of self-consistent microscopic theory of C-SET[3] and Caldeila-Leggett theory. We show the explicit expression of the cumulant generation function $\Omega(\{\chi_\alpha\})$ for all kinds of currents in the system. Here $\chi_\alpha$ ($\alpha$ = L, R) is the counting field (CF) of C-SET on side $\alpha$ introduced under current continuity conditions. Currents and cross correlation of noises are then obtained as

$$\begin{aligned} I_\alpha &\equiv \langle\, \mathscr{I}_\alpha \rangle = \partial_{\mathrm{i}\chi_\alpha}\, \Omega(\{\chi_\alpha\})\,|_{\chi_\alpha=0} \\ S_{LR}(\,\omega=0\,) &\equiv \int_{-\infty}^{\infty} \mathrm{d}t\, \langle\, [\,\delta\mathscr{I}_L(t), \delta\mathscr{I}_R(0)\,]_+ \,\rangle = \partial_{\mathrm{i}\chi_L}\,\partial_{\mathrm{i}\chi_R}\,\Omega(\{\chi_\alpha\})\,|_{\chi_\alpha=0} \end{aligned}$$

where $\mathscr{I}_\alpha$ is the current operator on side $\alpha$ and $\delta\mathscr{I}_\alpha \equiv \mathscr{I}_\alpha - \langle\, \mathscr{I}_\alpha \rangle$.

Note that, in this system, crossed AR and elastic cotunneling involve the virtual creation and propagation of a quasiparticle in superconductor and are taken into account up to infinite order of tunneling[4]. We discuss charging and energy dissipation effects on $I_\alpha$ and bunching-antibunching aspect of $S_{LR}(\omega=0)$.

[1] D. Beckmann, H. B. Weber and H. v. Löhneysen, Phys. Rev. Lett. **93** 197003-1 (2004)
[2] R. Melin and D. Feinberg, Phys. Rev. **B 70** 174509 (2004)
[3] S. Iwabuchi, *Physics of Mesoscopic Systems* (Maruzen, Tokyo) (1998)
V. Bubanja and S. Iwabuchi, Phys. Rev. **B84** 094501 (2011)
[4] For non perturbative treatment of cotunneling, see V. Bubanja and S. Iwabuchi, J. Phys. Soc. Jpn., **76** 073601 (2007)

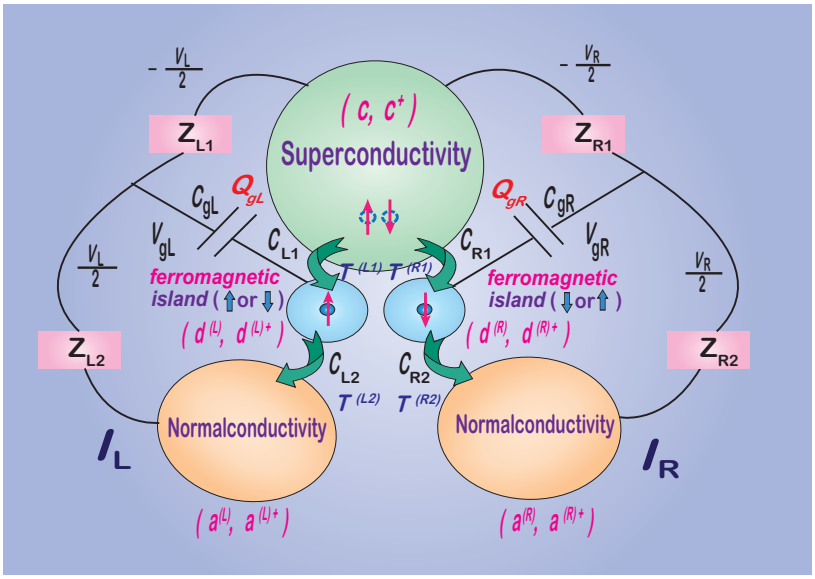


FIG.1: A generalized SSE structure consisting of superconducting electrode, double ferromagnetic islands (with gates) and normal conducting drains. Thick arrows in ferromagnetic islands denote majority spin orientations. Islands are Stoner metals and/or half metals. Environmental impedances $Z_{\alpha i}$ $(i = 1,2)$ as well as charging energy are nonperturbatively taken into account in the theory. Various quantum mechanical macroscopic charges, creation annihilation operators of electrons and tunnel matrices between junctions are also shown in the figure.

# Phonon Assisted Spin Orbit Transitions in Spin Interferometers

Geof Aers[1], Sergei Studenikin[1], Marek Korkusinski[1], Ghislain Granger[1], Alicia Kam[1] and Andy Sachrajda[1]

[1] *National Research Council of Canada, Ottawa, Canada K1A 0R6*
*e-mail: andy.sachrajda@nrc.ca*

Recently spin interferometers have been successfully realized experimentally in double and triple quantum dots [1-3]. The results have been effectively modeled by Landau-Zener-Stückelberg behavior associated with the relevant level anticrossing. The anticrossing is assumed to be related to the hyperfine interaction.

In this work we demonstrate that this underlying behavior is non-trivially and significantly modified in AlGaAs/GaAs based lateral quantum dots when the experiments are initiated with pulses incorporating very short rise times. Under these experimental conditions we will show that two new observations become apparent; a discrete sequence of additional resonance lines appears as the rise time becomes shorter and there is a dramatic 'apparent' increase in the gap at the anticrossing. These observations develop consistently as a function of both pulse rise time and experiment readout time. The experiments are performed in a triple quantum dot tuned to a double quantum dot regime.

To account fully for these novel observations a theoretical model was developed which combined acoustic phonon assisted spin-orbit transitions and Landau-Zener-Stückelberg behavior in a density-matrix calculation. The apparent gap widening is due to acoustic phonons generated by the high frequency probe pulse while the resonance lines are found to be associated with phonon cavity effects consistent with the device gate structure.

1. J. R. Petta, H. Lu, and A. C. Gossard, Science **327,** 669 (2010).
2. L. Gaudreau, et al. Nature Physics **8**, 54 (2012).
3. S. A. Studenikin, et al., Phys. Rev. Lett. **108**, 226802 (2012).

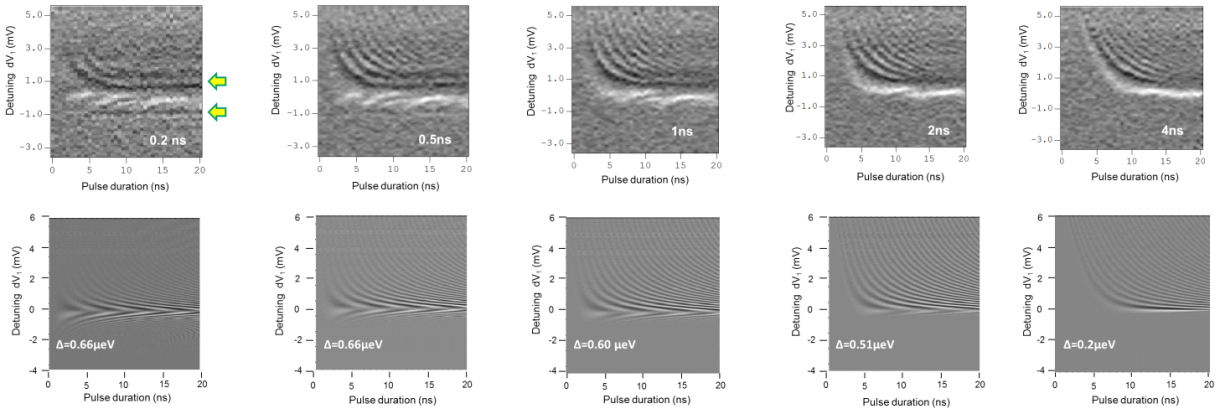


*Figure 1: Landau-Zener-Stückelberg coherent oscillations as a function of rise time (top- experimental results, lower- theoretical simulations not including phonon cavity effects).*

# Terahertz single electron photovoltaic effect in self-assembled InAs quantum dots

Y. Zhang[1], K. Shibata[1], N. Nagai[1], C. Ndebeka-Bandou[2], G. Bastard[2], and K. Hirakawa[1]

[1] *Institute of Industrial Science and INQIE, University of Tokyo, 4-6-1 Komaba, Meguro-ku, Tokyo 153-8505, Japan*

[2] *Laboratoire Pierre Aigrain, Ecole Normale Superieure, 24 rue Lhomond F75005, Paris*

*e-mail: hirakawa@iis.u-tokyo.ac.jp*

We have observed the terahertz (THz) induced single electron photovoltaic effect in self-assembled InAs quantum dots (QDs). We used a single electron transistor (SET) geometry that consists of a single InAs QD and nanogap electrodes coupled with a bowtie antenna [1]. Under a weak, broadband THz radiation, a photocurrent induced by THz intersublevel transitions in the QD is generated even when no bias voltage is applied to the SET [2]. The observed single electron photovoltaic effect is due to an energy-dependent tunneling asymmetry in the QD-SET. Moreover, the tunneling asymmetry changes not only with the shell, but also with the electron number in the QD, suggesting the manybody nature of the electron wavefunctions. The THz photovoltaic effect observed in the present QD-SET system may have potential applications to nanoscale energy harvesting.

[1] Y. Zhang, K. Shibata, N. Nagai, C. Ndebeka-Bandou, G. Bastard, and K. Hirakawa, Nano Lett. **15**, 1166 (2015).

[2] Y. Zhang, K. Shibata, N. Nagai, C. Ndebeka-Bandou, G. Bastard, and K. Hirakawa, Appl. Phys. Lett., in press.

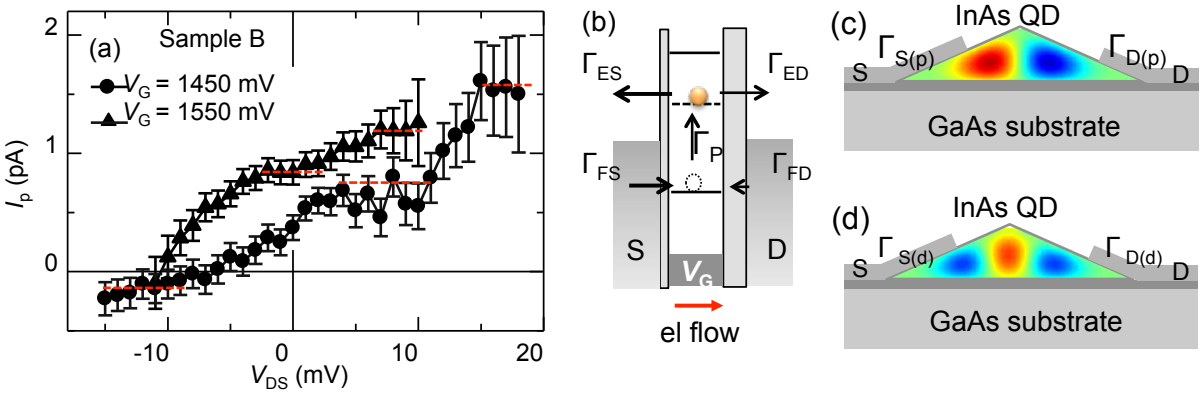


Fig. 1 (a) THz-induced photocurrent as a function of $V_{DS}$ measured on a QD-SET sample, (b) energy band diagram of a QD-SET, (c) and (d) schematic cross sections of a QD-SET sample and the wavefunction patterns calculated for the p- and d-shells, respectively.

# Transport though InAs self-assembled quantum dots controlled by sidegate voltages

Akira Oiwa[1], Ryoki Shikishima[1], Takashi Hirayama[1], Haruki Kiyama[1], Shoji Baba[2], Naomi Nagai[3], Kazuhiko Hirakawa[3], and Seigo Tarucha[2,4]

[1] *The Institute of Scientific and Industrial Research, Osaka University, Ibaraki, Osaka, 567-0047, Japan*

[2] *Department of Applied Physics, School of Engineering, The University of Tokyo, Hongo, Bunkyo-ku, Tokyo, 113-8654, Japan*

[3] *Institute of Industrial Science, The University of Tokyo, Komaba, Shibuya-ku, Tokyo, 153-8505 , Japan*

[4] *RIKEN Center for Emergent Matter Science (CEMS), Wako, Saitama, 351-0198, Japan*

*e-mail: oiwa@sanken.osaka-u.ac.jp*

In uncapped InAs self-assembled quantum dots (QDs) the electrical controls of g-factor [2]and spin-orbit interaction [3] have been demonstrated by combining conventional backgate and laterally coupled sidegates. Moreover the technique also enables one to control the Josephson current and Kondo effect associated with many body interaction [4]. The efficiency of such sidegates is more than an order of magnitude smaller than that of the backgate [4,5]. In this work we elucidate the mechanisms limiting the sidegate efficiency and discuss the transport properties of uncapped InAs QDs with improved device designs.

InAs QDs with a typical size of 100 nm are grown by molecular beam epitaxy. Device A has source and drain electrodes with a 200-nm-width. On the other hand, Device B has narrower electrodes with a 50-nm-width. First, we evaluate the lever arm of the sidegates. From a comparison between Device A and B, we have found that the screening effect by electron reservoirs is reduced in Device A with a narrow source-drain electrode. Then, with the improved device design, the sidegate dependence of the tunnel couplings has been evaluated. The results indicate the spatial modulation of electron wave function in the QD and the potential application to wave function mapping in QDs.

[1] M. Jung *et al*., Appl. Phys. Lett. **87**, 203109 (2005).

[2] S. Takahashi *et al*., Phys. Rev. Lett. **104**, 246801 (2010).

[3] Y. Kanai *et al.*, Nature nanotechnology **6**, 511 (2011).

[4] Y. Kanai *et al*., Phys. Rev. B **82**,054512 (2010).

[5] K. Shibata *et al*., Nature communications **4**, 2664 (2013).

# Effects of charging and energy dissipation on current and noise correlation in solid state entangler based on non perturbative full counting statistics

Yuri Sawamura[1], Yukimi Kanai[1], Megumu Mihata[2], Takeshi Inagaki[3]
and
Shuichi Iwabuchi[1]
[1]*Department of Physics, Graduate School of Humanities and Sciences, Nara Women's University, Nara 630-8506, Japan*
[2]*Microelectronics Center, TOSHIBA Corporation, Yokohama 247-8585, Japan*
[3]*Graduate School of Material Science, Nara Institute of Science and Technology, Ikoma 630-0192, Japan*
*e-mail:iwabuchi@cc.nara-wu.ac.jp*

Recently, much interest has been shown for quantum entanglement of electrons in solid state systems. Beyond the exploration of nonlocal quantum effects through the test of Bell's inequality, a controlled generation and manipulation of electronic entanglement is of great importance for quantum information and computation schemes. Hofstetter *et al.*[1] reported the evidence of nonlocal signal which could be attributed to crossed Andreev reflection in ultra-small Cooper pair splitter, which is nothing but a solid state entangler (SSE) consisting of two coupled superconducting-normal-normal C-SETs (FIG.1). Inspired by their experimental research, several authors have discussed current and noise correlation theoretically[2]. Nevertheless neither charging nor energy dissipation effects have been so far properly taken into account, although these effects are crucial to effective extraction and decoherence of quantum entanglement. For example, they could not have reproduced any sign of Coulomb gap and Coulomb staircases (oscillations) in currents.

We present the non perturbative theory of full counting statistics for SSE depicted in FIG.1, which properly describes charging effect as well as energy dissipation. We show the explicit expression of the cumulant generation function (CGF) for all kinds of currents in the system as

$$\begin{aligned}\Omega(\{\chi_\alpha\}) &\equiv \lim_{T\to\infty}\frac{1}{T}\log\left\langle T_{c_{\rm K}}\exp\left\{-\frac{\rm i}{\hbar}\int_{c_{\rm K}}{\rm d}\tau\,\mathscr{H}_T(\{\chi_\alpha\})(\tau)\right\}\right\rangle \\ &= \int_{-\infty}^{\infty}\frac{{\rm d}\omega}{2\pi}\,{\rm Tr}_{SK\otimes NG}\left\{\log\left[\frac{\hat{1}-\hat{g}_c(\omega)\hat{\Sigma}_c(\{\chi_\alpha\};\omega)}{\hat{1}-\hat{g}_c(\omega)\hat{\Sigma}_c(0;\omega)}\right]+\sum_{\alpha=L,R}\log\left[\frac{\hat{1}-\hat{g}_{a_\alpha}(\omega)\hat{\Sigma}_{a_\alpha}(\{\chi_\alpha\};\omega)}{\hat{1}-\hat{g}_{a_\alpha}(\omega)\hat{\Sigma}_{a_\alpha}(0;\omega)}\right]\right\},\end{aligned}$$

where $\chi_\alpha$ is the counting field (CF) introduced along Keldysh contour $c_{\rm K}$ defined above and below real time axis in interval $[-T/2,T/2]$, and $c$ ($a_\alpha$) denotes superconducting (normal drain on side $\alpha$) electrode. $\mathscr{H}_T(\{\chi_\alpha\})$ is CF dependent tunnel Hamiltonian, and $\hat{g}_\nu(\omega)$ and $\hat{\Sigma}_\nu(\{\chi_\alpha\};\omega)$ are, respectively, Green's function and self-energy of electrons in electrode $\nu$ defined in Schwinger-Keldysh⊗Nambu-Gorkov (SK⊗NG) space. Note that both charging and energy dissipation effects are taken into account in them, in the spirit of self-consistent microscopic theory of C-SET[3] and Caldeila-Leggett theory, respectively. Because of introduction of CFs satisfying current continuity conditions, we can get more transparent expressions for CGF than ever, which in turn leads to compact expressions for current cumulants, especially for cross correlations. Based on CGF obtained we will discuss charging and energy dissipation effects on branching currents and their crossed correlations. Some of tentative results for currents are shown in FIG.2. Furthermore, within the same theoretical framework, we consider the model of SSE as depicted in FIG.3 and will discuss Bell's inequality.

[1] L. Hofstetter, S. Csonka, J. Nygard and C. Schönenberger, Nature **461**, 960 (2009)
[2] J. Rech, D. Chevallier, T. Jonckheere and T. Martin, Phys. Rev. B **85**, 035419 (2012)
D. Chevallier, J. Rech, T. Jonckheere and T. Martin, Phys. Rev. B **83**, 125421 (2011)
[3] S. Iwabuchi, *Physics of Mesoscopic Systems* (Maruzen, Tokyo) (1998)
V. Bubanja and S. Iwabuchi, Phys. Rev. **B84**, 094501 (2011)

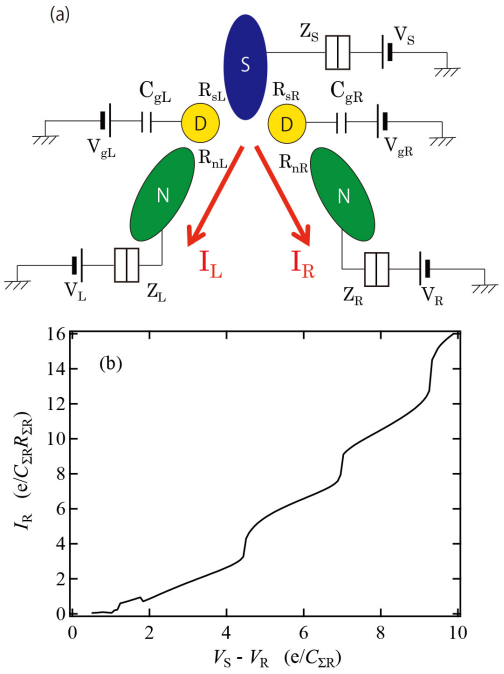


FIG.1: (a) The solid state entangler consisting of two C-SET structures. S(N) and D stand for the superconducting (normal-metallic) electrode and normal metallic island, respectively. Various resistances and capacitances are defined as usual. (b) Current $I_R$ flowing through the right C-SET as a function of the bias voltage $V_S - V_R$ in high impedance limit. Parameters are chosen tentatively. Coulomb gap and staircases are clearly seen in the current caused by direct and crossed Andreev reflections.

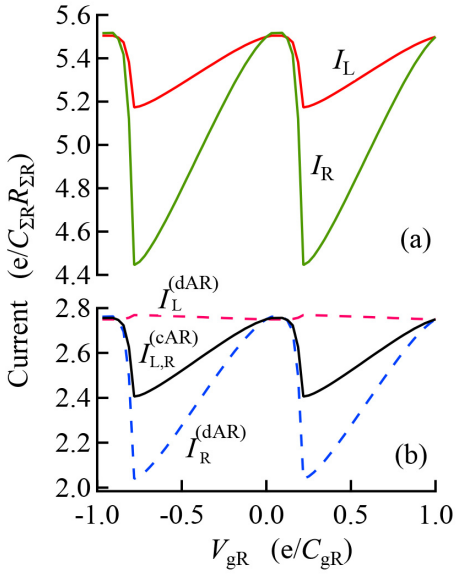


FIG.2: (a) Coulomb oscillations in the currents $I_L$ and $I_R$ flowing through left (right) C-SETs as a function of gate voltage of the right C-SET $V_{gR}$ with $V_{gL}$ fixed. (b) Current components caused by crossed and direct Andreev reflections flowing through C-SET on $\alpha$ (= L, R), $I_\alpha^{(cAR)}$ and $I_\alpha^{(dAR)}$. Bias voltages of the two C-SETs are tentatively chosen to be identical (no elastic co-tunneling limit). Correlated variation is clearly seen between $I_\alpha^{(cAR)}$ only, which corresponds to the bunching correlation: Second cumulant $S(\omega = 0)$ becomes positive. Furthermore, we can show that the charging effect (Coulomb blockade ) makes it possible for us to extract $I_\alpha^{(cAR)}$ signal only in a certain bias condition.

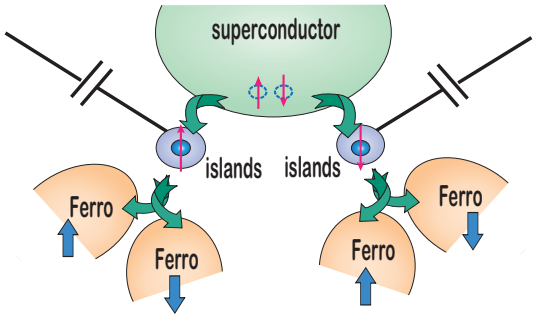


FIG.3: A generalized SSE structure consisting of superconducting-double normal metallic islands (with gates) - four ferromagnetic metallic drains. Thick arrows in ferromagnetic electrodes denote majority spin orientations. Environmental impedances are not shown here.

# Signatures and Detection of Majorana Zero Modes using Nano devices

Dong E. Liu[1], Alex Levchenko[2], and Roman M. Lutchyn[1]

[1] *Station Q, Microsoft Research, Santa Barbara, California 93106-6105, USA*
[2] *Department of Physics, University of Wisconsin-Madison, Madison, Wisconsin 53706, USA*
*e-mail: donl@microsoft.com*

Tunneling spectroscopy provides the simplest way to detect Majorana zero-energy modes (MZMs): a zero bias conductance peak (ZBP) with quantized peak height (2e^2/h). However, due to the large subgap states observed in tunneling experiments, the largest observed peak height was at most 30% of the predicted value. Therefore, it is a challenging task to exclude the other false-positive contributions, such as Kondo effects, disorders, and resonant Andreev scattering, which are ubiquitous. I theoretically proposed two simple local measurement schemes using tunable Nano devices to qualitatively distinguish Majorana modes with other false-positive signatures.

First of all, I redesigned a tunneling scheme by simply replacing the normal metallic lead in the tunneling spectroscopy with a resistive lead (with large resistance) so that dissipation plays an important role. I found that the ways that the dissipation effects renormalize the conductance is significantly different for Majorana and other cases. Therefore, the dissipation effect provides a way to qualitatively distinguish Majorana ZBP and other ZBP, and serves as a "Majorana signature filter" [1].

Secondly, we introduced a new setup involving a QD sensor closed to a MZM, and propose to measure its full counting statistics (FCS), of charge transport fluctuations. Using a Keldysh path-integral approach, we predicted that, for the symmetric QD-lead couplings, all the cumulants are independent of the microscopic parameters and exhibit a universal pattern. When the dot couples to other non-Majorana modes, FCS shows different non-universal results, which depend on all parameters. These results provide another complete tool set for detecting Majorana modes in tunneling transport measurements [2].

[1] D. E. Liu, Phys. Rev. Lett. 111, 207003 (2013).
[2] D.E.Liu, A. Levchenko, R. M. Lutchyn, arXiv:1503.00776 (2015).

# Electric-field control of quantum states in nanostructures by electric-double-layer gating

Kenji Shibata[1,2], Kenji Yoshida[2], and Kazuhiko Hirakawa[2]

[1] *Tohoku Institute of Technology, Sendai, Miyagi 982-8577, Japan*
[2] *IIS and INQIE, University of Tokyo, Meguro-ku, Tokyo, 153-8505, Japan*
*e-mail: kshibata@tohtech.ac.jp*

Electrical manipulation and read-out of quantum states in low dimensional nanostructures by nanogap metal electrodes is expected to bring about innovation in quantum information processing. However, electrical tunability of the quantum states is limited by the screening of gate electric fields. Electric-double-layer (EDL) transistors with ionic liquids as gate dielectric have recently emerged as a powerful tool in tuning the Fermi energy, $E_F$, in nanostructures [1]. The EDL formed at liquid/solid interfaces functions as nanogap capacitors with a huge capacitance and can accumulate or deplete charge carriers over a wide range. In this work, we demonstrate a new way to realize wide-range electrical modulation of quantum states of single self-assembled InAs quantum dots (QDs) and metal quantum point contacts (QPCs) with a liquid-gated EDL transistor geometry (Fig. 1(a)).

In single InAs QD transistors, it is found that the efficiency of EDL gating is 6-90 times higher than that of the conventional solid-gating. The quantized energy level spacing between the *s*- and *p*-orbitals, $\Delta E_{s\text{-}p}$, is modulated from ~15 meV to ~25 meV and the electron g-factor is electrically tuned over a wide range as seen in Figs. 1(b)-1(d). Such a field effect tuning can be explained by the modulation in the confinement potential of electrons in the QDs [2]. Furthermore, the use of optically transparent ionic liquids (Fig. 1(a)) as the gate dielectrics potentially allows us to optically manipulate single electron charge/spin states in QDs [3]. On the other hand, in metal QPC samples (Fig. 2(a)), the electric conductance shows quantized conductance plateaus and step-wise increase/decrease by $G_0$ as EDL gate voltage, $V_{EDL}$, is swept, as seen in Fig. 2(b). This indicates that the conductance in metal QPCs is successfully modulated by EDL gating. The electric-field control of conductance in metal QPCs opens a way for their application to the local charge sensing at room temperature, for example, to the local sensing of signal transduction in neuron where a large number of ions' flow transduces signals in the electrolyte solution [4].

[1] K. Ueno et al., Nature Materials **7**, 855 (2008).

[2] K. Shibata et al., Nature Communications **4**, 2664 (2013).

[3] K. Shibata et al., Phys. Rev. Lett. **109**, 077401 (2012).

[4] B. Alberts et al., Molecular Biology of the Cell, (Garland Science 2001).

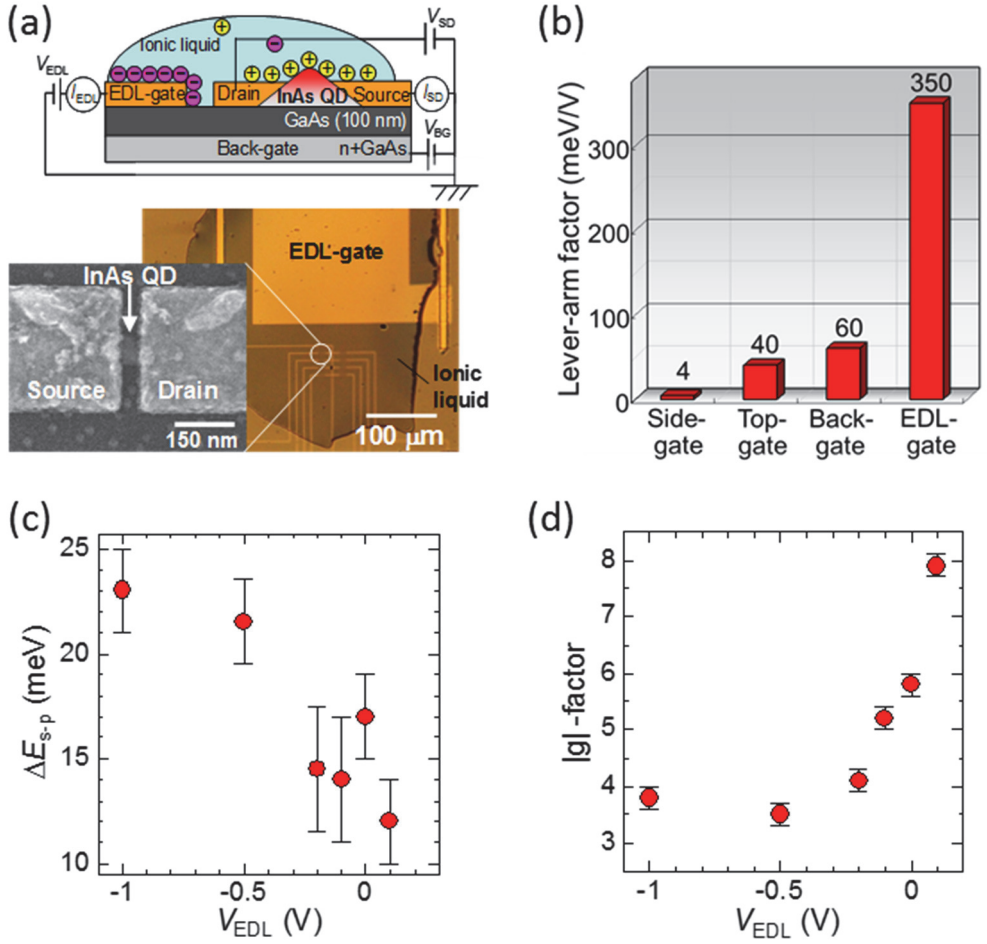


Fig. 1: (a) Schematic illustration (upper) and the microscope images (lower) of QD-EDL transistors. (b) Comparison of the gating efficiency with various gating methods. $V_{EDL}$ dependence of (c) $\Delta E_{s\text{-}p}$, and (d) electron g-factors of 1*s* state.

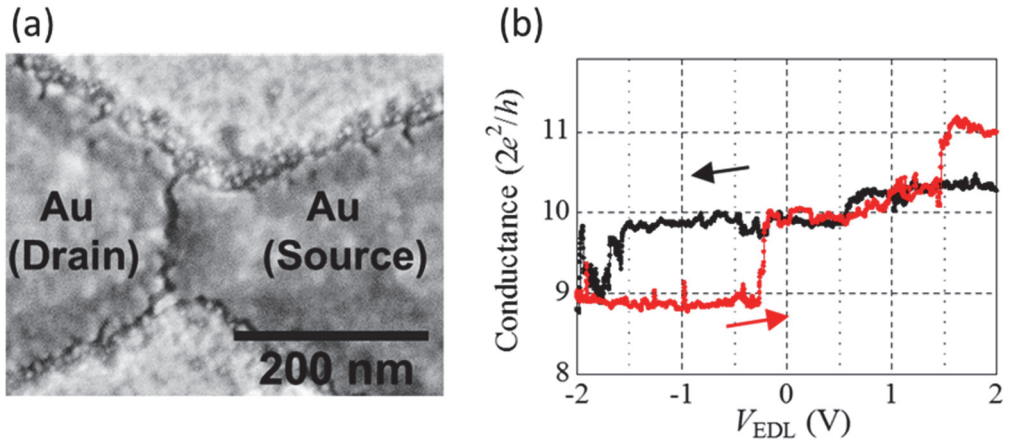


Fig. 2: (a) An SEM image of the metal QPC sample. (b) $V_{EDL}$ dependence of the conductance of the metal QPC measured at 220 K. The observed hysteresis may be attributed to the slow ion motion and the interfacial trap states.

# Formation of Au oxide layer for highly sensitive graphene photosensor toward single photon sensing

○Shohei Ishida[1], Yuki Anno[1], Shiho Kobayashi[1], Masato Takeuchi[2], Masaya Matsuoka[2], Kuniharu Takei[1], Takayuki Arie[1], Seiji Akita[1]

[1] *Department of Physics and electronics, Osaka Prefecture University, Osaka 599-8531, Japan*

[2] *Department of Applied Chemistry, Osaka Prefecture University, Osaka 599-8531, Japan*

*e-mail: ishida-4@pe.osakafu-u.ac.jp*

Graphene is expected for optical sensors for ultra-wide wavelength region from ultraviolet to terahertz which originates from zero-gap band structure. Recently, we reported highly photosensitive graphene filed-effect transistor (G-FET) with the Au native oxide layer on Au electrodes formed by natural oxidation process [1]. In this case, the oxidation of Au depends on the surrounding environment of Au. Thus, stable and controlled formation of Au oxide layer is still open subject. In this study, we investigate the formation of Au oxide layer using plasma or thermal oxidation process.

A pair of source and drain electrodes consisting of Cr/Au (5nm/30nm) was fabricated on highly doped Si substrate with a 300nm thick $SiO_2$ layer. The oxidation of the Au electrode was performed by RF plasma oxidation (a few minutes at room temperature) or simple thermal annealing in $O_2$ (1 atm) for 1 hours at 100~200 $^oC$, and the oxidized surfaces were examined by XPS. Then a monolayer graphene was transferred onto the substrate and trimmed by using oxygen plasma etching to form an FET channel (width × length = 5 × 3 $\mu m^2$), where the graphene was synthesized using low pressure chemical vapor deposition at 1000 $^oC$ using Cu foil as catalyst. In the case of plasma oxidation, the continuous shift of Dirac point ($V_{Dirac}$) under the light illumination (510nm, ~228mW/$cm^2$) was observed for the repeated cycle of measurements because of the pileup of the trapped charge and were hardly returned to the initial $V_{Dirac}$. This continuous shift of $V_{Dirac}$ is a serious problem for practical application. Generally, the shift of $V_{Dirac}$ mainly originates from the charge accumulation at the $SiO_2$ layer or charge impurities nearby graphene channel. Therefore, the plasma oxidation induces the serious charge trapping site on $SiO_2$ layer in addition to the formation of the Au oxide layer on the electrodes. On the contrary, in the case of thermal oxidation at 100~150 $^oC$, the shift of $V_{Dirac}$ was well suppressed, where the photosensitivity appears only at $V_{GS} > V_{Dirac}$. Note that no further shift of $V_{Dirac}$ was also observed for the repetitive measurements. The faster sweep rate of $V_{GS}$ is favorable for the photosensitivity owing to the lower dark current. At the sweep rate of $V_{GS}$ = 14V/s, high photoresponse of ~ $7.4\times10^5$ $AW^{-1}$ is achieved. The XPS spectra show the peak shifts are much smaller than those for the plasma oxidation, which indicates that the oxidized Au formed by the thermal oxidation process has smaller valence of Au than that formed by the plasma oxidation. These results are comparable to the G-FET with native Au oxide layer on electrodes [1]. Note that the G-FET with Au oxide layer formed at 200 $^oC$ showed poor photosensitivity with shift of $V_{Dirac}$, because the $Au_2O_3$, which is most stable Au oxide, is dissolved higher than 160 $^oC$. This was confirmed by the XPS spectrum for the Au oxide formed at 200 $^oC$. Thus, the thermal oxidation process is efficient for formation of the Au oxide layer for the highly photosensitive G-FET.

**Acknowledgements** This work was partially supported by JSPS KAKENHI Grant Number 25286010, and by the Iketani Science and Technology Foundation.

[1] S. Ishida et al, submitted

# Dephasing effect on a perfectly conducting channel in disordered graphene nanoribbons with zigzag edges

Yuji Shimomura and Yositake Takane

*Department of Quantum Matter, Graduate School of Advanced Sciences of Matter, Hiroshima University, Higashi-Hiroshima 739-8530, Japan*
*e-mail: shimomura25@hiroshima-u.ac.jp*

Electron transport in a disordered graphene nanoribbon with zigzag edges is crucially affected by a perfectly conducting channel without backward scattering that is stabilized if intervalley scattering of electrons is ignorable [1]. In the presence of such a perfectly conducting channel, the average dimensionless conductance $\langle g \rangle$ of the system decreases toward the quantized value of $\langle g \rangle = 1$ with increasing the system length $L$, and hence $\langle g \rangle$ does not vanish even in the limit of $L \to \infty$. This indicates that Anderson localization does not take place in this system. In the realistic case where intervalley scattering is sufficiently weak but not completely ignorable, the perfectly conducting channel is gradually destabilized with increasing $L$ and $\langle g \rangle$ eventually decays to zero. Here, we show that such destabilization of the perfectly conducting channel can be significantly relaxed by pure dephasing. We numerically calculate $\langle g \rangle$ in the presence of long-ranged impurities that induce weak intervalley scattering, taking dephasing effect into account. It is demonstrated that, in the presence of sufficient dephasing, the decay of $\langle g \rangle$ in the regime of $\langle g \rangle < 1$ is strongly suppressed and $\langle g \rangle$ remains nearly equal to 1 in a wide region of $L$. We expect that this encourages experimental efforts to detect a perfectly conducting channel in zigzag nanoribbons.

[1] K. Wakabayashi, Y. Takane, and M. Sigrist, Phys. Rev. Lett. **99**, 036601 (2007).

# Electronic structures of zigzag-edge nanoribbon lateral superlattices

Futo Hashimoto, Nobuya Mori, Osamu Kubo, and Mitsuhiro Katayama

*Graduate School of Engineering, Osaka University*
*2-1 Yamada-oka, Suita, Osaka 565-0871, Japan*
*e-mail: hashimoto@si.eei.eng.osaka-u.ac.jp*

Materials consisting of a single-atom-thick hexagonal lattice have been attracted much attention because of their unique electronic properties and emerging applications. Among them, graphene has been most extensively studied up to now. The electronic structures are strongly affected by the orientation of the edges [1, 2]. For example, one can open a significant band-gap by forming armchair-edge graphene nanoribbons (NRs), narrow strips cut out from a two-dimensional (2D) sheet of graphene. Recently, massively parallel silicon NRs are grown experimentally [3, 4]. Although it is not well understood whether the inter-NR interaction presents in such structures, it should be worth investigating how the interaction affects their electronic states. Here we calculate electronic structures of zigzag-edge NR lateral superlattices (LSLs) with changing the inter-NR interaction strengths, and investigate how the system evolves from isolated NRs (no inter-NR interaction) to a bulk 2D sheet (full interaction).

We consider zigzag-edge NR LSLs whose schematic diagram is given in Fig. 1. The NR width $N$ is defined as the number of the zigzag lines. We use a nearest-neighbor (NN) tight-binding model with a transfer integral of $t$ between NN atoms in a NR. We assume an inter-NR transfer integral of $\gamma$ between neighboring NRs. The system becomes isolated NRs when $\gamma = 0$, while it is a bulk 2D sheet when $\gamma = t$.

The left panels of Figs. 2(a)–(f) show the band structures of NR LSLs with $N = 5$ for different inter-NR interaction strengths. The right panels show the corresponding density-of-states (DOS); The solid lines represent the total DOS, $\rho_{\rm total}(E)$, and the dashed lines the local DOS, $\rho_{\rm edge}(E)$, of the edge atoms, i.e. 1A, $N$B, $(N+1)$A, 2$N$B atoms in Fig. 1. For $\gamma = 0$, a flat band appears at $E = 0$. This state completely localizes at the edge atoms at $k_x = \pi/a$ ($a$ is the lattice constant) [1, 2]. For $\gamma = t$, we see the Dirac point of a bulk 2D sheet appearing at $(k_x, k_y) = (2\pi/3a, 0)$. Note that we use a fixed rectangle unit cell of the size $L_x \times L_y = a \times \sqrt{3}Na$ for the entire parameter regime, $0 \le \gamma \le t$ (see Fig. 1). For the intermediate parameter regime, $0 < \gamma < t$, we find a coexisting of (almost) flat bands and the Dirac point. These flat bands appear at $E = \pm\gamma$, and originate in dimers on the edges, such as an atom-pair of $N$B and $(N + 1)$A atoms. These modes completely localize at the edges at $(k_x, k_y) = (\pi/a, 0)$ [see, also, Fig. 3 where we plot normalized DOS defined as $\rho_{\rm edge}(E)/\rho_{\rm total}(E)$]. The Dirac point locates at $k_x = k_{\rm D} \equiv 2\arccos[\frac{1}{2}(\gamma/t)^{1/N}]/a$ and $k_y = 0$ (see Fig. 4). Figure 5 shows $\gamma$-dependence of the velocity $v_x$ ($v_y$) parallel (perpendicular) to the NR axis near the Dirac point. At $\gamma = t$, the velocity dispersion is isotopic reflecting the isotropy of the bulk Dirac cone, and $v_x = v_y = v_0 \equiv \sqrt{3}at/2\hbar$. As $\gamma$ decreases, the velocity dispersion becomes anisotropic. However, the anisotropy is not so large as long as $\gamma$ is not too small (see the $v_y/v_x$ curve in Fig. 5).

In summary, we calculated electronic structures of zigzag-edge NR LSLs with varying $\gamma$, and found that both the almost flat bands and the anisotropic Dirac cone appear for $0 < \gamma < t$.

[1] M. Fujita *et al.*, J. Phys. Soc. Jpn. **65**, 1920 (1996). [2] K. Wakabayashi *et al.* Sci. Technol. Adv. Mattr. **11**, 054504 (2010). [3] A. Kara *et al.*, Surf. Sci. Rep. **67**, 1 (2012). [4] P. De Padova *et al.*, Nano Lett. **12**, 5500 (2012).

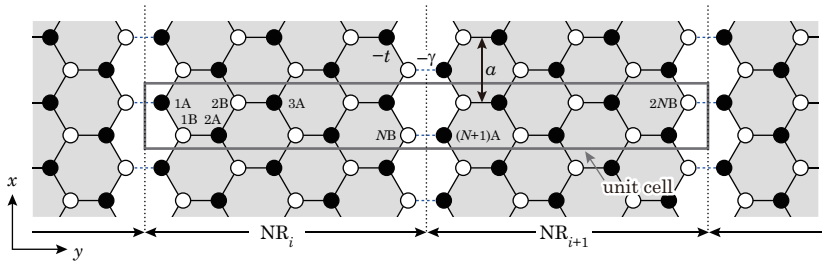


**Fig. 1**: Zigzag-edge NRs along the $x$-direction are coupled to the neighboring NRs with interaction strengths $\gamma$. The thick gray rectangle defines the unit cell.

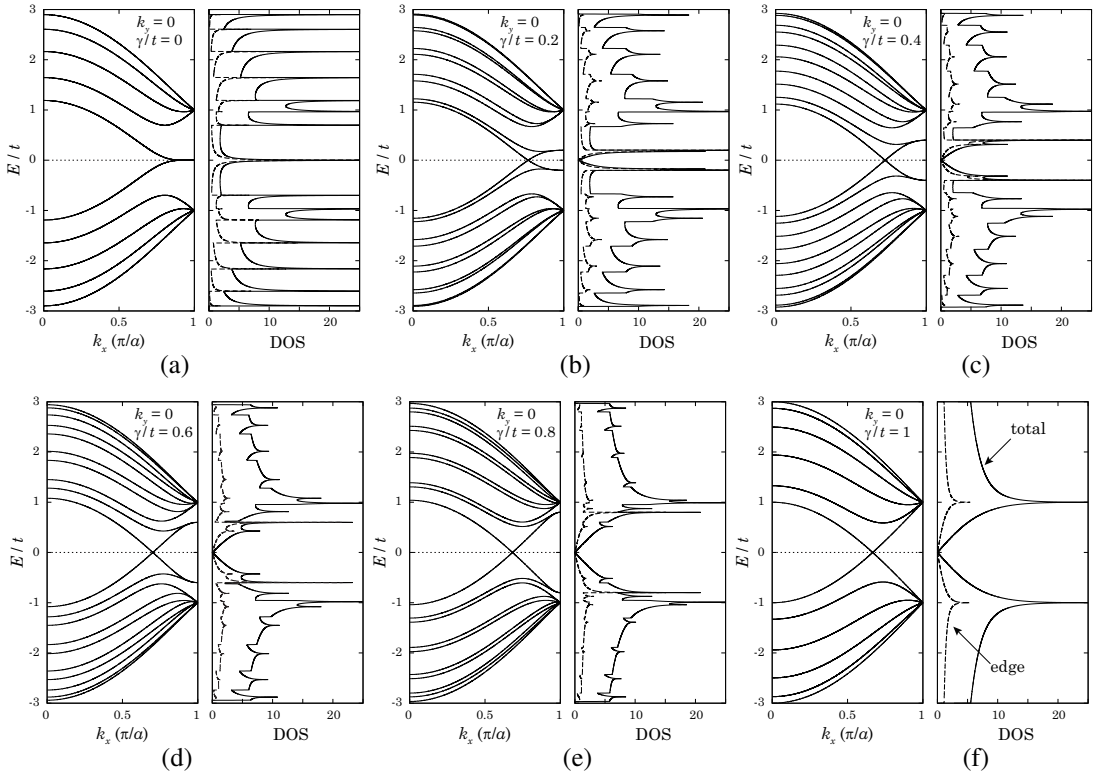


**Fig. 2**: Band structures (left panels) and DOS (right panels) for NR LSLs with $N = 5$ and $\gamma/t = 0$ (a), 0.2 (b), 0.4 (c), $\cdots$, 1 (f).

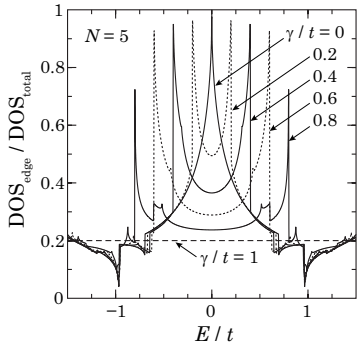


**Fig. 3** [left]: Normalized NR-edge DOS for $\gamma/t$ between 0 and 1 with 0.2 steps.

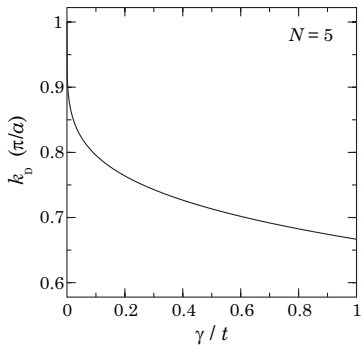


**Fig. 4** [center]: Dirac-point wavevector $k_{\rm D}$ *vs.* $\gamma$.

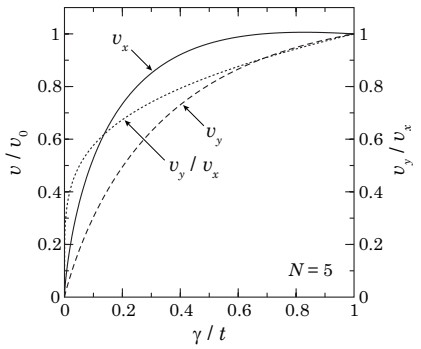


**Fig. 5** [right]: $\gamma$-dependence of the velocity $v_x$ ($v_y$) parallel (perpendicular) to the NR axis near the Dirac point. $v_0 \equiv \sqrt{3}at/2\hbar$ is the Fermi velocity of the bulk 2D sheet.

# Electron Transport in Densely-Packed Graphene Nanoribbons Formed on a Corrugated SiC Surface

Hirokazu Tanaka[1], Kohei Fukuma[2], Kohei Morita[2], Shingo Hayashi[2], Takashi Kajiwara[2], A. Visikovskiy[2], Satoru Tanaka[2], Akinobu Kanda[1]

[1] *Division of Physics and TIMS, Faculty of Pure and Applied Sciences, University of Tsukuba, 1-1-1 Tennodai, Tsukuba, Ibaraki 305-8571, Japan*

[2] *Department of Applied Quantum Physics and Nuclear Engineering, Kyushu University, Fukuoka 819-0395, Japan*

*e-mail: s1420235@u.tsukuba.ac.jp*

Formation of graphene nanoribbons (GNRs) is a promising approach to the band gap opening in graphene. However, conventional GNRs produced with top-down methods, such as oxygen plasma etching and chemical exfoliation, suffer degradation of transport properties due to uncontrollable edge structures. Recently one of the authors (S. Tanaka in Kyushu Univ.) proposed another approach to the GNR engineering, in which GNRs with moderate width (~ 100 – 200 nm) are placed on top of a corrugated substrate and the edge of each GNR is seamlessly connected to an insulating buffer layer. These GNRs are produced with a bottom-up method, thermal decomposition of a vicinal SiC substrate. We expect that the band gap is enhanced by the periodic potential modulation and the effect of edge scattering is weaker than that of the conventional GNRs due to the seamless connection to insulators. Furthermore, since the GNRs are densely ordered with a separation of ~ 0.5 μm, high current density is also anticipated.

Here, we report electron transport in these GNRs. An array including several tens of parallel GNRs is formed using oxygen plasma etching and is connected to Cr/Au electrodes using photolithography and lift-off. The two terminal resistance exhibited thermal activation behavior with an activation energy of 50 – 100 meV, which is much larger than a band gap expected for GNRs with a similar width (~ several meV). The temperature dependence of the four terminal resistance is weaker than that of Coulomb blockade behavior, indicating that the electron transport mechanism of our GNRs is different from that of conventional GNRs.

# Boundary between mono- and bi-layer graphene as a valley filter

Takeshi Nakanishi[1] and Tsuneya Ando[2]

[1] *Nanomaterials Research Institute, AIST*
*1-1-1 Umezono, Tsukuba 305-8568, Japan*
[2] *Department of Physics, Tokyo Institute of Technology*
*2-12-1 Ookayama, Meguro-ku, Tokyo 152-8551, Japan*

Graphene consists of a two-dimensional hexagonal crystal of carbon atoms, in which electron dynamics is governed by the Dirac equation. The electronic states have various intriguing features. In fact, the wave functions are characterized by spinor whose orientation is inextricably linked to the direction of the electron momentum in a different manner between monolayer and bilayer graphenes, and are strongly affected by the actual structure in the vicinity of edges. The purpose of this paper is to study the boundary between monolayer and bilayer graphenes and show a valley polarization in transmission probability through the boundary[1].

We consider the boundary of monolayer and bilayer graphene, in which layer 1 in bilayer graphene is continuously connected to the monolayer graphene and layer 2 is terminated along a straight edge having zigzag or armchair structures. Boundary conditions between monolayer and bilayer graphene are derived in an effective-mass scheme. The results show that the envelope function in layer 1 of the bilayer graphene is continuously connected to monolayer graphene, as expected, but the condition in layer 2 sensitively depends on the edge structure and mixes the K and K' valleys at the armchair structure and does not at the zigzag structure. The strong dependence on the edge structure is mostly taken care of by evanescent modes present in the bilayer graphene and does not manifest itself so much in the transmission between traveling modes.

The transmission probability vanishes at zero energy or the Dirac point due to the boundary conditions and increases roughly in proportional to the wave vector perpendicular to the boundary when the Fermi level is raised under the condition that the electron density in both layers remains the same. The transmission probability varies strongly as a function of the incident angle and its maximum appears at an angle deviating from the vertical direction depending on the K and K' points (Figure 1 shows an example for a zigzag structure). This asymmetry is opposite between the K and K' points, showing that strong valley polarization can be induced across the interface of monolayer and bilayer graphenes.

## References

[1] T. Nakanishi, M. Koshino and T. Ando, Phys. Rev. **B 82** (2010) 125428.

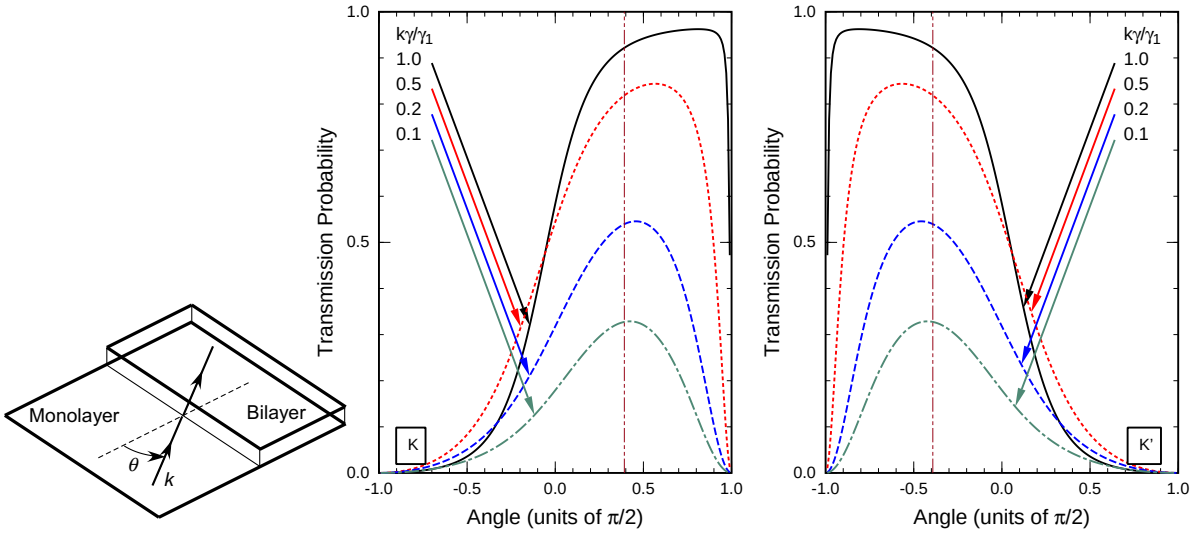


**Fig. 1** Transmission probability through a zigzag boundary as a function of the incident angle for several values of the wave vector $k$ (left and right for K and K' electrons, respectively, incident from the monolayer). The angle is measured from the direction perpendicular to the boundary. A vertical line shows maximum $\pm\sin^{-1}(1/\sqrt{3}) \approx \pm 0.196\pi$ estimated for small $k$.

# Encapsulated Graphene/Superconductor Junctions: Formation and Electron Transport

Katsuhide Yarimizu[1], Kenta Katakura[1], Youiti Ootuka[1], Kenji Watanabe[2], Takashi Taniguchi[2], Keiji Ueno[3], Hikari Tomori[1,4], Akinobu Kanda[1]

[1] *Division of Physics and TIMS, Faculty of Pure and Applied Sciences, University of Tsukuba 1-1-1 Tennodai, Tsukuba, Ibaraki 305-8571, Japan*

[2] *National Institute for Materials Science (NIMS), Tsukuba, Ibaraki 305-0047, Japan*

[3] *Department of Chemistry, Saitama University, Saitama 338-8570, Japan*

[4] *PRESTO-JST, Kawaguchi, Saitama 332-0012, Japan*

*e-mail: s1520270@u.tsukuba.ac.jp*

In a normal metal/superconductor (NS) interface, an incident electron with low energy is converted to a Cooper pair and a hole is reflected. This process is called Andreev reflection. In a conventional NS interface, a reflected hole traces the path of incident electron (retroreflection), while in a graphene/superconductor (GS) interface, *specular* reflection can occur for the electron energy close to the Dirac point.[1] This specular Andreev reflection has never been confirmed experimentally, presumably because the charged impurities on the graphene surface cause the spatial fluctuation of the Dirac point. On the other hand, it is known that the number of charged impurities is dramatically decreased by encapsulation of the graphene device with hexagonal boron nitride (hBN) layers.[2] In this work, we apply this technique to GS junctions and investigate the electron transport of the encapsulated GS junctions.

We used $NbSe_2$ thin layer as a superconductor. We fabricated hBN/$NbSe_2$/graphene/hBN heterostructures using the so-called “van der Waals assembly” technique, in which exfoliated thin layers are stacked under microscope in a dry environment.[3] An example is shown in the figure, where a graphene/$NbSe_2$ junction is sandwiched between hBN layers. Device fabrication and its electron transport will be presented in the poster session.

[1] C. W. J. Beenakker, Phys. Rev. Lett. 97, 067007 (2006).

[2] C. R. Dean et al., Nat. Nanotechnol. 5, 722 (2010).

[3] L. Wang et al. Science 342, 614 (2013).

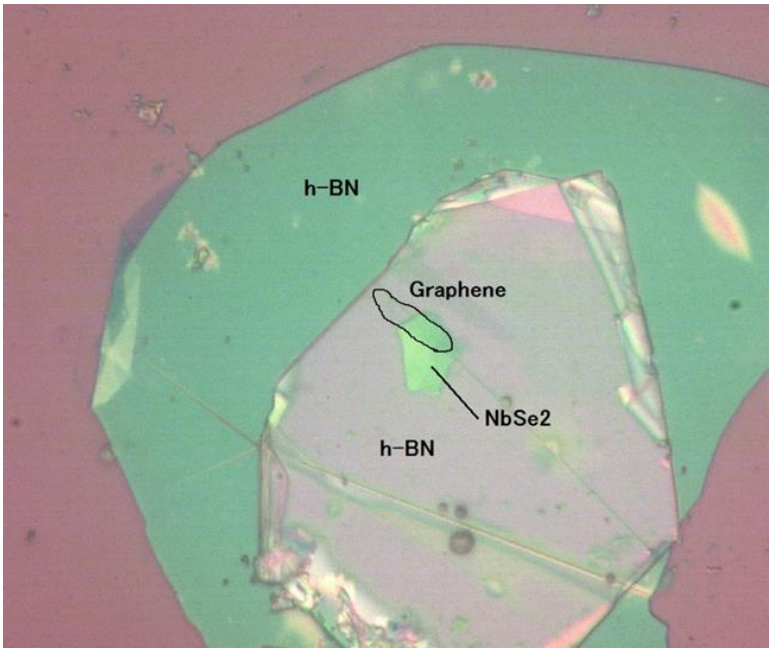


Figure: An optical microscope image of a graphene/$NbSe_2$ junction sandwiched between hBN layers.

# Control of Q-factor and nonlinearity of carbon nanotube mechanical resonator by electrostatic force

Masaaki Yasuda, Kuniharu Takei, Takayuki Arie, and Seiji Akita
*Department of Physics and Electronics, Osaka Prefecture University,*
*Sakai, Osaka 599-8531, Japan*
*e-mail: akita@pe.osakafu-u.ac.jp*

Carbon nanotube (CNT) mechanical resonators can be applied to high sensitivity force sensors because of their minute mass and high mechanical strength. Quality-factor (Q-factor) control enhances the sensitivity, and nonlinearity control expand their applications. Here, we demonstrate the control of Q-factor and nonlinearity by electrostatic force induced by electron beam irradiation inside a scanning electron microscope (SEM).

Cantilevered CNTs as resonators were supported by SU-8 layers on a Si substrate, where the CNTs were synthesized by chemical vapor deposition with post annealing treatment. SU-8 and thin native oxide layer on Si substrate are electric insulator, so that charges induced by the electron beam are accumulated on the insulator surface and cause non-uniform electrostatic field around the CNT cantilever. The electric potential on the SU-8 surface induced by the charge-up was successfully estimated to be ~ 1 kV from the comparison between the static deflection of CNT cantilever and finite element method (FEM) analysis. As a result of the pile-up charges on the insulator, the Q-factor improved about 5 times from 630 to 3200 inside SEM. In case of harmonically oscillating mechanical resonators, it was reported that the phase retarding force induced by external perturbations affects the velocity dependent damping.[1] We found that the velocity dependent damping was reduced by the retardation of the electrical charge on the CNT resonator owing to the insulator support, which results in the improvement of the "effective" Q-factor. Additionally, non-uniform electric field induced by the pile-up charge induces the nonlinearity on the resonance property, which changed from hardening to softening as the amount of charge increased. The FEM analysis revealed that the observed nonlinearity change was caused by the change of charge distribution. Thus, we have successfully demonstrated not only more than 5 times improvement of the effective Q-factor but also the control of nonlinear behavior from hardening to softening of the CNT mechanical resonator by using the pile-up electrostatic charge.

**Acknowledgements** This work was partially supported by JSPS KAKENHI Grant Number 25286010, and by the Iketani Science and Technology Foundation.

[1] C. Metzger, I. Favero, A. Ortlieb, and K. Karrai, Phys. Rev. B **78,** 035309 (2008).

# Tunnel barrier formation in multi-walled carbon nanotubes by Ar atom or Ga focused ion beam irradiation.

Tomohiro Yamaguchi[1], Hiroshi Tomizawa[1,2], Seiji Akita[3], and Koji Ishibashi[1,2,4]

[1] *Advanced Device Laboratory, RIKEN, 2-1 Hirosawa, Wako, Saitama 351-0198, Japan*
[2] *Department of Applied Physics, Tokyo University of Science, 6-3-1 Niijuku, Katsushika-ku, Tokyo 125-8585, Japan*
[3] *Department of Physics and Electronics, Osaka Prefecture University, 1-1 Gakuen-cho, Nakaku, Sakai, Osaka 599-8531, Japan*
[4] *RIKEN Center for Emergent Matter Science (CEMS), 2-1 Hirosawa, Wako, Saitama 351-0198, Japan*
*e-mail: tyamag@riken.jp*

Carbon nanotubes have attracted a great deal of attention as a material for quantum dot (QD)-based devices owing to their small diameter. The technique indispensable for fabrication of functional nanodevices based on QDs is to form the desired tunnel barriers with enough controllability and reproducibility. In contrast to single-walled carbon nanotubes, multi-walled carbon nanotubes (MWNTs) are not sensitive to defects or environments and their interface with the metal contacts is ohmic in most cases. These should make it possible to design more flexibly and to fabricate more complex QD-based devices. In this presentation, we report the fabrication and characterization of tunnel barriers formed in MWNTs by Ar atom beam [1] or Ga focused ion beam (FIB) irradiation technique.

In the former technique, Ar atom beam irradiated MWNTs through the openings in the resist layer. The resistances after irradiation increased, and varied from sample to sample even though they were irradiated at the same condition. The resistances appear to be related to the heights of the formed tunnel barrier estimated from the Arrhenius plots. In spite of large variation in the resistance, there were some samples with resistances suitable for a QD formation. We observed a honeycomb pattern in the sample with triple barriers in the charge stability diagram which suggests the formation of the double coupled QDs.

In the case of Ga FIB, the range of the resistance variation was much smaller than the former. The room-temperature resistance has a positive correlation with the barrier height and is possibly controlled by the Ga ion dose to a certain degree. In the sample with double barriers, a Coulomb diamond was observed showing formation of a single QD.

These results demonstrate the potential of our techniques towards the at-will fabrication of QD-based nanodevices.

[1] H. Tomizawa et al., J. Appl. Phys. **118**, 044306 (2015).

# Electron transport on a surface of weak topological insulators with step edges

Takashi Arita and Yositake Takane

*Department of Quantum Matter, Graduate School of Advanced Sciences of Matter, Hiroshima University, Higashi-Hiroshima 739-8530, Japan*
*e-mail: m146037@hiroshima-u.ac.jp*

Weak topological insulators (WTIs) consist of stacked atomic layers, each of which can be identified as a two-dimensional quantum spin-Hall insulator (2D-QSHI). A 2D-QSHI has an energy gap in the bulk, but possesses a one-dimensional helical edge channel as gapless low-energy excitations. Hence, only on the side surface of a WTI, low-energy states are formed by the hybridization of helical edge channels arising from stacked layers. Since the resulting surface states are described by a massless Dirac equation in the low-energy limit, the corresponding particles are called Dirac electrons. Dirac electrons in a WTI show an unusual feature that depends on whether the number of layers is even or odd. If it is even, the helical edge channels acquire a finite-size gap owing to the hybridization. Contrastingly, in the odd case, there arises one hybridized helical channel with gapless linear energy dispersion.

Focusing on the odd case, we consider the side surface with step edges that significantly modify the excitation spectrum of Dirac electrons [1]. Regardless of step edges, one helical channel with gapless linear dispersion persists and plays the role of a perfectly conducting channel without backward scattering. We show that, by manipulating step edges on the side surface in a certain manner, pseudo helical channels with a nearly gapless linear dispersion can be created in addition to the helical channel existing from the outset. One expects that such pseudo helical channels enhance the electronic conductivity of the system. To examine this, we numerically calculate the average conductivity in the presence of disorder by using a simple model for Dirac electrons [1]. It is shown that the average conductivity significantly increases owing to the contribution from pseudo helical channels.

[1] T. Arita and Y. Takane, J. Phys. Soc. Jpn. **83**, 124716 (2014).

# Doping Effect of Dielectric Encapsulation Layer in $WSe_2$ Field Effect Transistors

Seung-Pil Ko[1], Jiung Cho[2], Jong Mok Shin[1], Ho Kyun Jang, Min Youl You, Jun-Eon Jin and Gyu-Tae Kim[1]

[1] *School of Electrical Engineering, Korea University, Seoul 136-713, South Korea*
[2] *Advanced Material Research Center, Korea Basic Science Institute, Gangneung 210-702, South Korea*
*e-mail: gtkim@korea.ac.kr*

As the scaling of the logic transistor is accelerated, the research for new channel materials is being continued. For low power consumption in the logic devices, we need to improve the gate controllability and lower the off leakage current. In that perspective, it is possible for two dimensional materials such as $WSe_2$ and $MoS_2$ to scale down to a monolayer which corresponds to 0.7 nm. This property can enable the extreme electrostatic gate control. They also show large bandgap energies compared to Si and Ge devices leading to a high on-off ratio [1]. However, the doping techniques to control Fermi energy in two dimensional materials are critical issues. Recently there have been several chemical doping results [2]. But those methods are not stable and electrical properties can be changed with semiconductor process like rinsing [3]. In this work, we present the stable n-doping and p-doping effects via dielectric encapsulation layer. Due to the fixed charges in the dielectric layer, device parameters such as threshold voltage and on-current are changed. To make $WSe_2$ field effect transistors, the $WSe_2$ channel layer was mechanically exfoliated onto $SiO_2$/Si substrate. We defined the source and drain by e-beam lithography and metallization process. Dielectric encapsulation layer is deposited by atomic layer deposition (ALD) method. The $WSe_2$ FETs show the p-type characteristics. $Al_2O_3$ encapsulation layer plays a role as electron charge transfer via field effect. So threshold voltage is negatively shifted and on-current is slightly decreased. On the contrary, the $WSe_2$ FETs with $HfO_2$ encapsulation layer show p-type doping effect so that threshold voltage is positively shifted. Using fixed charges in the dielectric layers, we can adjust threshold voltage of $WSe_2$ FETs.

[1] W. Liu et al., Nano Lett., 13, 1983-1990 (2013).
[2] H. Fang et al., Nano Lett., 12, 3788-2792 (2012).

# Analysis of Ultra-High-Speed Image Sensor with Monte Carlo Simulation

Natsumi Minamitani[1], Vu Truon Son Dao[2], Kazuhiro Shimonomura[2],
Takeharu Goji Etoh[2], Yoshinari Kamakura[1], and Nobuya Mori[1]

[1] *Osaka University, 2–1 Yamada-oka, Suita, Osaka 565–0871, Japan*
[2] *Ritsumeikan University, 1–1–1 Nojihigashi, Kusatsu, Shiga 525-8577, Japan*
*e-mail: minamit@si.eei.eng.osaka-u.ac.jp*

Application of high-speed video cameras is expanding to various fields of sciences and engineering, and further increase of the frame rate is still demanded. In 2011, the speed of 16.5 M frames per second (fps) was achieved with the backside-illuminated (BSI) CCD [1], and we are now trying to achieve 10 Gfps using the BSI multi-collection-gate (MCG) technique [2] (Fig. 1). In this study, we computationally investigate the fundamental properties of electron transport to understand and design the ultimate limit of the frame rate in BSI MCG image sensor, one of which is considered to be determined by the transit time dispersion of photoelectrons [2].

We assumed a simple simulation system as shown in Fig. 2, and the electron stochastic motion inside the structure was computed using the Monte Carlo (MC) simulator [3], whose accuracy has been validated through the comparison with the various experimental data of Si, e.g., as shown in Fig. 3. Fig. 4 shows the MC simulation results of the distribution of the electron transit time. The standard deviation $\sigma$ extracted from the distribution is plotted in Fig. 5 (a), suggesting that $\sigma$ can be reduced with decreasing *W* and/or increasing *E*, although for both parameters there exist limitations imposed by other device design considerations [2]. In Fig. 5 (b), $\sigma$ and *W* are normalized to the quantities characterizing the system, i.e., the mean transit time $\tau$ ($\equiv W/v_d$) and the diffusion length $L_n$ ($\equiv \sqrt{D_{||}\tau}$), respectively. It was found that the simulated data lie on the common curve, indicating the relationship $(\sigma/\tau) \sim (W/L_n)^{-1}$, and thus $\sigma \sim (D_{||}^{1/2} v_d^{-3/2}) \times \sqrt{W}$. The prefactor $D_{||}^{1/2} v_d^{-3/2}$ determines the electric field dependence of $\sigma$; note that Fig. 6 suggests almost no benefit is expected in terms of $\sigma$ reduction by increasing *E* larger than >> ~10 kV/cm, which originates from the hot carrier effect.

[1] T. G. Etoh et al., "A 16 Mfps 165 kpixelbackside-illuminated CCD," *ISSCC2011*, p.406.
[2] T. G. Etoh et al., "Toward 1Gfps: Evolution of Ultra-high-speed Image Sensors -ISIS, BSI, Multi-Collection Gates, and 3D-stacking-," *IEDM2014*, p.255.
[3] T. Kunikiyo et al., "A Monte Carlo simulation of anisotropic electron transport in silicon including full band structure and anisotropic impact ionization model," *J. Appl. Phys.* **75**, 297 (1994).

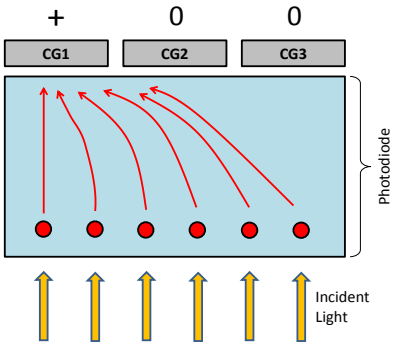


**Fig. 1:** Schematic view explaining the basic concept of BSI MCG image sensor. The photoelectrons are collected under the collection gate (CG) to which positive voltage is applied. If the selected CG is switched rapidly, then the electrons generated at different time frames are collected by the different CGs. To make this mechanism work well, the variation of the electron transit time must be much smaller than the switching time.

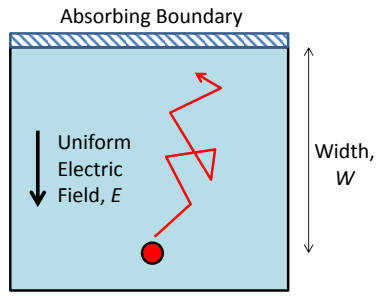


**Fig. 2:** Schematic view of the system simulated in this study. A simple one dimensional structure was assumed, and the absorbing boundary condition was imposed at the top surface. Initially, $10^3$ electrons were put at the depth of $W$, and their stochastic motions under the uniform electric field $E$ were simulated until all the electrons were absorbed at the top boundary. Then, the distribution of the electron transit times was recorded.

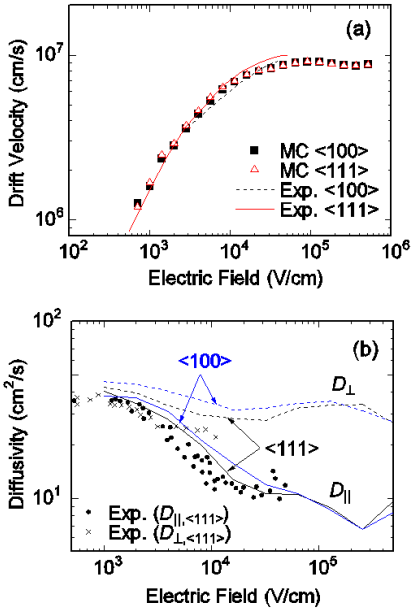


**Fig. 3:** Comparison of the MC simulation results with the experimental data for (a) the drift velocity $v_d$ and (b) the diffusivity $D$ in bulk Si plotted as a function of the electric field $E$. The electric field was applied along <100> and <111> directions. In (b), the transverse ($D_{||}$) and the longitudinal ($D_{\perp}$) components (along the field direction) are plotted.

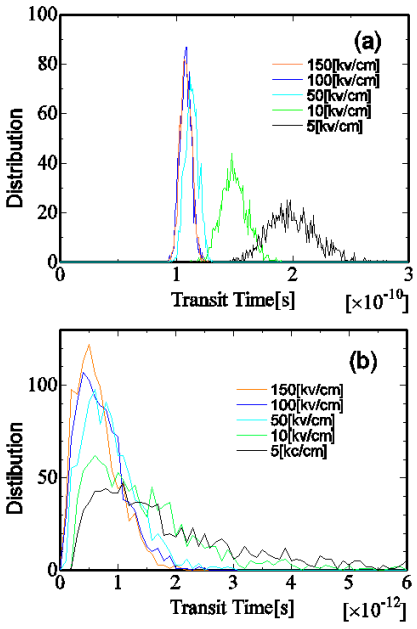


**Fig. 4:** Distribution of electron transit time for the traveling distance $W$ of (a) 10 μm and (b) 0.1 μm simulated with various electric fields $E$ ranging from 5 to 150 kV/cm.

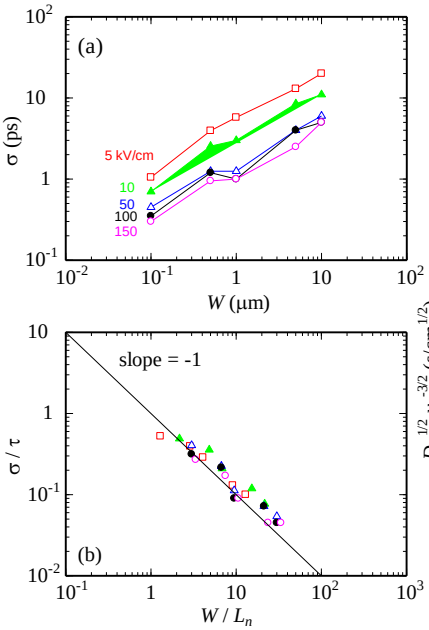


**Fig. 5:** Standard deviation $\sigma$ of the electron transit time plotted as a function of $W$ (a). In (b), $\sigma$ and $W$ are normalized by the mean transit time ($\tau \equiv W/v_d$) and the diffusion length ($L_n \equiv \sqrt{D_{||}\tau}$). All data lie on the same line.

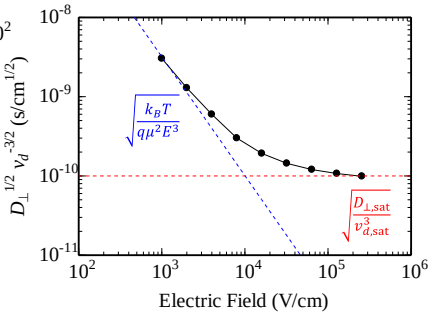


**Fig. 6:** The prefactor which determines the electric field dependence of the standard deviation of the transit time, i.e., $\sigma \sim (D_{||}^{1/2} v_d^{-3/2}) \times \sqrt{W}$. The dashed lines represent the asymptotic characteristics in the limits of low (blue) and high (red) electric fields. The values for $D_{||}(E)$ and $v_d(E)$ are taken from the simulation data shown in Fig. 3.

# Theoretical calculation of impact ionization rate for 4H-SiC in the *GW* approximation

K. Konaga[1)], T. Kotani[2)], R. Fujita[1)], Y. Kamakura[1)], N. Mori[1)]
[1)] Division of Electrical, Electronic and Information Engineering, Osaka University, Suita, Osaka 565-0871, Japan
[2)] Department of Applied Mathematics and Physics, Tottori University, Tottori 680-8552, Japan
E-mail: konaga@si.eei.eng.osaka-u.ac.jp

Impact ionization is one of the most important factors limiting the performance of power devices. However, there are still many unclear points about the properties and mechanism of impact ionization in SiC. In this study, we present the theoretical investigation of impact ionization rate in bulk 4H-SiC based on the state-of-the-art *ab initio* calculations.

Band structure of bulk 4H-SiC was computed with quasiparticle selfconsistent *GW* (QSGW) method using the `ecalj` code [1] as shown in Fig.1. In the band calculation, a small correction was added to precisely reproduce the experimental gap energy of $E_g$ = 3.26 eV. Then, the impact ionization rate was calculated also with the `ecalj` code from the quasiparticle width in the *GW* approximation [2]. In Fig. 2 the calculated impact ionization rate is plotted as a function of the energy for the primary electrons ($E > E_c$) and the primary holes ($E < E_v$). It is found that, compared at the same carrier energy, i.e., $E_e = E - E_g$ for electrons and $E_h = -E$ for holes, the ionization rate initiated by holes is larger than that for electrons. Note that this is consistent with the experimental observation for the ionization coefficients of electrons and holes in 4H-SiC [3,4]. However, the experimental data also suggested that there exists a strong anisotropy in the ionization coefficients especially for electrons depending on the crystal orientation [3], while the ionization rate calculated in this study exhibits only weak anisotropy, i.e., it is almost determined by $E$, but not strongly dependent on the wave vector direction.

To understand the characteristics of the ionization coefficients, the information about not only the ionization rate, but also the carrier energy distribution at a given electric field is necessary. Fig. 3 plots the iso-energy surfaces for the conduction bands of 4H-SiC inside the first Brillouin zone, indicating the strong anistropic nature between $\langle 0001 \rangle$ and $\langle 11\bar{2}0 \rangle$ directions. The conduction minima locate at the M-point. If the equiribrium low-energy electrons are accerelated by an electric field along the $\langle 0001 \rangle$ direction, they could hardly reach up to the ionization threshold energy $E_{\mathrm{th}}$ (= $2E_g$ for electrons) due to the energy gap between the lowest two and the higher conduction bands (Fig. 4a) [5]. Actually, the electron-phonon scattering spreads the hot electron distribution in $k$-space away from the M-L line, and thus they can be heated up to > $E_{\mathrm{th}}$. But it is considered that the hot electrons are not easily generated compared to the case of the field accerelation along $\langle 11\bar{2}0 \rangle$; looking at the conduction band structure along the M-Γ direction, there exists paths to gain the kinetic energy (see, Fig. 1). As shown in Fig. 4b, this is also the case for the holes. These properties are qualitatively consistent with the experimental observations, but for quantitative analysis the introduction of more rigorous simulation method, such as the full-band Monte Carlo simulation [6], is neccesary.

In summary, we have calculated the impact ionization rate of electrons and holes in 4H-SiC using the `ecalj` code based on QSGW method. The calculated results have suggested that (1) the ionization rate initiated by holes is larger than that for electrons, and (2) the ionization rate exhibits only weak anisotropy. The strong anisotropy observed in the measured ionization coefficients is considered to originate from the characteristics of the hot carrier generation depending on the field direction.

[1] T. Kotani, J. Phys. Soc. Jpn. 83, 094711 (2014); https://github.com/tkotani/ecalj/
[2] T. Kotani and M. van Schilfgaaede, Phys. Rev. B 81, 125201 (2010).
[3] H. Niwa, J. Suda, and T. Kimoto, Materials Science Forum 778-780, 461 (2014).
[4] T. Hatakeyama, Phys. Status Solidi A 206, 2284 (2009).
[5] S.Nakamura, H.Kumagai, T.Kimoto, H.Matsunami, Appl. Phys. Lett. 80, 3355 (2002).
[6] T. Hatakeyama, T. Watanabe, T. Shinohe, K. Kojima, K. Arai, and N. Sano, Appl. Phys. Lett. 85, 1380 (2004).

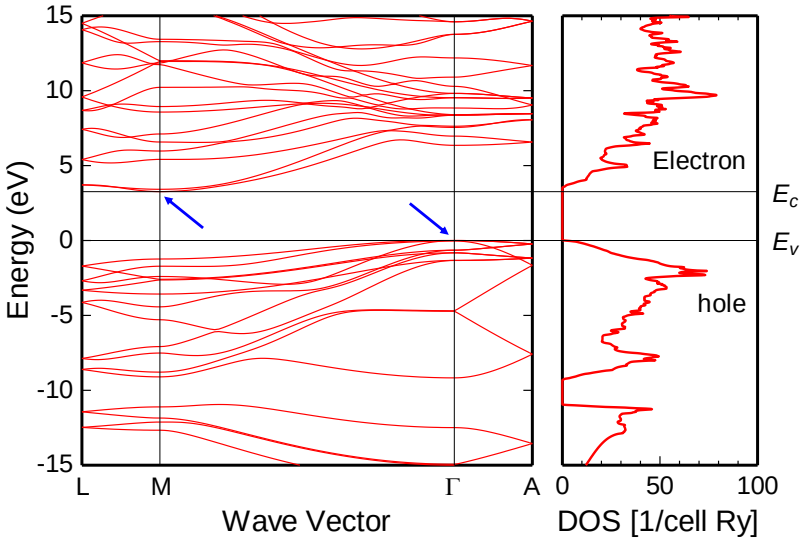


Fig. 1 Band structure and density of states (DOS) of 4H-SiC calculated by QSGW method. The bottom of the conduction band and the top of the valance band are located at M- and G-points, respectively, as indicated by arrows.

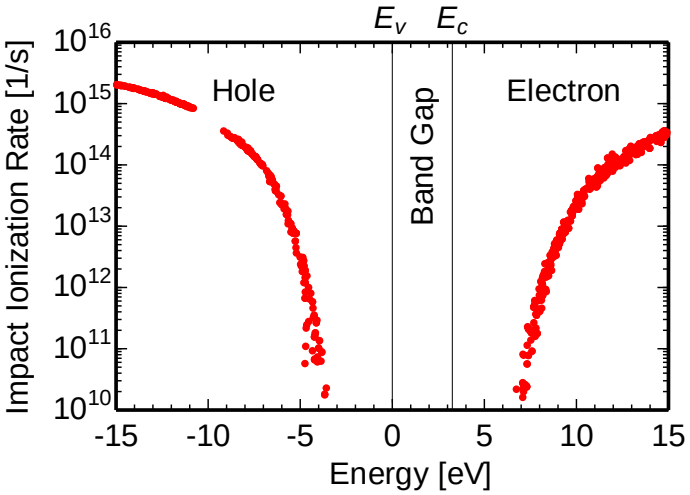


Fig. 2 Calculated impact ionization rate plotted as a function of energy measured from the top of the valence band. The dots represent the results calculated at various *k*-points inside the Brillouin zone.

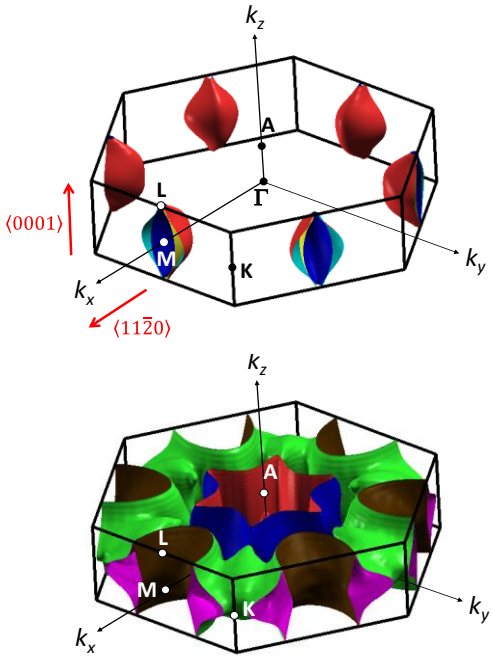


Fig. 3 Iso-energy surfaces for the conduction bands of 4H-SiC inside the first Brillouin zone at (top) $E$ = 3.71 eV and (bottom) $E$ = 6.52 eV (= $2E_g$; impact ionization threshold energy $E_{th}$).

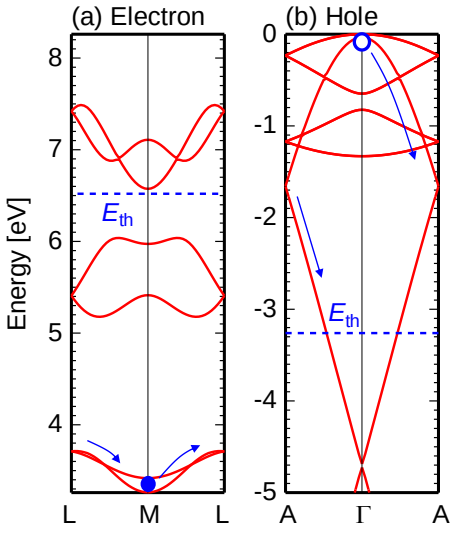


Fig. 4 Zoom-up view of the band diagram along ⟨0001⟩ direction around (a) the bottom of the conduction band and (b) the top of the valence band. The impact ionization threshold energies $E_{th}$ for electrons and holes are indicated by the bule dashed lines. If the equiribrium electrons at M-point are accerelated by an electric field along ⟨0001⟩, they cannot reach up to $E_{th}$; while the holes at Γ-point have a path to do it. Although the electron-phonon scattering spreads the hot electron distribution in *k*-space away from the M-L line (and thus they can actually be heated to > $E_{th}$), it is considered that the hot electrons are not easily generated compared to the holes.

# Comparison of Slab and Block Decomposition Strategies for the Two-Dimensional Wigner Monte Carlo Method

Josef Weinbub, Paul Ellinghaus, Mihail Nedjalkov, and Siegfried Selberherr
*Institute for Microelectronics, TU Wien, Gußhausstraße 27-29/E360, 1040 Vienna, Austria*
*e-mail: weinbub@iue.tuwien.ac.at*

Both stochastic and deterministic methods have been applied to solve the one-dimensional Wigner equation. However, only the Wigner Monte Carlo method, using the signed-particle technique [1], has made multi-dimensional Wigner simulations viable thus far [2]; a multi-dimensional approach is essential for the simulation of realistic semiconductor devices. The primary challenge lies in the fact that the essential *annihilation* algorithm requires the entire phase space to be represented by an array whose size is proportional to the dimensionality and resolution of the phase space – this quickly results in exorbitant memory requirements which easily exceed the limited memory of a single workstation [3]. A spatial domain decomposition approach has been introduced for the one-dimensional Wigner Monte Carlo method [3] and successfully extended to two-dimensional simulations [4]. The implementations use a message passing interface (MPI) technique and are based on the Wigner Ensemble Monte Carlo simulator which is part of the free open source ViennaWD simulation package [5].
Two domain decomposition techniques – a uniform slab and a uniform block decomposition – for two-dimensional problems are compared. The performance of the two approaches is evaluated by simulating a representative physical problem. Figure 1 shows the evolution of three wave packets over 300fs within a 128nm x 128nm simulation, providing 16 dopants acting as potential barriers. Our results (Figure 2) for 16, 32, 64, and 128 MPI processes show that the slab decomposition method is superior to the block decomposition approach. This result is especially interesting, as it shows that the much simpler to implement slab decomposition method is an excellent method for parallelizing highly memory intensive two-dimensional Wigner Monte Carlo quantum simulations based on the signed-particle method.
The computational results have been achieved using the Vienna Scientific Cluster (VSC).

[1] M. Nedjalkov et al., Phys. Rev. B, **70**(11), DOI:10.1103/PhysRevB.70.115319 (2004).
[2] J. Sellier et al., Comput. Phys. Commun., **185**(10), DOI:10.1016/j.cpc.2014.05.013 (2014).
[3] P. Ellinghaus et al., J. Comput. Electron., **14**(1), DOI:10.1007/s10825-014-0635-3 (2015).
[4] J. Weinbub et al., J. Comput. Electron., DOI:10.1007/s10825-015-0730-0 (2015).
[5] ViennaWD, http://viennawd.sourceforge.net/.

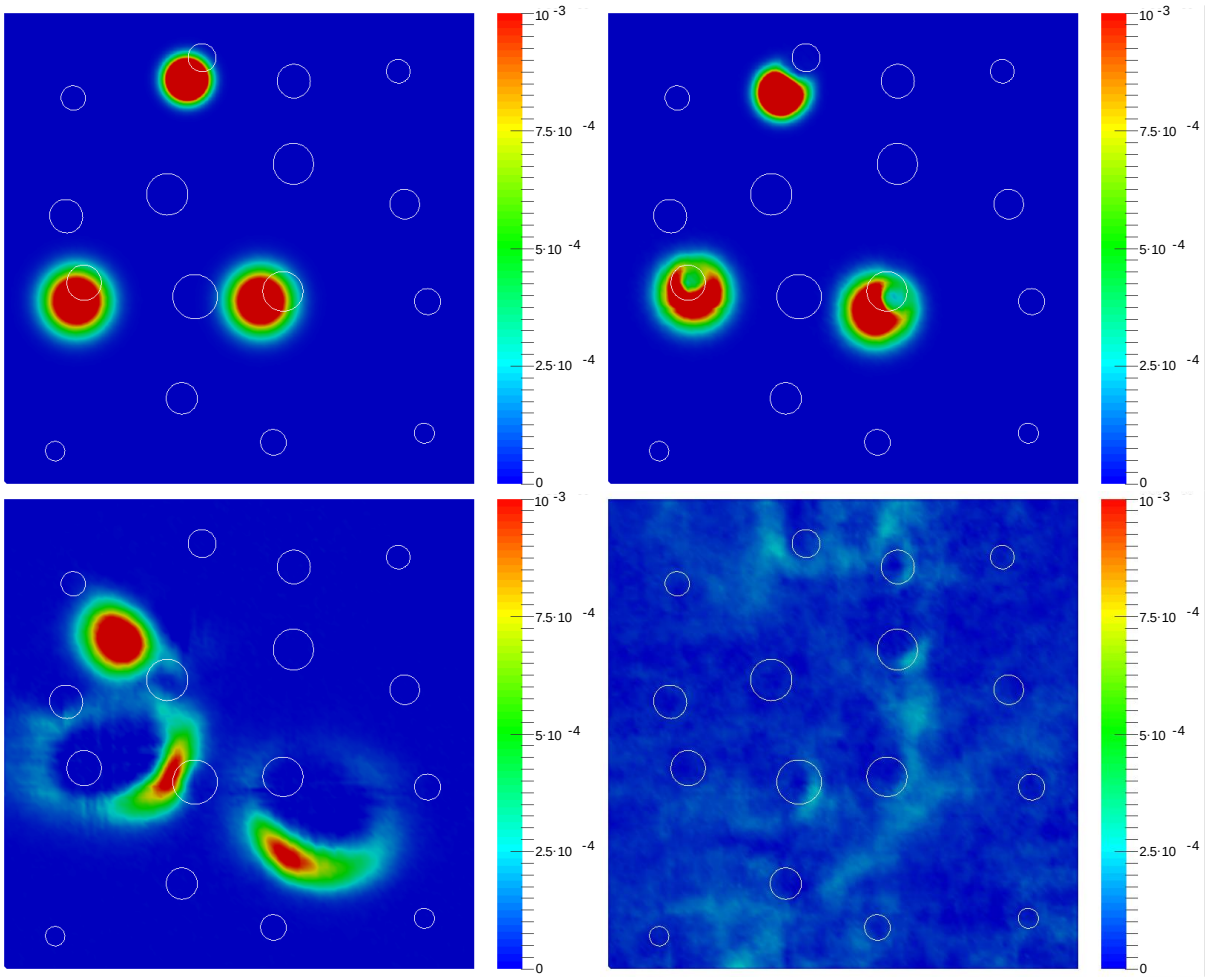


*Figure 1: Normalized density (i.e. probability) at 0 fs, 10 fs, 50 fs, and 300 fs (top left, top right, bottom left, bottom right). White cricles denote locations of dopants.*

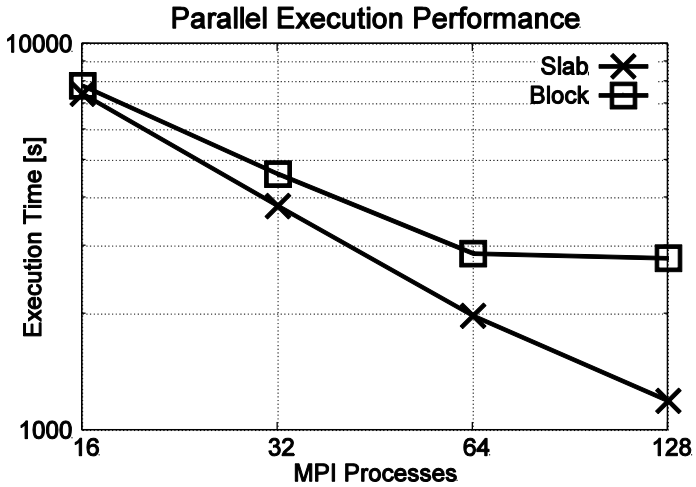


*Figure 2: Comparison of the execution times between the slab and the block decomposition approaches.*

# Convergence of stationary Wigner equation with inflow boundary conditions

Anton Arnold[1], Ruo Li[2], Tiao Lu[2], and Zhangpeng Sun[2]

[1] *Institute for Analysis and Scientific Computing, Vienna Technology University, Vienna,*
[2] *CAPT, HEDPS, LMAM, IFSA Collaborative Innovation Center of MoE, School of Mathematical Sciences, Peking University, Beijing, China*
*e-mail: tlu@math.pku.edu.cn*

We propose in this paper a well-posed semi-discretization of the stationary Wigner equation with inflow BCs, making use of the Whittaker-Shannon interpolation formula with shifted sampling points. The convergence of the solutions of the discrete problem to the continuous problem is then analyzed, providing certain regularity of the solution of the continuous problem.

# Uncertainty and quantum correlation in Wigner transport equations

Kyoung-Youm Kim[1] and Saehwa Kim[2]

[1]*Department of Electrical Engineering, Sejong University, Seoul 05006, Korea*
[2]*Department of Information and Communications Engineering, Hankuk University of Foreign Studies, Gyeonggi-Do 17035, Korea*
*e-mail: kykim@sejong.ac.kr*

Here, we discuss two fundamental characteristics of the discrete Wigner transport equation [1,2] resulting from the uncertainty principle. First, the discretized momentum space results in a kind of positional uncertainty of electrons [1]. We show that this uncertainty determines the maximum length of nonlocal potential correlation. As a result, the finer the momentum resolution of the discrete Wigner function is, the longer the region for nonlocal potential correlation becomes. Next, electrons can have positional uncertainty inside the device [3]. We prove that this uncertainty sets a minimum momentum resolution of the discrete Wigner function to be $h/(2L)$, where $h$ and $L$ denote the Planck constant and the length of the device, respectively. Therefore, the smaller the device is, the larger the minimum momentum resolution should be. We show numerically that its violation deteriorates the simulation results significantly.

[1] K.-Y. Kim, J. Appl. Phys., **102**, 113705 (2007).
[2] K.-Y. Kim, Jpn. J. Appl. Phys., **47**, 358–360 (2008).
[3] K.-Y. Kim and S. Kim, Solid-State Electron., **111**, 22–26 (2015).

# Phase-Space Functions and Entanglement: A Role for Wigner Functions

**D. K. Ferry**

*School of Electrical, Computer, and Energy Engineering*
*Arizona State University, Tempe, AZ 85287-5706* ferry@asu.edu

The Wigner function has been studied for more than eight decades, in the quest to develop a phase-space formulation of quantum mechanics. But, it is not the only phase-space formulation. What is little appreaciated is that they can give new insights into many quantum properties such as entanglement, which is not normally observable. That is, when two distinct wave functions are combined as one, such as occurs in an entangled state, the Wigner function shows distinct behavior which indicates the entanglement, a result that is not seen in other approaches such as the wave function itself or the density matrix. Hence, this leads us to an important conclusion, these phase-space representations contain information about the quantum nature that does not have a counterpart in the classical phase space function. As a result, the Wigner function has become useful in quantum information theory, an application which will be highlighted in this talk.

# Wigner representation of electron dynamics in presence of thermal dephasing in disordered systems

Bartlomiej Spisak[1] and Maciej Woloszyn[1]

[1] *AGH University of Science and Technology, Faculty of Physics and Applied Computer Science, Al. A. Mickiewicza 30, 30-059 Krakow, Poland*

*e-mail: bjs@agh.edu.pl*

Electron transport phenomena in disordered systems demonstrate the non-Markovian properties due the quantum interference of the conduction electrons in the absence of mechanisms which destroy the time-reversal invariance. One of the possible manifestations of the quantum interference in the disordered systems is the weak localization of the carriers. The effect stems from the coherent propagation of the electrons which are multiply scattered on the spatially distributed ions.

In the present contribution, an influence of an effective thermal field due to the dynamics of ions on the weak localization is considered in terms of the generalized kinetic equation in the Wigner representation. Within this approach, the weak localization manifests itself by the singularity for the multiple backward scattering of the carriers, and we show that this singularity is removed by the considered dephasing mechanism.

[1] G. J. Morgan, M. A. Howson, and K. Saub J. Phys. F **15**, 2157 (1985).

[2] B. J. Spisak Transport properties and localisation of one-electron states in systems with disturbed translational symmetry, Libron Press, Kraków 2013 - in Polish.

# Toward atom scale ultra low power electronic circuitry

Robert Wolkow

*Department of Physics, University of Alberta*
*and National Institute for Nanotechnology, Edmonton, Alberta Canada*

Decades of academic study of silicon with scanned probe and related techniques have made it possible to now envisage a silicon-based, atom-scale, ultra-low power circuitry that merges with and enhances CMOS electronics technology.

A key step was made in 2008 when single silicon dangling bonds on an otherwise H-terminated surface were shown to behave as ultimate small quantum dots[1]. Because all such dots are identical, and spacing between dots can be identical, and dots can be placed very closely to achieve strong interaction, and because many, many dots can be printed easily there appears to be prospects for interesting circuitry. The same dots can be deployed to make "passive" elements like wires and to make active elements of diverse kinds including quantum cellular automata with the prospect of room temperature operation, and single electron transistors (SETs) of extremely narrow device to device variation.

Among most recently published work I will describe are single-electron, single-atom transport dynamics[2] and the use of multi-probe STM to show surface conduction among collectives of DBs[3]. Just published STM spectral studies of silicon atoms will be shown and the remarkable roles of controlled single atom charge state change and of near surface dopants will be identified[4].

The preparation and characteristics of a robust, readily repairable, single atom tip and its varied applications to imaging and fabrication will be described also.

[1] M. Baseer Haider, Jason L. Pitters, Gino A. DiLabio, Lucian Livadaru, Josh Y. Mutus, and Robert A. Wolkow, Phys.Rev.Lett., **102**, 046805 (2009), and patent issued recently.

[2] Marco Taucer, Lucian Livadaru, Paul G. Piva, Roshan Achal, Hatem Labidi, Jason L. Pitters, and Robert A. Wolkow, Phys. Rev. Lett., **112**, 256801 (2014)

[3] Bruno V. C. Martins, Manuel Smeu, Lucian Livadaru, Hong Guo, and Robert A. Wolkow, Phys. Rev. Lett., **112**, 246802 (2014)

[4] H. Labidi, M.Taucer, M.Rashidi, M.Koleini, L.Livadaru, J.Pitters, M.Cloutier, M.Salomons and Robert A Wolkow, New J. Phys., 17, 073023 (2015)

# Nanowire Transistor Performance at the Scaling Limit
# Comprehensive DD, EMC and NEGF simulation study

A. Asenov[1, 2],Y. Wang[1,3], A. Talib[1], X. Wang[1], V. Georgiev[1], E. Towie[2], S. M. Amoroso[2], A. R. Brown[2], B. Cheng [2], D. Reid[2], C. Riddet[2], X. Liu[3], J. Kang[3]

[1] Device Modeling Group, School of Engineering, University of Glasgow, Glasgow, G12 8LT, UK

[2] Gold Standard Simulations Ltd., 11 Somerset Place, Glasgow, G3 7JT, UK

[3] Institute of Microelectronics, Peking University, Beijing 100871, China

asen.asenov@glasgow.ac.uk

Problems with the oxide thickness and doping-controlled electrostatic integrity of conventional 'bulk' CMOS transistors have prompted interest in thin-body and 3D transistor architectures, which have improved electrostatic control resulting in steeper sub-threshold slope (SS), reduced drain-induced barrier lowering (DIBL), and therefore reduced channel leakage compared to bulk transistors. Tolerance to low channel doping additionally boosts mobility and performance and reduces local (statistical) variability. This research and corresponding technology development has culminated in the introduction of 28nm fully depleted silicon-on-insulator (FDSOI) CMOS by ST Microelectronics and 22nm and 14nm FinFET CMOS by Intel [18] and Samsung. It has been speculated that the scalability of FDSOI can extend planar CMOS technology down to 10nm and FinFETs can extend CMOS technology down to 7 nm. Even better electrostatic integrity, offered by gate-all-around nanowire transistor (NWT) architectures may be needed to extend CMOS scaling beyond the 7 nm mark.

In this paper we have studied the performance of silicon nanowire transistors (NWT) for application in advanced CMOS technologies. The 3D simulations were carried with the drift-diffusion and ensemble Monte Carlo modules of the GSS 'atomistic' simulator GARAND in which accurate quantum mechanical corrections were introduced, based on the solution of the Schrödinger equation in 2D cross-sections along the direction of the transport. Results based on the density gradient approach that has been calibrated with respect to the Poisson-Schrödinger corrections are also presented. The simulated NWTs have cross-sections and dimensional characteristics representative of the transistors expected at 7nm CMOS technology. Different gate lengths, cross-section shapes, spacer thicknesses and doping steepness were considered. We have also estimated the optimal gate length for different NWT design conditions.

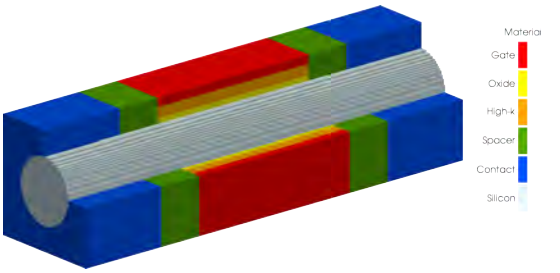


| $T_{interfacial\ layer}$, $T_{high\text{-}k}$ (nm) | 0.6, 1.2 |
|---|---|
| Gate length (nm) | 10-24 |
| Spacer thickness (nm) | 3.0, 5.0 |
| S/D peak doping ($cm^{-3}$) | $2\times10^{20}$ |
| Doping roll-off (nm/dec) | 1.0, 1.5, 2.0 |
| Channel doping ($cm^{-3}$) | $10^{14}$ |
| Substrate orientation | (001) |
| Nanowire orientation | <110> |

Fig. 1 Naznowire transistor (NWT) schematics and design parameters

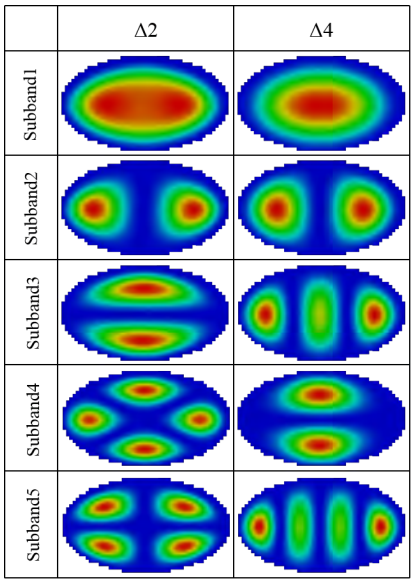


Fig 2 Wave functions in the two-fold and four-fold degenerate valley in the cross-section of an elliptical Si NWT

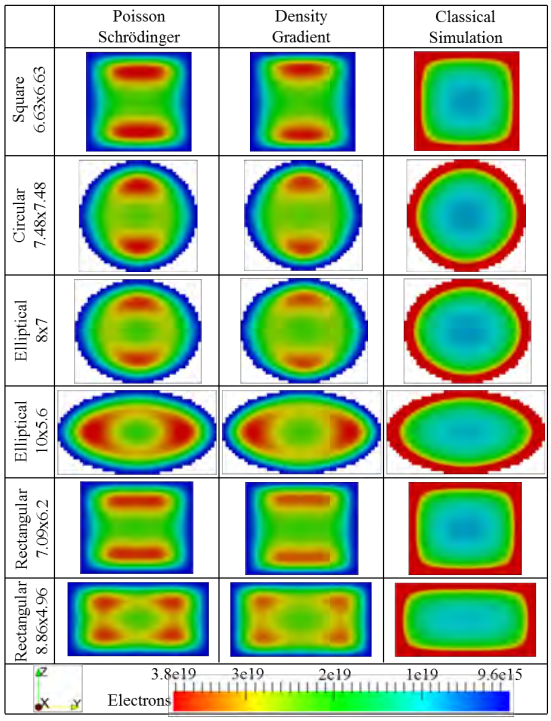


Fig. 3 Different NWT cross-sections simulated in this paper. Comparison of the charge distribution in the nanowire cross-section obtained from Poisson-Schrödinger, density gradient the classical DD simulations at Vg=0.65V

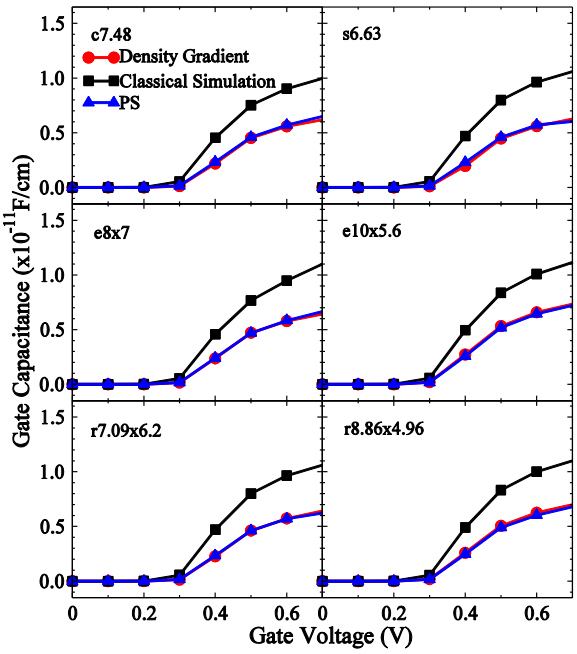


Fig. 4 Capacitance-voltage (C-V) characteristics of the simulated NWT with different cross-sections.

# Multi-Scale Modeling of Self-Heating Effects in Silicon Nanoscale Devices

A. R. Shaik[1], S. S. Qazi[1], R. L. Daugherty[1], A. Laturia[1], E. Bury[2], B. Kaczer[2], K. Raleva[3] and D. Vasileska[1]

[1]*School of Electrical Computer and Energy Engineering, Arizona State University, Tempe, AZ, USA*

[2]*IMEC, Belgium*

[3]*Faculty of Engineering and Information Technology, University Sts. Cyril and Methodius, Skopje, Republic of Macedonia*

*e-mail: vasileska@asu.edu*

In this paper we present a novel multi-scale simulation approach that combines circuit level simulations performed with SILVACO Atlas with an electro-thermal Monte Carlo device simulation to uncover the temperature of the hot-spot in the device under test. The GIGA3D SILVACO Atlas module simulates the thermal transport characteristics at the interconnect level, providing temperature boundary conditions for the device-level simulation. The device-level simulator then solves for self-heating throughout the device.

The simulation results are compared with device level temperature measurements based on the temperature dependence of the sub-threshold slope of a planar MOSFET; the variations in the sub-threshold slope can be used to determine the temperature in the hot-spot. Two devices are operated in either common source or common drain configuration. One device functions as a *heater*, the device under test (DUT), while the other device functions as a *sensor*. The sub-threshold slope of the sensor varies in direct relation to the temperature in the heater device. From the extracted subthreshold slopes, using the EKV method, the corresponding average sensor temperatures are determined for different bias conditions ($V_{DS}$ and $V_{GS}$). The goal of the multi-scale simulations is two-fold: (1) to reproduce the sensor temperature variation for a given structure and bias conditions and (2) once matching in the sensor temperature is achieved, to extrapolate the peak heater temperature. By comparing the simulation results with the experimental results for the sensor temperature, we are able to determine the temperature of the hot-spot in the heater.

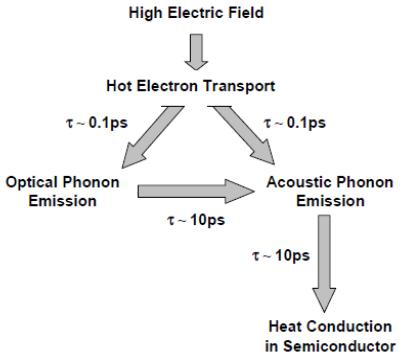


Fig. 1. This diagram shows the basic mechanism by which energy is exchanged from high energy electrons and the phonon bath.

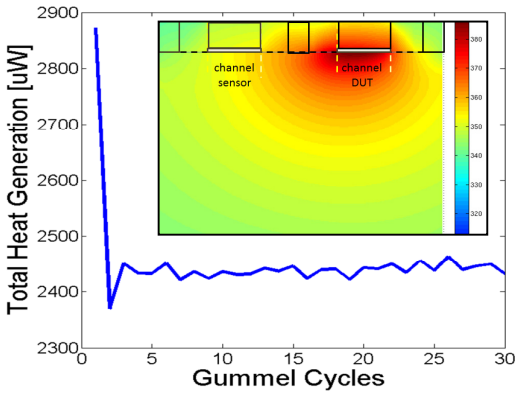


Fig. 2. Convergence of the global Gummel loop. Inset shows converged lattice temperature profile.

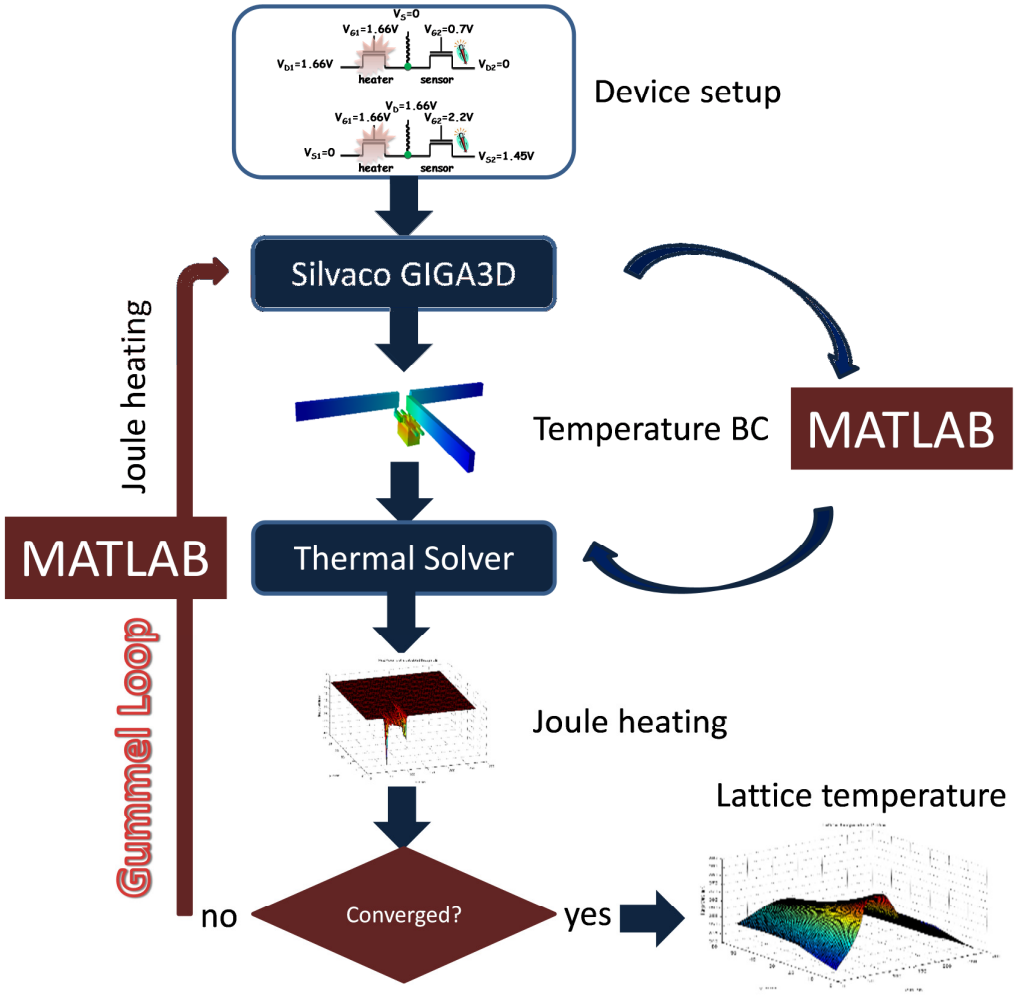


Fig. 3. Multiscale model implemented in this work.

# Coupled Electrical and Thermal Transport in Hybrid Graphene-Silver Nanowire Transparent Conducting Electrodes

David B. Janes[1,3], Suprem R. Das[2,3], Ruiyi Chen[1,4], Sajia Sadeque[1,3], Kerry Maize[1,3], Yuki Mori[5], Doosan Back[1,3], Ali Shakouri[1,3], and Muhammad A. Alam[1,3]

1. *School of Electrical and Computer Engineering, Purdue University, West Lafayette, IN 47907*
2. *Department of Physics, Purdue University, West Lafatette, IN 47907*
3. *Birck Nanotechnology Center, Purdue University, West Lafayette, IN 47907*
4. *Department of Information Science and Electronic Engineering, Zhejiang University, Hangzhou, 310027, China*
5. *Osaka University, Osaka, Japan.*

*Email: janes@ecn.purdue.edu*

Nanostructured conductors being considered as potential replacements for transparent conducting oxides include large-area graphene (grown by chemical vapor deposition) and random networks of metallic nanowires. The performance of these materials is limited by high-resistance grain boundaries and wire-wire junction resistances, respectively. Hybrid networks consisting of a network of metallic nanowires coupled with a single layer of graphene have been proposed [1] and demonstrated experimentally [2, 3], including sheet resistances below 20 ohms per square at 90% transparency[3]. The basic model of conduction [1] consists of co-percolation between the two conductive layers (nanowire network and graphene), with each layer bridging the conductive gaps in the other layer. In this presentation, we describe current-voltage characteristics and transient thermoreflectance (TR) imaging of nanowires and hybrid networks. Transient TR imaging provides information on the time-dependence of self-heating and cooling, with various magnifications providing resolutions ranging from individual hot-spots (e.g. nanowire junctions) to macroscopic regions. A thermal conductance model considering both vertical (substrate) and lateral (heat spreading through network) elements can be used to understand thermal transport in the device. Since self-heating occurs at resistive links in conductive pathways, the ability to resolve local heating versus diffusion effects allows a more detailed understanding of the distribution of conductive paths and resistance bottlenecks in the distributed conductors. Extensions to other materials systems will also be discussed.

[1] C. Jeong, et al, *Nano Lett.* **11**, 5020 (2011)

[2] I.N. Kholmanov, et al., *Nano Lett.* **12,** 5679 (2012)

[3] R. Chen, et al., *Advanced Functional Materials* **23**, 5150 (2013).

# Band gap due to inter-wall interaction in flattened carbon nanotubes

Takeshi Nakanishi[1] and Tsuneya Ando[2]

[1] *Nanomaterials Research Institute, AIST*
*1-1-1 Umezono, Tsukuba 305-8568, Japan*
[2] *Department of Physics, Tokyo Institute of Technology*
*2-12-1 Ookayama, Meguro-ku, Tokyo 152-8551, Japan*

Flattened carbon nanotubes are new kinds of quantum wires topologically different from the conventional wires fabricated at semiconductor heterostructures. The flattened carbon nanotubes are distinguished from single wall carbon nanotubes by inter-layer couplings in a collapsed region. The purpose of this study is to show electronic states of the flattened carbon nanotubes[1].

The flattened carbon nanotubes consist of fully collapsed region with layer spacing of 3.3$\mathring{A}$ and curved regions. The fully collapsed region is a bilayer graphene, whereas one of the curved regions is a part of a carbon nanotube or a mono-layer graphene. We theoretically study effects of inter-wall interaction in collapsed carbon nanotubes, first directly calculating effective inter-wall interaction within an effective-mass scheme and second regarding collapsed tubes as ribbons of bilayer graphene with closed edges described by boundary conditions explicitly derived. Within the effective-mass scheme, effects of inter-wall interactions are shown to be important in non-chiral nanotubes such as zigzag and armchair, as shown in Fig. 1 (a). In fact, with the increase in the width of the flattened region, the band structure approaches that of a bilayer ribbon in which the electron motion in the ribbon-width direction is discritized. In chiral nanotubes, inter-wall interaction can essentially be neglected except in the vicinity of non-chiral tubes. Inter-wall interactions diminish rapidly when chiral angle deviates from zigzag or armchair, although the decay is slower in the vicinity of the armchair tube.

For armchair and zigzag nanotubes, the same results can be derived by calculating boundary conditions corresponding to the closed-edge structure in which the top and bottom layers are smoothly connected through a monolayer graphene. Figure 1 (b) shows an example of calculated energy, when the flattened region has the structure of AB stacked bilayer graphene. The bottom of the conduction band is fixed at zero energy, while the top of the valence band is lowered, forming a band gap, because the anti-bonding state corresponding to the top of valence band in bilayer graphene does not satisfy the boundary condition.

## References

[1] T. Nakanishi, and T. Ando, Phys. Rev. **B 91** (2015) 155420.

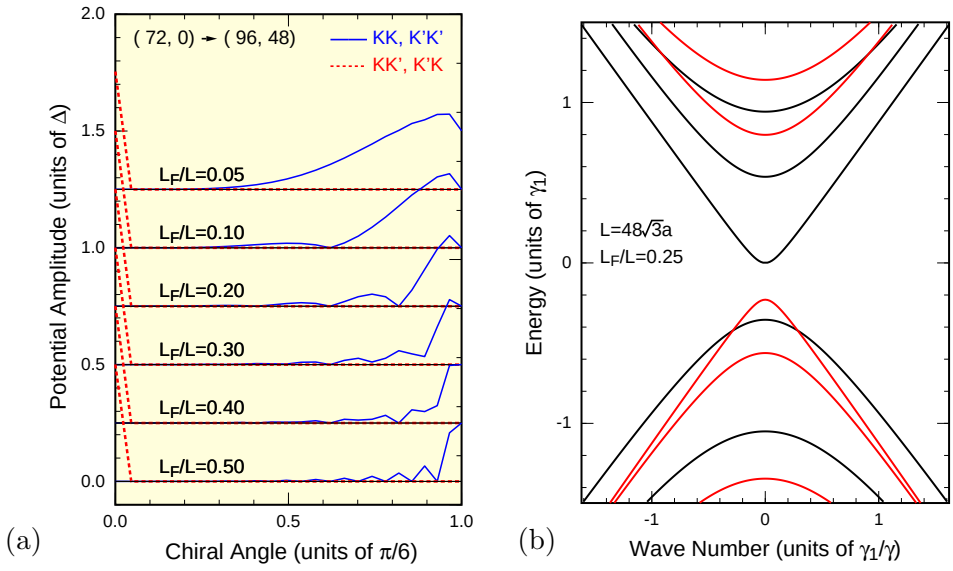


**Fig. 1** (a) Some examples of the potential amplitude in the dominant-term approximation as the function of chiral angle $\eta$. (b) Calculated band structure of a collapsed armchair tube.

# Magnonic Holographic Read-Only Memory

F. Gertz[1], A. Kozhevnikov[2], Y. Filimonov[2], and A. Khitun[1]

[1]*Electrical Engineering Department, University of California - Riverside, Riverside, CA, USA, 92521*

[2]*Kotel'nikov Institute of Radioengineering and Electronics of Russian Academy of Sciences, Saratov Branch, Saratov, Russia, 410019*

In this work, we consider the possibility of building Magnonic Holographic Read-Only Memory (MH-ROM) devices exploiting spin wave interference for read-out. MH-ROM consists of a grid of magnetic waveguides connected via cross junctions. Some of the cross junctions have a hole in the center of junctions, others have not. The presence/absence of the hole is assigned to the memory states 0 and 1, respectively, We present experimental data showing spin wave propagation modification in the permalloy cross junction due to the presence of the hole. The results show prominent spin wave modulation which is applicable for application in MH-ROM. Similar to the optical CD-ROM, the internal memory states can be recognized via wave interference. The advantages of using of spin wave instead of optical beams are scalability and compatibility with conventional electronic devices. The memory density scales invers proportional to the operational density. According to the estimates, the memory density of MH-ROM can be 1Tb/cm$^2$ at $\lambda$=100nm. We discuss the physical limitations and physical constrains associated with the spin wave interference. The development of MH-ROMs opens a new horizon for building scalable holographic devices compatible with conventional electronic devices. he development of spin-based logic circuitry requires a new type of interconnects capable of reliable magnetic signals transmission through micrometer-scale distances at room temperature.

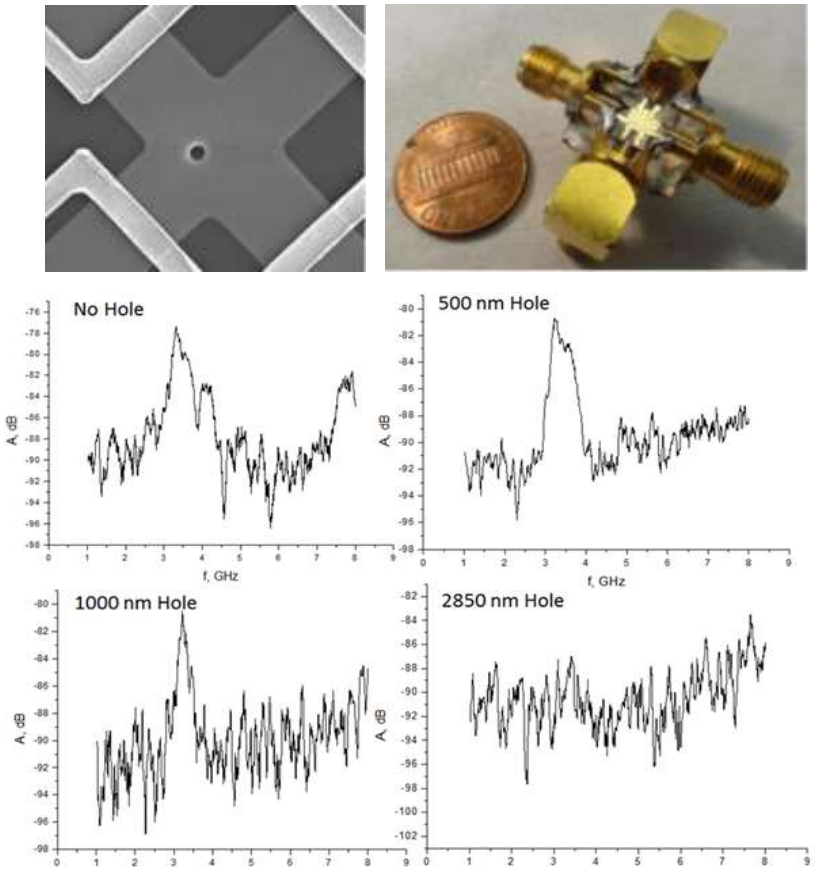


Figure 1, (A) SEM angled image of Py cross structure with 500nm hole. (B) Photo of the packaged device with microwave input/output ports used for connection to VNA. Permalloy single cross structure is seen in the center. (C) Experimental data on the spin wave transport between ports 1 and 3. (C1) There is no hole in the junction; (C2) Hole radius is 500nm; (C3) Hole radius has been increased to 1000nm; (C4) Hole radius has been further increased to 2850 nm.

# Modeling Reliability and Metastability of CdTe Photovoltaics*

Da Guo[1], Richard Akis[1], Dragica Vasileska[1], Daniel Brinkman[2], Christian Ringhofer[2], Andrew Moore[3] and Igor Sankin[4]

[1]*School of ECEE, Arizona State University, Tempe, AZ 85287, USA*
[2]*School of MSS, Arizona State University, Tempe, AZ 85287, USA*
[3]*Department of Physics, Colorado State University, Fort Collins, CO 80523, USA*
[4]*First Solar Inc., Perrysburg, OH 43551, USA*
*e-mail: vasileska@asu.edu*

Performance of CdTe solar cell, similarly to performance of any other semiconductor device is uniquely defined by device geometry and properties of semiconductor regions such as band parameters, distribution and parameters of doping and trapping/recombination centers. However, when the above variables cannot be measured precisely, predictive simulation of device performance becomes rather challenging, and CdTe PV devices exemplify such situation. Moreover, predictive simulation of CdTe devices becomes even more challenging due to low temperature diffusion and reaction of Cu-related centers, phenomena that is known to strongly affect the device causing both short-term metastabilities and permanent changes in device performance [1]. In this work, we present a 1D diffusion-reaction solver that was develop to overcome these challenges by accurate simulation of electrically active centers in the device structure as-fabricated, and evolution of these centers under stress conditions. The solver was used in this work to support our hypotheses that explain limited Cu incorporation (also known as Cu solubility limits in CdTe [2]), tight self-compensation of Cu-related donors and acceptors [3], and rapid changes in atomic concentration of Cu in absorber as function of stress conditions [4].

* This work was supported by the Department of Energy SunShot Program, PREDICTS AWARD DE-EE0006344. The authors would also like to thank Dr. Su-Huai Wei and Dr. Ji-Hui Yang from NREL for providing the first principle calculated defect parameters.

[1] A. Pudov, M. Gloeckler, S. Demtsu, J. Sites, K. Barth, R. Enzenroth, *et al*., "Effect of back-contact copper concentration on CdTe cell operation," in Proceedings of the 29th IEEE Photovoltaic Specialists Conference, New Orleans, LA, 2002.
[2] J. Ma, S.-H. Wei, T. A. Gessert, and K. K. Chin, "Carrier density and compensation in semiconductors with multiple dopants and multiple transition energy levels: Case of Cu impurities in CdTe," Physical Review B, vol. 83, 2011.
[3] J. Perrenoud, L. Kranz, C. Gretener, F. Pianezzi, S. Nishiwaki, S. Buecheler, et al., "A comprehensive picture of Cu doping in CdTe solar cells," Journal of Applied Physics, vol. 114, 2013.
[4] A. Moore, T. Fang, and J. Sites, "Cu profiles in CdTe Solar Cells," in Proceedings of the 42nd IEEE Photovoltaic Specialists Conference, New Orleans, LA, 2015.

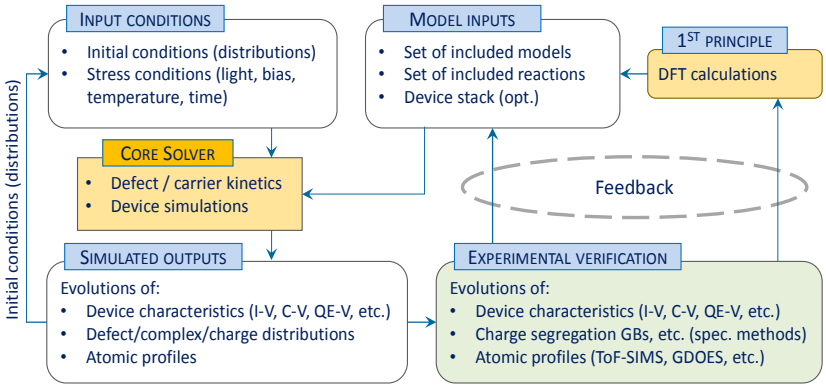


Fig. 1. Unified diffusion-reaction/device solver – multi-scale computation with feedback (https://nanohub.org/tools/predicts1d/)

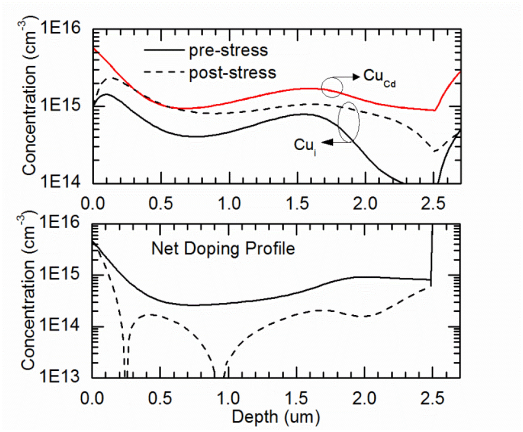


Fig. 2. Defect profiles and corresponding doping profiles simulated after a 200°C 220s anneal and two-hour open circuit stress in a standard CdS/CdTe solar cell. Extra $Cu_i$ moved into CdTe layer due to small built-in electric field under OC condition, which reduced the p-type net doping during the stress.

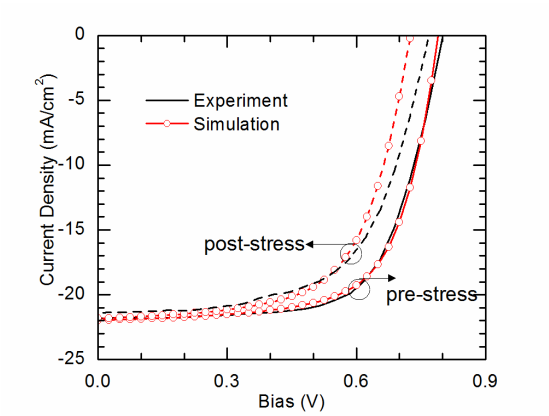


Fig. 3. Comparison between simulated and experimental IV curves of the CdTe solar cell before and after the stress. Loss in p-doping caused the reduction of $V_{OC}$, hence the conversion efficiency.

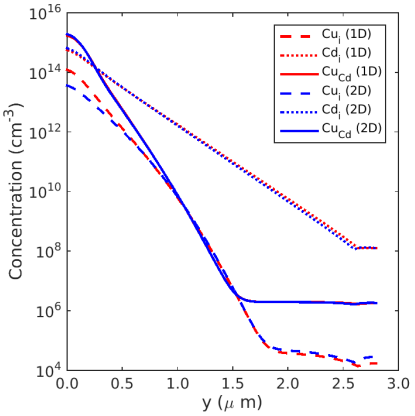


Fig. 4. Comparison of the concentration of $Cu_i$, $Cd_i$ and $Cu_{Cd}$ for the 1D finite-difference scheme and the 2D finite-element method scheme finished by a standard 200°C 220s anneal from a finite Cu source. Although the time step employed for the 2D case is 100 times larger than the 1D time step, the difference between these profiles is negligible.

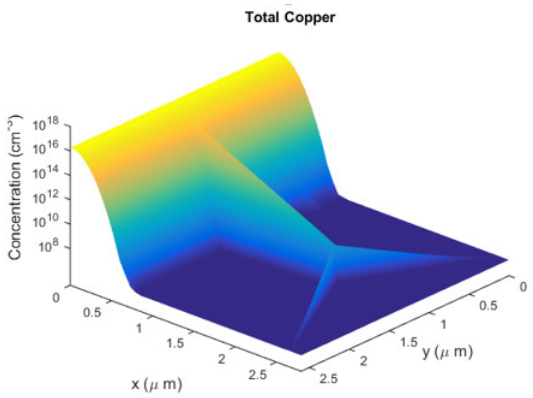


Fig. 5. The 2D FEM scheme allowed the inclusion of grain-boundary enhanced diffusion of Cu in the simulation. A fork-shaped grain-boundary was assumed in this 2D simulation. Clear segregation of Cu along the boundary was achieved.

# Wideband spectroscopic probe for near-zone field mapping

Daniel van der Weide
*Department of Electrical & Computer Engineering,*
*University of Wisconsin, Madison WI 53706 USA*
*e-mail: danvdw@engr.wisc.edu*

Although they can be numerically computed, experimentally determining the full set of electric and magnetic field components on a sample with arbitrary spatial and temporal resolution remains elusive. An ideal probe would exert minimal perturbation of the fields proximal to the sample surface, yet also enable reciprocal use as a three-dimensional (3D) field exciter, e.g. for photoconductive detection for mapping coupled semiconductor quantum dots[1]. Wedge-shaped indirect electro-optic probes have allowed mapped one lateral near-zone electric field component with subpicosecond resolution[2], but shrinking the wedge to a point shape diminishes both sensitivity and field component selectivity[3]. Point probes (such as atomic-force microscope [AFM] tips) excite, scatter[4] or detect[5] the surface-normal electric field; a loop probe (on an AFM cantilever) is the dual of the point probe, and works with only one magnetic field component[6].

Building on slot antennas (already proven in THz spectroscopy[7]) for in-plane fields and the inherent polarization isolation of crossed slots, I describe a new electrode configuration that can use dual-source (e.g. comb[8]) driving waveforms for coherent excitation and linear detection of wideband (DC-THz) near-zone electric fields in three dimensions.

[1] R. H. Blick, D. W. van der Weide, R. J. Haug and K. Eberl, Physical Review Letters **81** (3), 689-692 (1998).

[2] T. Löffler, T. Pfeifer, H. G. Roskos, H. Kurz and D. W. van der Weide, Microelectronic Engineering **31** (1-4), 397-408 (1996).

[3] B. Rosner, J. Peck and D. W. van der Weide, IEEE Transactions on Antennas and Propagation **50** (5), 670-675 (2002).

[4] F. Keilmann, Infrared Physics Technology **36** (1), 217-224 (1995).

[5] B. T. Rosner and D. W. van der Weide, Review of Scientific Instruments **73** (7), 2505-2525 (2002).

[6] V. Agrawal, P. Neuzil and D. W. van der Weide, Applied Physics Letters **71** (16), 2343-2345 (1997).

[7] D. W. van der Weide, J. S. Bostak, B. A. Auld and D. M. Bloom, Applied Physics Letters **62** (1), 22-24 (1993).

[8] D. W. van der Weide, J. Murakowski and F. Keilmann, Proc. SPIE **3828**, 276-284 (1999).

# Directional and Polarized Emission from a Periodically Nanostructured Phosphor Film

Yasuhisa Inada, Akira Hashiya, Mitsuru Nitta, Shogo Tomita and Taku Hirasawa

*Advanced Research Division, Panasonic Corporation, 1006 Kadoma, Kadoma City, Osaka 571-8501, Japan*

*e-mail: inada.yasuhisa@jp.panasonic.com*

Controlling the directionality and polarization direction of photon emission is a significant challenge for a wide variety of optical and photonic devices. Most studies have focused on modifying spontaneous emission by confining photons in an extremely small space using microcavities, photonic crystals or plasmonic structures [1]. These methods have major potential for use in photonic devices such as low-threshold lasers and single-photon sources; however, more commonly used optical devices such as lighting, displays and projectors require directional and polarized light sources with high brightness.

In this presentation, we demonstrated resonantly enhanced directional and polarized emission using a luminescent nanostructured-waveguide resonance (LuNaR). Our concept is based on coupling between the emitters in the waveguide and a resonant guided mode which interacts resonantly with a periodic nanostructure and hence outcouples via diffraction (Fig. 1). Our samples were prepared by depositing YAG:Ce phosphor onto a nanograting fabricated on the top of a silica substrate. We showed that the directionality and the polarization direction of the LuNaR emission can be controlled by tuning the dimensions and the geometry of the nanograting. The measured dependence of the resonant enhancement on the outcoupling rate, which varied with grating depth, agreed closely with analytical theory.

[1] M. Pelton, Nature Photonics, **9**, 427 (2015).

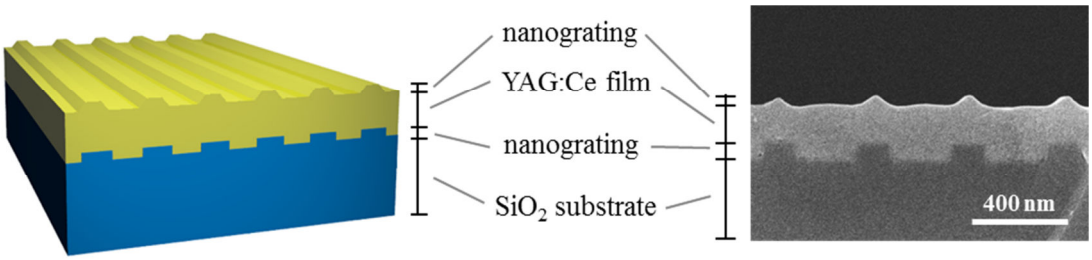


**Figure 1**. Schematic (left) and SEM image of a LuNaR structure

# Antenna-Coupled Single-Metal Nanoscale Thermocouples: Where is the Hot Spot?

Gergo P. Szakmany, Alexei O. Orlov, Gary H. Bernstein, and Wolfgang Porod

*Center for Nano Science and Technology, Department of Electrical Engineering, University of Notre Dame, Notre Dame, IN 46556, USA*
*e-mail: porod@nd.edu*

Antenna-coupled single-metal nanoscale thermocouples (ACNTC) for infrared (IR) detection were characterized with various antenna designs. The response of a nanoscale thermocouple (NTC) depends upon the location of the hot spot relative to the NTC junction. Radiation-induced antenna currents lead to localized heating along the resonant antenna element, and we use this as a tool to study the NTC response as we control the location of the hot spot by engineering the antenna structure.

We constructed ACNTCs with three different designs, as shown in Fig. 1a. The devices were patterned by electron beam lithography, and 45-nm-thick Ni was deposited by electron beam evaporation. In all cases, the widths of the narrow lead lines and the antenna were 70 nm and the widths of the wide lead lines were 300 nm.

We performed polarization-dependent measurements of the devices, using a $CO_2$ laser operating at 10.6 μm, and a half-wave plate to rotate the polarization. The open-circuit voltage response of the devices is shown in Fig. 1b, which clearly demonstrates that the response of the devices varies with the lead geometry. The response of design #1 is similar to the previously reported antenna-coupled detectors, *i.e.*, it is maximum when the polarization of the incident IR wave is parallel to the antenna axis, and is minimum at perpendicular polarization. In contrast, the measured $V_{OC}$ of design #2 changes sign at perpendicular polarization, which is unexpected from such a detector. Furthermore, the measured response of design #3 shows a large open-circuit voltage at 45 deg and 135 deg (relative to design #1) with opposite signs. This indicates that the lead lines themselves behave as an antenna, and are in resonance with the 10.6 μm IR excitation. In addition, the sign change indicates that the hot junction moves along the antenna-lead lines as the polarization angle of the incident IR radiation changes from parallel to cross polarization, as shown in Fig. 2.

By engineering the antenna structure, we constructed an integrated polarization sensitive ACNTC. The narrow segments not only act as an antenna but also form, together with the wider wire segments, NTC junctions. Depending on the polarization of the incident IR radiation, either the left or the right antenna is in resonance, and heating occurs there. As a result, the polarization dependent response is symmetric around zero as shown in Fig. 3.

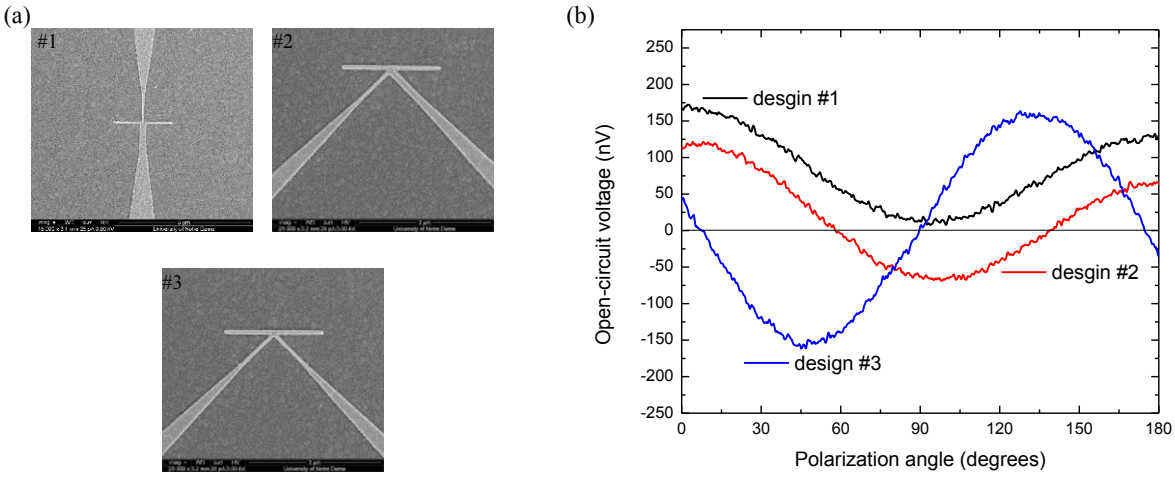


Figure 1. (a) SEM images of ACNTCs with various lead line geometries. (b) Polarization-dependent responses

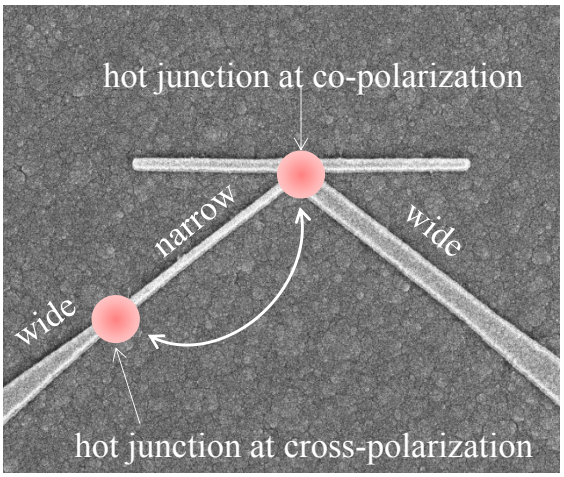


Figure 2. Shift of the hot junction. At cross polarization, the hot junction moves because the length of the lead lines are comparable to the effective dipole length, and therefore act as an antenna.

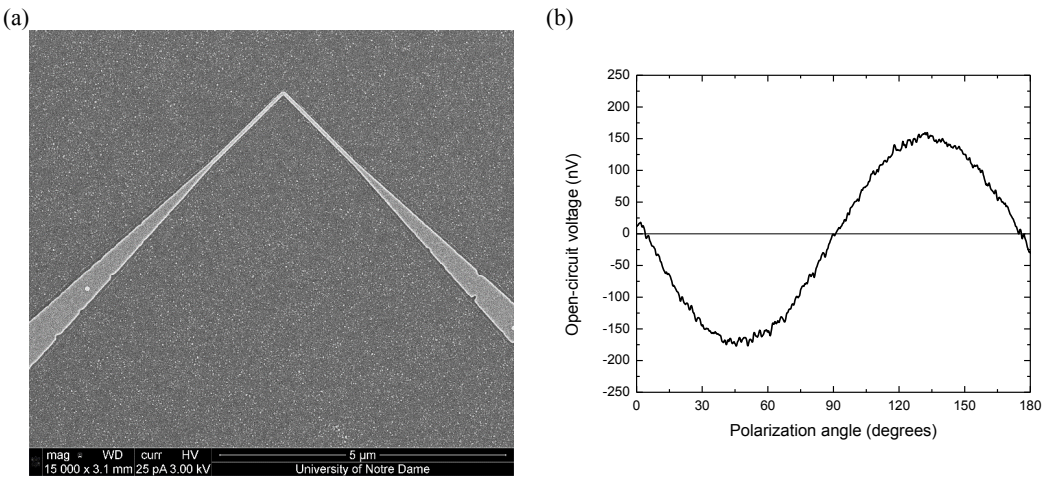


Figure 3. Integrated antenna-coupled single-metal nanothermocouple. (a) SEM image, (b) Polarization-dependent response.

# Topological Energy Transduction

Timothy Phillip[1] and Matthew J. Gilbert[1]

[1] *Department of Electrical and Computer Engineering, University of Illinois – Urbana-Champaign, Urbana, IL 61801*

*e-mail: matthewg@illinois.edu*

The on-chip inductor is a circuit element of vital importance, but that receives comparatively little attention. These passive elements help to minimize distribution losses and achieve fast transient responses to aid in the overall goal of more efficient computing. The currently used air-core inductors have very low inductances and thus additional magnetic materials must be added to improve the energy storage resulting from the electromagnetic response[1]. Furthermore, only select magnetic materials may be used to ensure that the inductors operate within the desired frequency range. Yet of the materials that boast the proper frequency range, the fabrication remains quite difficult as the magnetic anisotropy and the magnetic domain structure must be carefully controlled so as to ensure good magnetic performance.

To circumnavigate the issues with current on-chip inductors, we propose the nanoscale inductor, shown in **Fig. 1(A)**, which consists of a 3D time-reversal invariant topological insulator with ferromagnetic islands patterned on the surface. The operation of the topological inductor is based on the fact that when a DC applied field drives a current, the quantum anomalous Hall effect, i.e., the development of a quantized Hall voltage without the presence of a magnetic flux, causes a dissipationless current to flow through the islands in a direction that depends on the magnetic orientation, as shown in **Fig. 1(B)**. By utilizing alternating magnetization directions on successive islands, we predict the formation of an induced magnetic field, shown in **Fig. 1(C)**, and a highly resistive state, thereby allowing the system to act as an inductor storing maximal magnetic energy for efficient power management. We quantify the performance enhancements over other current and proposed inductor technologies in **Tab. 1**. We find that the topological inductor outperforms other current and proposed technologies in both Q factor and speed making it an extremely attractive candidate for inductor needs of post-CMOS architectures.

[1] N. Wang, et al., *Journal of Applied Physics* **111**, 07E732 (2012).

[3] D. S. Gardner, et al., *IEEE Transactions on Magnetics* **45**, 4760–4766 (2009).

[4] D. Sarkar, et al., *IEEE Transactions on Electron Devices* **58**, 853–859 (2011).

[5] H. Li and K. Banerjee, *IEEE Transactions on Electron Devices* **56**, 2202–2214 (2009).

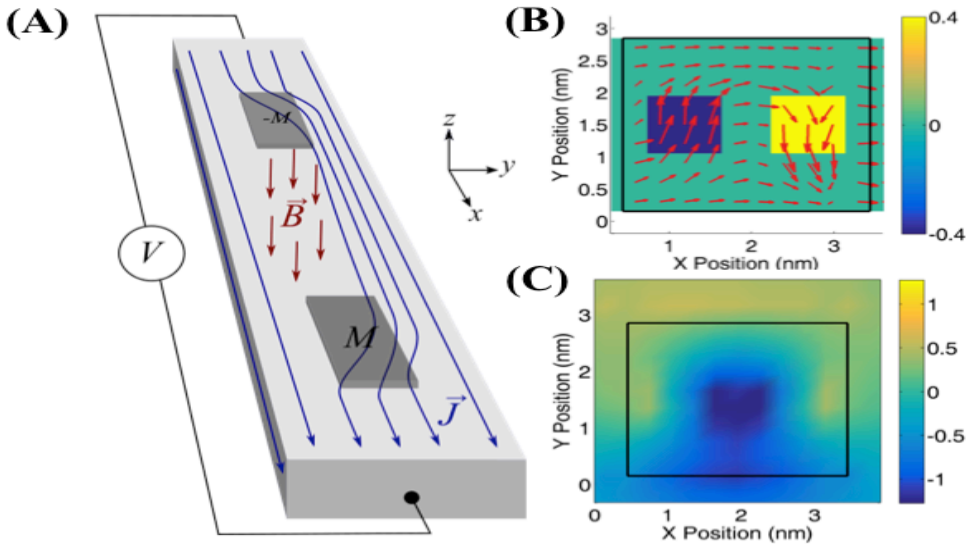


**Figure 1: (A)** Schematic of the proposed topological inductor design. Islands of alternating up and down magnetization (±*M*) are placed on the surface of a topological insulator. This steers the surface current into a loop using the QAHE. The rotating current density *J* generates the magnetic field *B* and concentrates the flux in between the islands resulting in an increased inductance. **(B)** Snapshot of current flow in the inductor structure demonstrating the current steering by the QAHE with an *x*-directed electric field. The islands of different magnetization indicated by the colored squares create a current transverse to the applied electric field, which effectively creates a current loop. **(C)** The magnetic field *B* profile (in mT) for the same snapshot in time with the location of the TI indicated by the rectangular outline. The flux can clearly be seen to be concentrated between the islands. These numerical results have been obtained using our hybrid time-dependent quantum transport / FDTD electromagnetics tool on a 2D solution mesh.

| *Inductor* | *Peak Q* | *Cut-off Frequency* |
|---|---|---|
| *Cu*[3] | *7* | *0.2 GHz* |
| *Graphene*[4] | *38* | *150 GHz* |
| *MWCNT*[5] | *100* | *150 GHz* |
| *SWCNT*[5] | *20* | *150 GHz* |
| ***Topological Inductor*** | ***405*** | ***300 THz*** |

**Table I**: Characteristics of various on-chip inductors comparing the topological inductor to other proposed solutions.

# Acoustic control of optical properties and spins in quantum wells

Tetsuomi Sogawa, Haruki Sanada, Yoji Kunihashi, and Hideki Gotoh

*NTT Basic Research Laboratories, NTT Corporation, Atsugi, Japan*
*e-mail: sogawa.tetsuomi@lab.ntt.co.jp*

Surface acoustic waves (SAWs) are known to provide a dynamic lateral modulation of the band structure of quantum wells (QWs), i.e., dynamic dots or wires, while conventional quantum nanostructure fabrication processes have certain detrimental effects. Furthermore, the band modulation introduced by SAWs differs qualitatively from that induced by static modulation, because its temporal and spatial dependence allows the dynamic control of the material properties. In this report, we discuss such dynamic optical properties as photoluminescence (PL) quenching induced by a lateral piezoelectric field and the polarization anisotropy of PL spectra caused by strain-induced band mixing [1, 2], and acoustic spin manipulation capability [3].

The investigations were performed on a sample containing 8 GaAs single QWs with various well thicknesses. Four inter-digital transducers (IDTs) were formed to generate SAWs propagating along the [110] and [1-10] directions, as illustrated in Fig. 1. The SAW frequency of 820 MHz was synchronized with excitation light pulses from a mode-locked Ti-sapphire laser. Low temperature (4 K) spatially resolved PL spectra were measured using a confocal micro-PL setup with a spatial resolution of approximately 1 μm. The PL was spectrally analyzed by using a spectrometer connected to a charge-coupled device (CCD) detector or a synchronously scanning streak camera. Figures 2 (a)-(d) show time-resolved PL spectra obtained under various SAW conditions. The interference of two or four acoustic beams formed 1D or 2D standing SAWs, which caused strong bandgap modulation. On the other hand, the quadrupole SAW fields caused saw-toothed spectral structures, as shown in Fig. 2(d). Stroboscopic PL mapping measurement demonstrated that the carriers move along a looped path following the local minima of the bandgap modulation by the quadrupole SAWs. We also discuss the spin behaviors under the spatial motion driven by the SAW fields [4].

[1] T. Sogawa et al., Phys. Rev. B **80**, 075304 (2009)
[2] T. Sogawa et al., Phys. Rev. B **86**, 035311 (2012)
[3] H. Sanada et al., Phys. Rev. Lett. **106**, 216602 (2011)
[4] H. Sanada et al., Nature Physics **9**, 280 (2013)

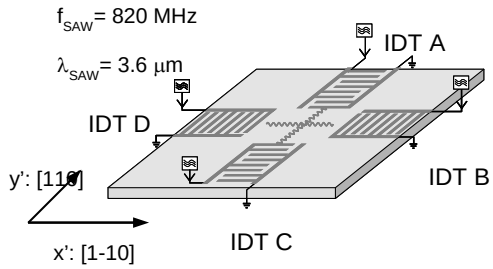


Figure 1: Schematic illustration of the sample structure

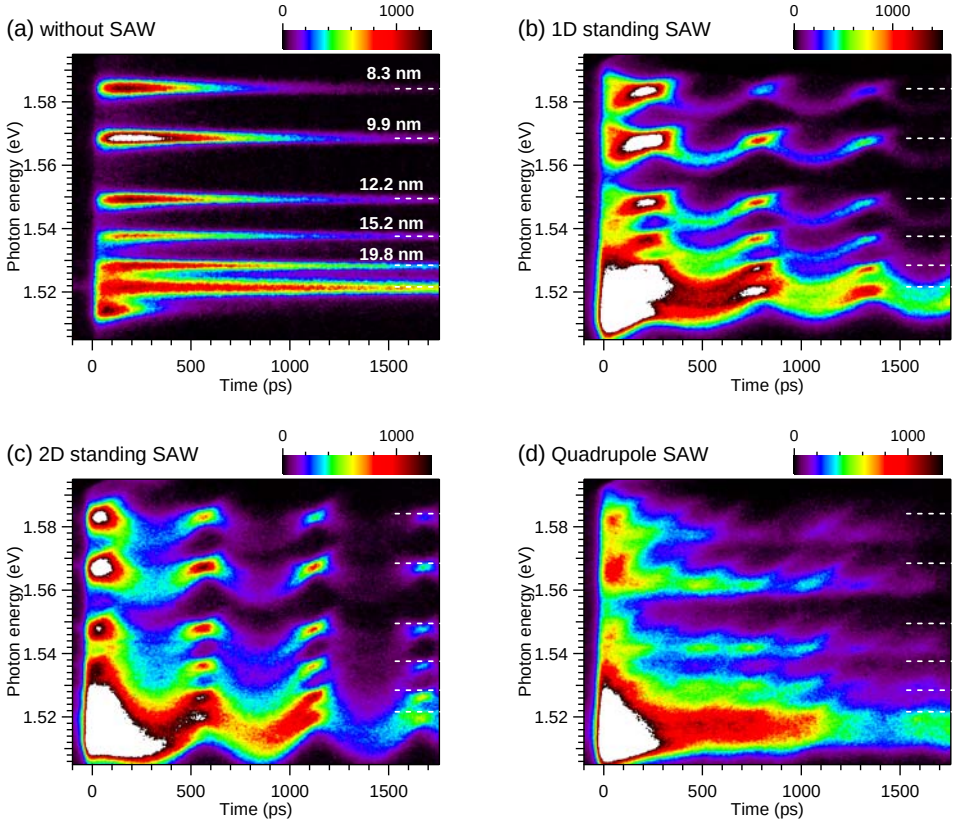


Figure 2: (a) Time-resolved PL spectra from several QWs in the absence of a SAW,
(b) with 1D standing SAWs along the [110] direction,
(c) with 2D standing SAWs, and (d) with quadrupole SAWs

# Tuning Phonon Transport at Nanoscale: Direct Evidence of the Acoustic Phonon Spectrum Modification and its Effect on Heat Conduction

Fariborz Kargar, Sylvester Ramirez, Hoda Malekpour and Alexander A. Balandin

*Phonon Optimized Engineered Materials (POEM) Center, Bourns College of Engineering, University of California – Riverside, Riverside, California 92521 USA*
*Spins and Heat in Nanoscale Electronic Systems (SHINES) Center, University of California-Riverside, Riverside, California 92521 USA*
*E-mail: balandin@ece.ucr.edu*

An ability for fine-tuning heat fluxes at nanoscale offers tremendous benefits for heat removal from state-of-the-art electronics and nano-energy applications, e.g. via increasing efficiency of the thermoelectric energy conversion in nanostructured materials. There is a growing realization that effective control of thermal conduction in nanostructures should rely not only on the phonon – boundary scattering but also on the spatially induced modifications of the acoustic phonon spectrum. The theory predicted that confinement of acoustic phonons – the main heat carriers in semiconductors – changes the phonon scattering rates modifying the thermal conductivity [1-2]. However, direct experimental evidence of the acoustic phonon dispersion changes in nanostructures is still scarce. No experimental studies have correlated the thermal conductivity with changes in the acoustic phonon spectrum. In this work, we used a set of nanoporous alumina membranes with the pore diameter, *D*, decreasing from 180 nm to 25 nm. The samples with the hexagonally arranged pores were selected to have the same porosity $\phi \approx 13\%$. We used the Brillouin-Mandelstam spectroscopy (BMS) to determine the acoustic phonon energies and group velocities. The BMS data revealed the bulk-like phonon spectrum in the samples with *D*=180-nm pores and spatial confinement induced modifications in the acoustic phonon spectra of the samples with 40-nm and 25-nm pores (see Figure). The velocity of the longitudinal acoustic (LA) phonons decreased by 10%. The observed changes in the acoustic phonon spectrum were in line with the elastic continuum calculations. The cross-plane and in-plane thermal conductivities measured by the "laser flash" technique [3] were analyzed in correlation with the acoustic phonon spectrum. Our data suggests that both phonon-boundary scattering and phonon confinement effects influence the heat conduction in the considered nanostructures with the feature sizes below ~40 nm.

The work at UC Riverside was supported as part of the DOE Spins and Heat in Nanoscale Electronic Systems (SHINES) Center under Award # SC0012670.

[1] See for review A.A. Balandin and D.L. Nika, Materials Today, 15 266 (2012).

[2] P. Goli, H. Ning, X. Li, C.Y. Lu, K. S. Novoselov and A. A. Balandin, Nano Letters, 14, 1497 (2014).

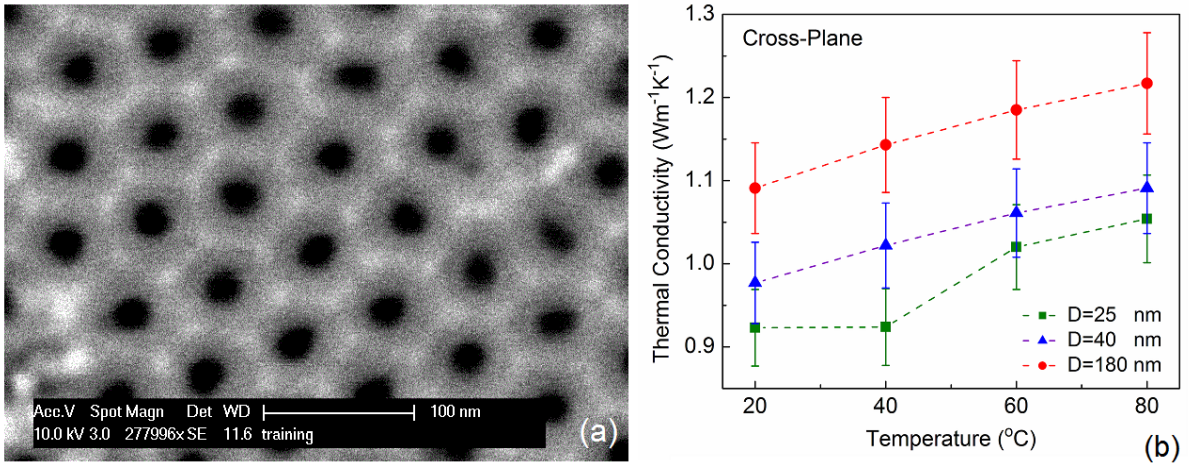


**Figure 1:** (a) SEM image of one of the examined porous alumina samples. (b) Cross-plane thermal conductivity of porous alumina membranes with the pore diameter $D$=25 nm, $D$=40 nm, $D$=180 nm and the corresponding inter-pore distances $H$=65 nm, $H$=105 nm and $H$=480 nm. Despite large difference in feature sizes all samples had the same porosity $\phi$=13%.

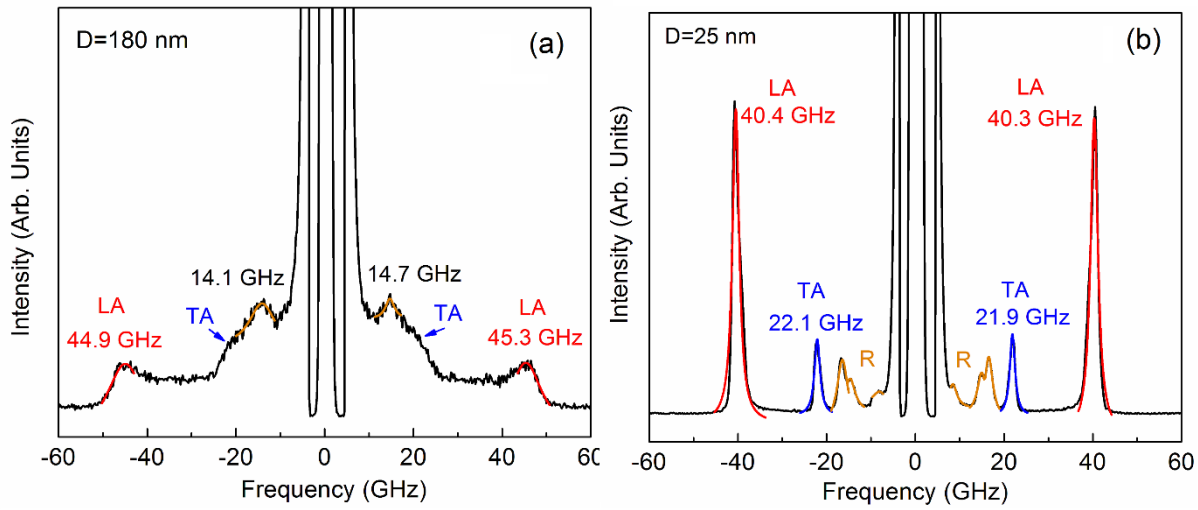


**Figure 2:** Brillouin-Mandelstam scattering spectra for the samples with (a) $D$=180 nm and (b) $D$=25 nm. The results are shown for the incident angle of 40°. Note a shift in the LA and TA phonon peaks with decreasing pore size D and inter-pore distance H indicating a reduction in the phonon group velocity. Multiple peaks in $D$=25 nm sample were attributed to the "ripple" phonon scattering (indicated with orange color). The BMS data presents direct evidence of the phonon confinement effects in nanostructures.

# Simulating the Ising Hamiltonian with phonons

Imran Mahboob, Hajime Okamoto and Hiroshi Yamaguchi*
*NTT Basic Research Laboratories, NTT Corporation, Atsugi-shi, Kanagawa 243-0198, Japan*
*yamaguchi.hiroshi@lab.ntt.co.jp

Solving intractable mathematical problems in simulators composed of atoms, ions, photons or electrons has recently emerged as a subject of intense interest [1]. Here we extend this concept to phonons that are localised in spectrally pure resonances in an electromechanical system which enables their interactions to be exquisitely fashioned via electrical means [2]. We harness this platform to emulate the Ising Hamiltonian whose spin 1/2 particles are replicated by the phase bistable vibrations from a parametric resonance where multiple resonances play the role of a spin bath [3]. The coupling between the mechanical spins is created by generating thermomechanical two-mode squeezed states which impart correlations between resonances that can imitate a ferromagnetic, random or an anti-ferromagnetic state on demand [4]. These results suggest that an electromechanical simulator could be developed for the Ising Hamiltonian in a non-trivial configuration namely with a large number of spins and multiple degrees of coupling [5].

[1] I. Buluta and F. Nori, Science **326**, 108 (2009).
[2] S. R. Sklan, AIP Advances **5**, 053302 (2015).
[3] I. Mahboob and H. Yamaguchi, Nature Nanotech. **3**, 275 (2008).
[4] I. Mahboob et al., Phys. Rev. Lett. **113**, 167203 (2014).
[5] I. Mahboob et al., arXiv 1505.02467 (2015).

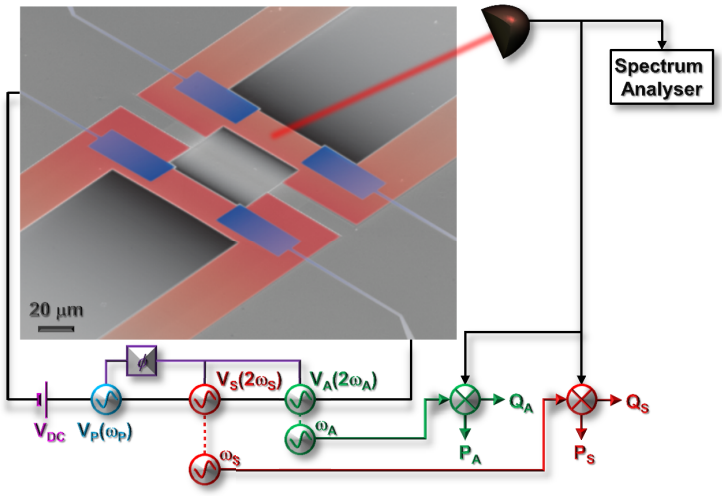


Figure 1: A false colour electron micrograph of the coupled mechanical resonators sustaining the symmetric and asymmetric vibration modes. The measurements were performed at room temperature and in a high vacuum and the mechanical vibrations were detected via a laser interferometer which was demodulated either in a spectrum analyser or in a phase sensitive detector utilising the homodyne mixing setup detailed in the circuit schematic. Five signal generators were employed with two piezoelectrically activating the parametric resonances at $2\omega_n$, two generating the reference signals for the phase sensitive detectors at $\omega_n$ and the fifth creating the coupling between the parametric resonances via parametric down-conversion when activated at $\omega_p$.

# Spin-dependent Trap-assisted Tunneling in Ferromagnet-Oxide-Semiconductor Structures

Viktor Sverdlov and Siegfried Selberherr

*Institute for Microelectronics, TU Wien, Gußhausstraße 27-29, 1040 Vienna, Austria*
*e-mail: {Sverdlov|Selberherr}@iue.tuwien.ac.at*

Silicon is an ideal material for spintronic applications due to its weak spin-orbit interaction and long spin lifetime [1,2]. Spin injection from a ferromagnetic electrode into n-type silicon was claimed at room [3] and elevated [4] temperatures. However, the amplitude of the spin-accumulation signal extracted from a three-terminal injection method [2,3] is orders of magnitude higher than predicted [1]. The reasons for this discrepancy are currently heavily debated [1,5-8]. Recently an alternative interpretation of the three-terminal signal based on spin-dependent magnetoresistance due to trap-assisted resonant tunneling was proposed [5]. However, the effects due to finite spin lifetime [6] were not taken into consideration. Here we investigate in detail the role of spin relaxation and decoherence on a trap in determining the trap-assisted tunneling magnetoresistance.

To elucidate the role of spin relaxation and decoherence we introduce the corresponding relaxation terms into a Lindblad equation for the density matrix evolution of spin on a trap. This results in coupled master equations for the density matrix elements in the presence of the spin lifetime $T_1$ and decoherence time $T_2$ ($T_2 \leq T_1$) and the tunneling rates $\Gamma_N$ from silicon and $\Gamma_\pm = \Gamma_F(1\text{-}p)$ to the ferromagnet (Fig.1). The current $I$ due to tunneling via a trap is different from $I_0 = \Gamma_F \Gamma_N /(\Gamma_F + \Gamma_N)$ and depends on the angle $\Theta$ between the spin quantization axis and the magnetization orientation.

$$I = e\frac{\Gamma_F(\Theta)\,\Gamma_N}{\Gamma_F(\Theta)+\Gamma_N},$$

$$\Gamma_F(\Theta) = \Gamma_F\left(1 - p^2\,\Gamma_F T_1\left\{\frac{cos^2\Theta}{\Gamma_F T_1+1} + \frac{T_2}{T_1}\frac{sin^2\Theta(\Gamma_F T_2+1)}{\omega_L^2 T_2^2+(\Gamma_F T_2+1)^2}\right\}\right). \quad (1)$$

$\omega_L$ is the Larmor frequency and $p$ is the ferromagnetic interface current polarization. In the case $T_1 = T_2 \to \infty$ the corresponding expression in [5] is recovered. In complement to [5], when $\Gamma_F T_1 = \Gamma_F T_2 \ll 1$, the resistance dependence on the magnetic field is of a Lorentzian shape with the half-width determined by the inverse spin lifetime. A short spin relaxation time suppresses the "spin blockade" [5] at small $\Theta$ (Fig.2) in a similar fashion as the reduction of spin polarization $p$ (Fig.3). Counterintuitively, due to a suppression of the last term in (1) at fixed $T_1$, the amplitude of the $I(\Theta)$ modulation becomes larger for shorter $T_2$ (Fig.4). In contrast to [5], at finite $T_1$ the modulation of $I(\Theta)$ is present at any trap position relative to the contacts (Fig.5). Finally, an unusual non-monotonic dependence with $T_2$ of the magnetoresistance half-width as a function of the perpendicular magnetic field **B,** with the linewidth decreasing, at shorter $T_2$ is shown in Fig.6.

This work is supported by the European Research Council through the grant #247056 MOSILSPIN.

[1] R.Jansen, *Nature Mater.* **11**, 400 (2012)
[2] V.Sverdlov, S.Selberherr, *Phys.Rep.* **585,**1 (2015)
[3] S.P.Dash *et al.*, *Nature*, **462**, 491 (2009)
[4] C.Li *et al.*, *Nature Commun.* **2**,245 (2011)
[5] Y.Song, H.Dery, *PRL* **113**, 047205 (2014)
[6] V.Sverdlov, S.Selberherr, *SpinTec*,114 (2015)
[7] A.Spiesser *et al.*, *PR*B ***90***, 205213 (2014)
[8] K.-R.Jeon *et al.*, *PR*B, **91**, 155305 (2015)

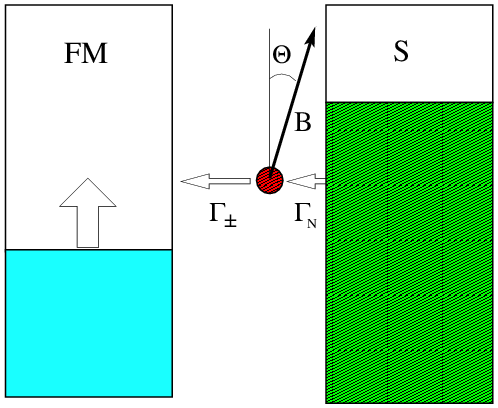


*Fig.1: The trap is connected to electrodes with the rates $\Gamma_N$ and $\Gamma_\pm$. A magnetic field **B** defines the trap spin quantization axis OZ' at an angle Θ to the magnetization orientation OZ in the ferromagnet.*

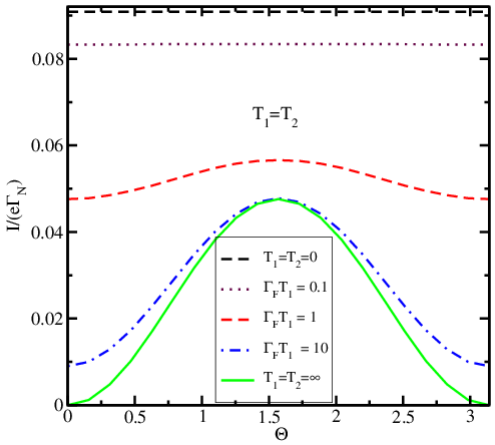


*Fig.2: Current in units of $e\Gamma_N$ as a function of Θ for p=1 $\Gamma_N/\Gamma_F$ = 10, $\omega_L/\Gamma_F$ = 1, and several values of $T_2$=$T_1$.*

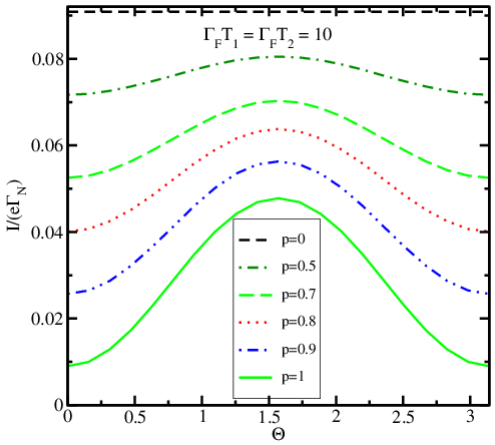


*Fig.3: Current as a function of Θ, for $\Gamma_N/\Gamma_F$ = 10, $\omega_L/\Gamma_F$ = 1, $\Gamma_F T_1 = \Gamma_F T_1$ = 10, and several values of p.*

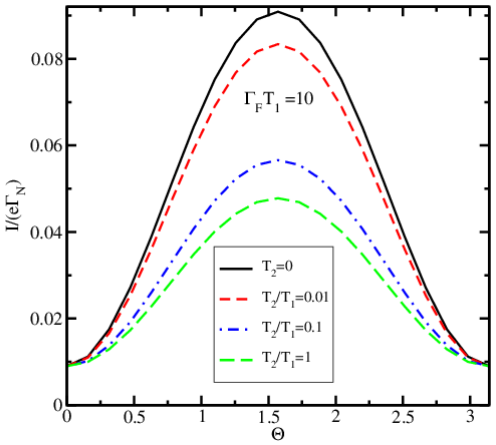


*Fig.4: Current as a function of Θ, for p=1, $\Gamma_N/\Gamma_F$ = 10, $\omega_L/\Gamma_F$ = 1, $\Gamma_F T_1$ = 10, and several values of $T_2/T_1$.*

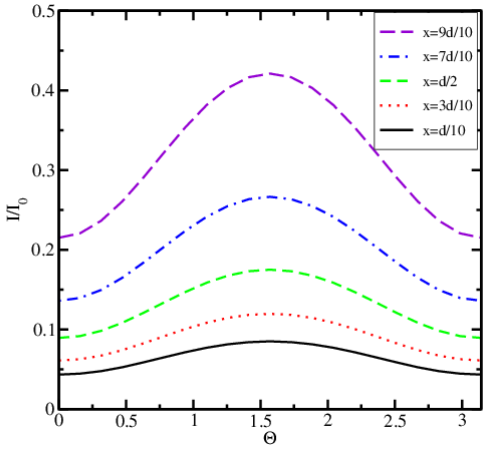


*Fig.5 Normalized current as a function of the position x relative to silicon, for p=1, $\Gamma_N=\Gamma_0 \exp(-x/d)$ , $\Gamma_F=\Gamma_0 \exp(-(d-x)/d)$, $T_2$=$T_1$, $\omega_L T_2 = \Gamma_0 T_2$ =10,*

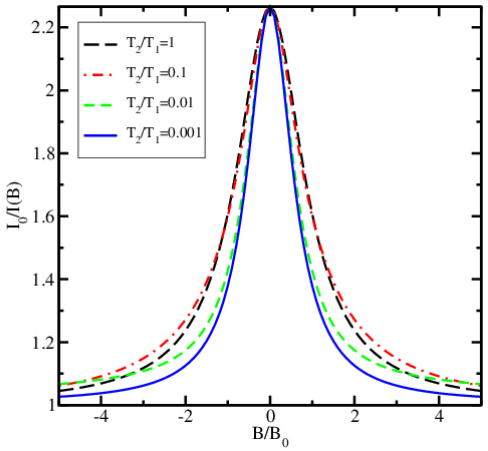


*Fig.6: Magnetoresistance signal as a function of the perpendicular magnetic field **B** for several $T_2/T_1$, for p=0.8 and $\Gamma_F T_1$ = 10. The field $\mathbf{B}_0$ is parallel to the magnetization in the ferromagnet.*

# A Novel Method of SOT-MRAM Switching

Alexander Makarov, Thomas Windbacher, Viktor Sverdlov, and Siegfried Selberherr

*Institute for Microelectronics, TU Wien, Gußhausstraße 27-29, 1040 Vienna, Austria*
*e-mail: Selberherr@TUWien.ac.at*

Three-terminal memory cell structures based on a magnetic tunnel junction (MTJ) are promising candidates for future generations of magnetic memory [1]. In particular, three-terminal devices with spin-orbit torque (SOT) switching have already been proposed [2]. Typically, a SOT memory cell is an MTJ fabricated on a heavy metal channel with large spin-orbit interaction, wherein the free layer is in direct contact with the heavy metal channel. Spin torque generated by a current through the channel induces the magnetization switching. However, one shortcoming is that an external magnetic field is required to provide deterministic switching [3]. The second shortcoming of this memory type compared to the conventional spin transfer torque memory is that it demands more space and thus leads to a lower area density because of the second transistor required for writing [1]. In this work we propose an external magnetic field free method of soft magnetic layer switching based on two consecutive orthogonal sub-nanosecond in-plane current pulses. We investigate the proposed method by means of extensive micromagnetic simulations and discuss a possibility of using this method in building 1Transistor-1MTJ memory cells in a cross-point architecture.

In the proposed method the soft magnetic layer switching is governed by the torques generated in the metal channel by charge currents (Fig.1). The first pulse is necessary for tilting the magnetization of the free layer from its stable state in order to create a small initial angle. The second pulse is used for switching the free layer to a new state (Fig.2). As our simulations show (Fig.3a), the switching probability for the proposed write scheme is 1, when the second pulse width is in the range 2.63-9.1ns. Furthermore, we demonstrated the absence of switching in the case of using only one of the two pulses, as this switching is an unwanted event and leads to the loss of information in half-selected cells in a cross-point architecture (Fig.3b, Fig.3c). Finally, potential memory cells architectures with this switching method are shown in Fig.4.

[1] D. Suzuki et al., Jpn.J.Appl. Phys. **54**, 04DE01 (2015).

[2] S. Fukami et al., INTERMAG BB-06 (2015).

[3] L. Liu et al., Phys.Rev.Lett. **109**, 096602 (2012).

This work is supported by the European Research Council through the grant #247056 MOSILSPIN.

Figure 1. Schematic illustration of the proposed method of soft magnetic layer switching. In (b), (c) The direction of the charge current is shown by big arrows, the direction of the spin current is given by small arrows.

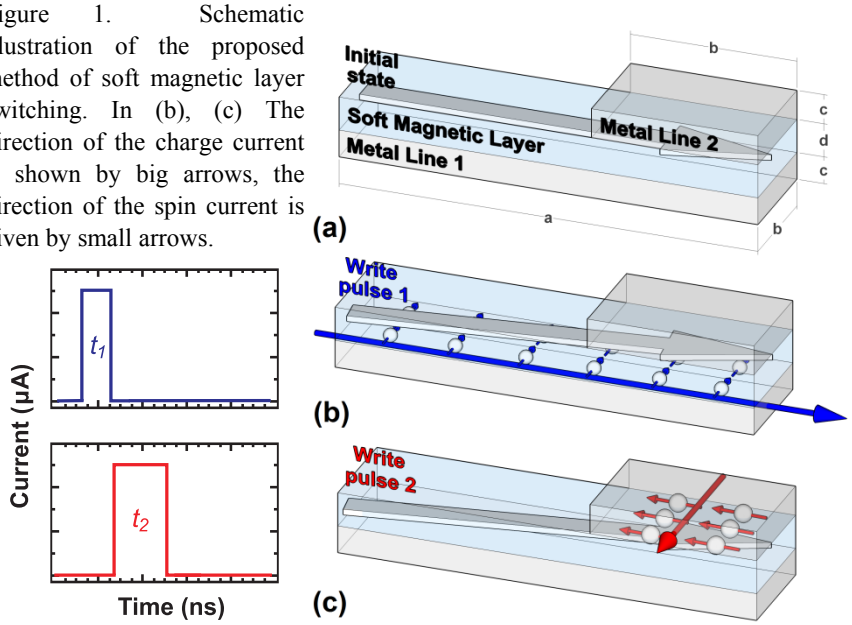


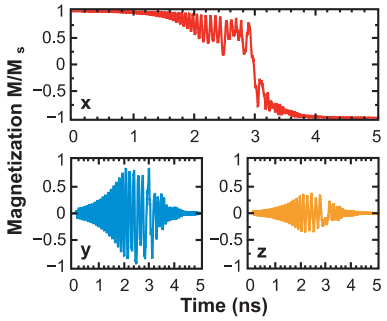


Figure 2. Magnetization components as a function of time for the "two write pulses" scheme: (top) *x*-component; (bottom - left) *y*-component; (bottom - right) *z*-component. The current is 10μA.

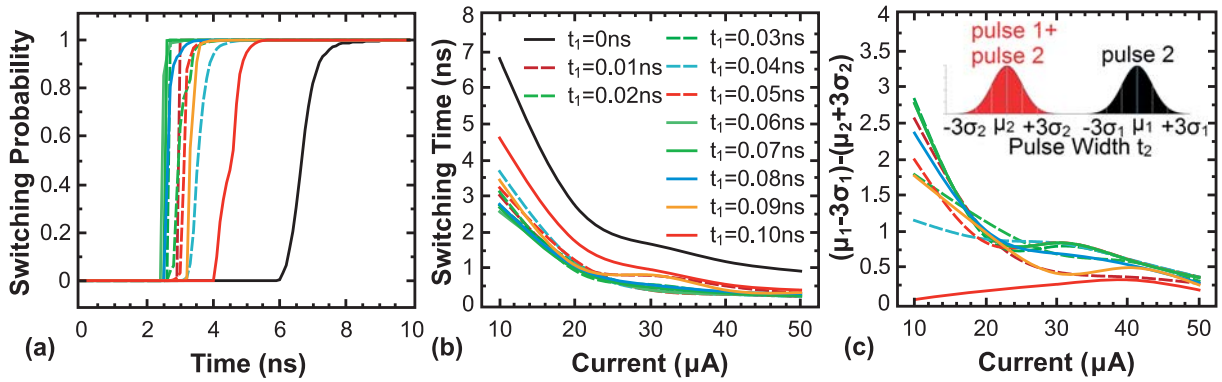


Figure 3. (a) Switching probability for the proposed scheme as a function of time for different values of pulse width $t_1$. For estimating the switching probability, 250 simulations of switching were performed with each pulse width $t_1$; (b) Switching time as a function of current for different values of pulse width $t_1$; (c) The difference between the minimum value of the pulse width $t_2$ required to achieve a non-zero probability of switching by using the "write pulse 2" scheme ($\mu_1$-3$\sigma_1$) and a value of the pulse width $t_2$ needed to achieve guaranteed switching with the "two write pulses" scheme ($\mu_2$+3$\sigma_2$) as a function of current.

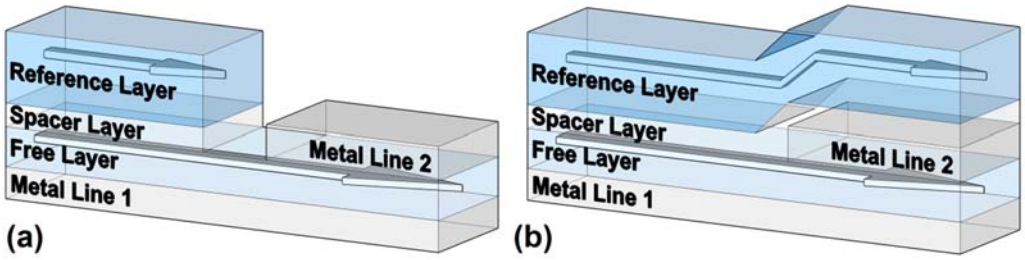


Figure 4. Schematic illustration of two memory cell structures with switching of the free layer based on the proposed "two write pulses" scheme.

# Quantum Hall effect in twisted bilayer graphene

Tomoki Machida[1,2], Satoru Masubuchi[1], Naoko Inoue[1], Reina Kashiwagi[1], Sei Morikawa[1], Kenji Watanabe[3], and Takashi Taniguchi[3]

[1] *Institute of Industrial Science, University of Tokyo, Tokyo 153-8505, Japan*
[2] *INQIE, University of Tokyo, Tokyo 153-8505, Japan*
[3] *National Institute for Materials Science, Tsukuba 305-0044, Japan*
*e-mail: tmachida@iis.u-tokyo.ac.jp*

We present experimental studies on the Landau level quantization in twisted bilayer graphene by employing magnetotransport measurements and cyclotron resonance absorption of mid-infrared light. Mechanically-exfoliated graphene layers were stacked with a twisted angle of $\theta \sim$ 0.4, 1.7, 4.0 degree and encapsulated by hexagonal boron nitride (h-BN) using the all-dry transfer technique of atomic layers. In low magnetic fields, the twisted bilayer graphene exhibited quantum Hall plateaus at $\nu$ = 4, 12, 20,..., (8$n$+4),... The absence of quantum Hall plateau at $\nu = 8n$ is contracted to the Landau level quantization in Bernal-stack bilayer graphene. In high magnetic fields, quantum Hall plateau developed at $\nu$ = 8, 16, 24,..., and the magnetic field at which $\nu$ = 8$n$ quantum Hall plateau develops depended systematically on the twisted angle of graphene layers. Temperature dependence of longitudinal resistance at the quantum Hall regime revealed that the activation energy of the quantum Hall states followed a sequence of $E_{\nu=4} > E_{\nu=12} > E_{\nu=20}$, ..., $> E_{\nu=16} > E_{\nu=8}$, which is different from $E_{\nu=4} > E_{\nu=8} > E_{\nu=12} > E_{\nu=16} > E_{\nu=20}$,... in the Bernal-stack bilayer graphene. The observed transition of Landau level degeneracy between eightfold and fourfold is attributed to a topological change of the Fermi surface at van Hove singularity point. The characteristic Landau level quantization was investigated also by using the cyclotron resonance absorption of mid-infrared light with a wavelength ~ 10 μm, where the splitting of the resonance peak was observed.

# Quantum transport in hBN/graphene/hBN heterostructures with one-dimensional edge contacts

Katsuyoshi Komatsu, Eichiro Watanabe, Daiju Tsuya, Kenji Watanabe, Takashi Taniguchi, and Satoshi Moriyama

*National Institute for Materials Science, Tsukuba, Ibaraki 305-0044, Japan*
*e-mail: KOMATSU.Katsuyoshi@nims.go.jp*

Recently, heterostructures of two-dimensional materials such as graphene, hexagonal boron niteride (hBN), molybdenum disulfide, etc., have attracted great interests because they form superlattices which allow band engineering as well as use of multiple degenerate degrees of freedom. The quantum transport in Graphene/hBN heterostructures in high magnetic fields showed a fractal spectrum known as Hofstadter butterfly [1-4]. We have measured the quantum transport properties of encapsulated hBN/graphene/hBN heterostructures with one-dimensional edge contacts (Fig. 1) as well as a Hall bar geometry, prepared by a dry transfer method similar to that in reference 5. Back-gate voltage dependence of the resistivity is shown in figure 2. We obtained a high mobility ~150,000 $cm^2/Vs$ near the Dirac point ($V_g$ ~ 0.3 V) at 5 K. The secondary peak at $V_g$ ~ -21 V corresponds to a cloned Dirac point come from moiré pattern due to the 1.8 % lattice mismatch between graphene and hBN. From this voltage, we can estimate the alignment angle between graphene and hBN, $\theta$ = 0.7-0.8° and the moiré superlattice size ~11 nm. In the conference, we will discuss the detail of quantum transport properties of the sample in magnetic fields.

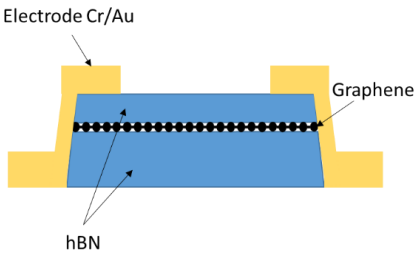


Fig. 1. Structure of hBN/graphene/hBN device with one-dimensional edge contacts.

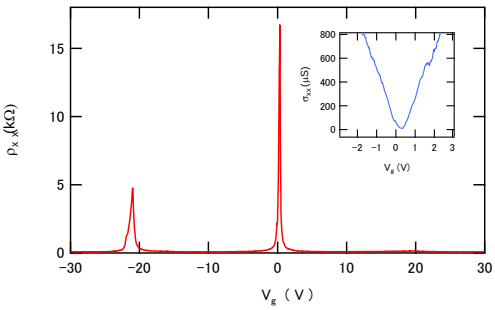


Fig. 2. Back-gate voltage dependence of resistivity ($\rho_{xx}$) and conductivity ($\sigma_{xx}$) near the Dirac point (inset).

[1] C. R. Dean et al., Nature 497, 598 (2012)
[2] L. A. Ponomarenko et al., Nature 497, 594 (2013).
[3] G. L. Yu et al., Nature Physics 10, 525 (2014).
[4] B. Hunt et al., Science 340, 1427 (2013).
[5] A. V. Kretinin et al., Nano Letters 14, 3270 (2014).

# Negative Compressibility of the Bubble and Stripe Phases in the Quantum Hall Regime

Benedikt Friess[1], Vladimir Umansky[2], Bernd Rosenow[3], Yang Peng[4], Felix von Oppen[4], Klaus von Klitzing[1], and Jurgen Smet[1]

[1] *Max Planck Institute for Solid State Research, Stuttgart, Germany*
[2] *Weizmann Institute of Technology, Rehovot, Israel*
[3] *University of Leipzig, Leipzig, Germany*
[4] *Freie Universtät Berlin, Berlin, Germany*
*e-mail: b.friess@fkf.mpg.de*

Physical systems which are subject to competing interactions acting on different length scales often evolve in geometrical patterns such as bubbles and stripes. Also in the quantum Hall regime such patterns are believed to appear as a modulation of the charge density due to the competition between the repulsive direct Coulomb interaction and the attractive exchange interaction [1]. So far, these density modulated phases have been studied mostly by resistance measurements [2]. Characteristic transport signatures are a reappearance of the integer quantum Hall effect for the bubble phase and strong resistance anisotropy in case of the stripe phase (Fig. 1a).

Here, we pursue a different approach to measure the conductivity in the bubble and stripe phases based on surface acoustic waves (SAW). The periodic movement of the sound wave traveling along the surface of the sample causes an oscillating electric field in the piezoelectric GaAs/AlGaAs heterostructure. Depending on the conductivity of the electronic system, the electrons will screen this electric field more or less effectively, which can be detected as a phase shift of the SAW. Perfect screening corresponds to zero phase shift. Poor screening causes a positive phase shift. We have used this technique to probe the conductivity along the perpendicular crystal directions [110] and [1-10] (Fig. 1b). Interestingly, the measurement reveals strong, distinct features for both types of charge density waves. For the stripe phase, a strong anisotropy is evident also in the SAW transmission. Surprising is the observation of a negative phase shift for both the bubble and the stripe phase. Such a slowing-down of the surface acoustic wave has not been observed so far. We attribute it to an overscreening of the SAW caused by the negative compressibility of the electron system in the bubble and stripe phase. Plausible alternative interpretations were addressed, but it was possible to exclude them. Also the fragile reentrant states in the second Landau level exhibit negative compressibility. Our experiments clearly indicate the presence of an attractive interaction between the charge carriers in the bubble and stripe phases.

[1] M. M. Fogler, A. A. Koulakov, and B. I. Shklovskii, Phys. Rev. B 54, 1853 (1996). A. A. Koulakov, M. M. Fogler, and B. I. Shklovskii, Phys. Rev. Lett. 76, 499 (1996).
[2] R. R. Du et al., Solid State Commun. 109, 389 (1999). M. P. Lilly et al., Phys. Rev. Lett. 82, 394 (1999). K. B. Cooper et al., Phys. Rev. B 60, 285 (1999).

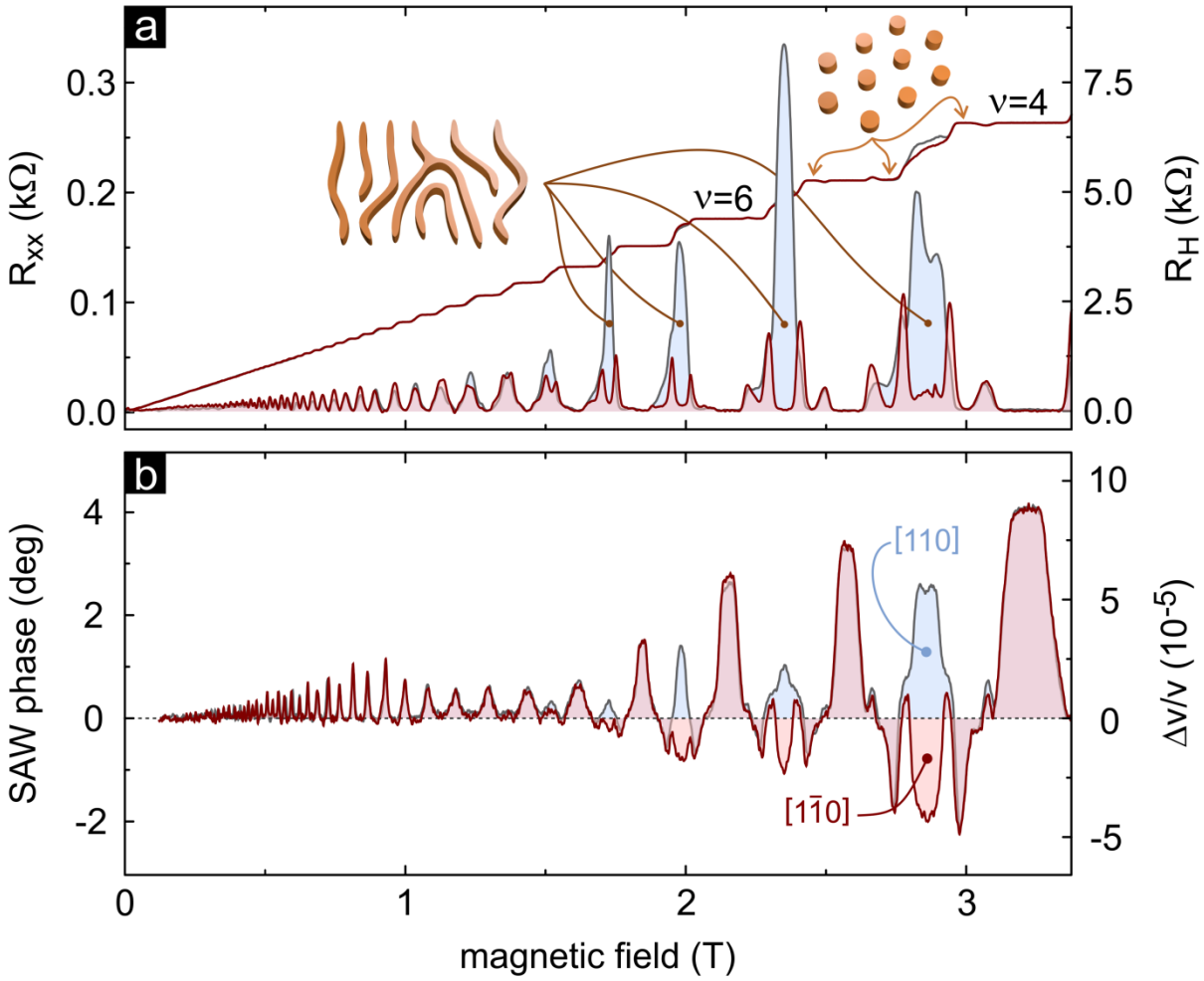


Fig.1 (a) Longitudinal and Hall resistance as a function of the magnetic field along the orthogonal crystal directions [110] (blue) and [1-10] (red). (b) Phase shift and velocity change of surface acoustic waves.

# Superconductivity Induced Topological Phase Transition at the Edge of Even Denominator Fractional Quantum Hall States

Maissam Barkeshli and Chetan Nayak

*Station Q, Microsoft Research, Santa Barbara, CA 93106-6105, USA*
*e-mail: mbarkeshli@gmail.com*

We show that every even-denominator fractional quantum Hall (FQH) state possesses at least two robust, topologically distinct gapless edge phases if charge conservation is broken at the boundary by coupling to a superconductor. The new edge phase allows for the possibility of a direct coupling between electrons and emergent neutral fermions of the FQH state. This can potentially be experimentally probed through geometric resonances in the tunneling density of states at the edge, providing a probe of fractionalized, yet electrically neutral, bulk quasiparticles. Other measurable consequences include a charge e fractional Josephson effect, a charge e/4q quasiparticle blocking effect in filling fraction p/2q FQH states, and modified edge electron tunneling exponents.

[1] M. Barkeshli and C. Nayak, arXiv: 1507.06305

# Spin-split and spin-unpolarized incompressible strips revealed by optical local spin injection

S. Nomura,[1], S. Mamyouda,[1] H. Ito,[1] Y. Shibata,[1] Y. Ootuka,[1]
S. Kashiwaya,[2] M. Yamaguchi,[3] H. Tamura[3] and T. Akazaki[3]

[1]*Division of Physics, University of Tsukuba, Tsukuba, Ibaraki 305-8571, Japan*
[2]*National Institute of Advanced Industrial Science and Technology, Tsukuba, Ibaraki 305-8568, Japan*
[3]*NTT Basic Research Laboratories, Atsugi, Kanagawa 243-0198, Japan*
*e-mail:nomura.shintaro.ge@u.tsukuba.ac.jp*

We report on our findings of a clear evidence for the formation of spin-split incompressible strips induced by the exchange energy enhanced spin-gap as revealed by local spin injection using a circularly polarized near-field scanning optical microscope (CP-NSOM) in a dilution refrigerator [1]. An NSOM has not been used for illumination of circularly polarized light because small tensions or torsions at an NSOM probe tip often provoke strain-induced birefringence. We have succeeded in fabricating probe tips with small disturbance of the polarization and in systematically controlling the polarization of the light emitted from the probe tip.

Figures 1(a) and 1(b) show degree of polarization of the first spatial derivative of photovoltage $P_+$ for $B > 0$ and $P_-$ for $B < 0$, respectively, measured by locally illuminating near the edge of a Hall-bar structure of a GaAs/$Al_{0.3}Ga_{0.7}$As single heterojunction sample. Black and white curves are the positions of the spin-unpolarized and polarized incompressible strips calculated based on a local-spin-density approximation formalism [2] for a fourth order polynomial confinement potential. Remarkably, we have found that $|P_\pm|$ is close to unity along the position of the spin-split incompressible strips (white dashed curve). By contrast, $|P_\pm|$ along the position of the spin-unpolarized incompressible strips is small (black curve). Calculated electron occupations near the Fermi-level in Fig. 2 indicate that the positions of the incompressible strips of our sample are better reproduced by using a fourth order polynomial confinement potential than a parabolic confinement potential. Our CP-NSOM opens up new opportunities to study spin-related phenomena in a variety of nanostructures. In particular, our results may contribute to studies of spin-valley couplings in transition metal dichalcogenide thin films, chiral molecules, and the edge states in the topological insulators.

[1] S. Mamyouda, H. Ito, Y. Shibata, S. Kashiwaya, M. Yamaguchi, T. Akazaki, H. Tamura, Y. Ootuka, and S. Nomura, Nano Lett. **15**, 2417 (2015).

[2] S. Nomura, S. Mamyouda, H. Ito, Y. Shibata, T. Ohira, L. Yoshikawa, Y. Ootuka, S. Kashiwaya, M. Yamaguchi, H. Tamura, and T. Akazaki, Appl. Phys. A, (published online, DOI 10.1007/s00339-015-9420-9, 2015).

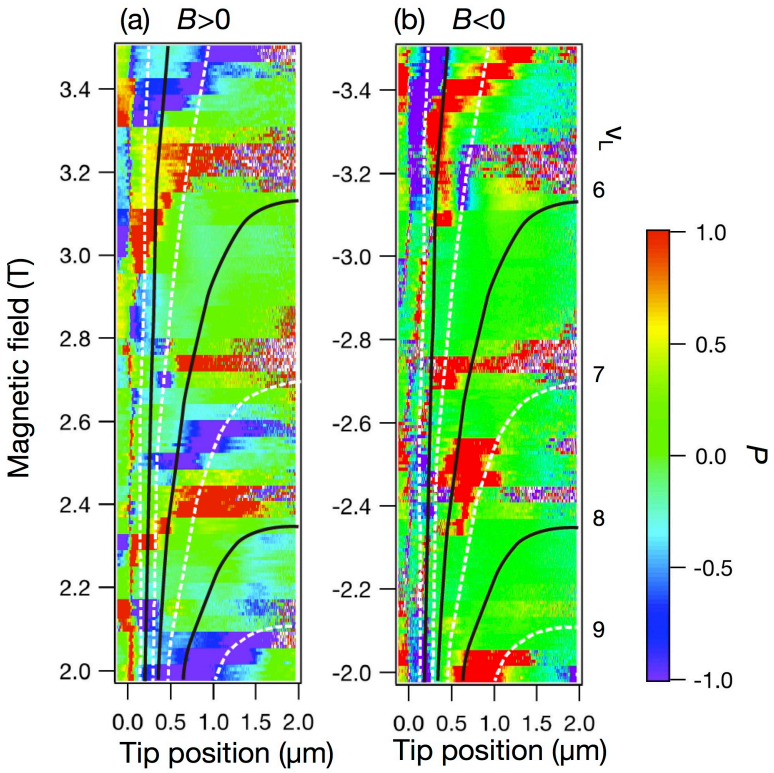


**Figure 1.** (a) Degree of polarization of the first spatial derivative of photovoltage $P_+$ for $B > 0$ and (b) $P_-$ for $B < 0$. Black and white curves are the positions of the spin-unpolarized and polarized incompressible strips as derived from Fig. 2(a) for a fourth order polynomial confinement potential. Adapted with permission from [1]. Copyright (2015) American Chemical Society.

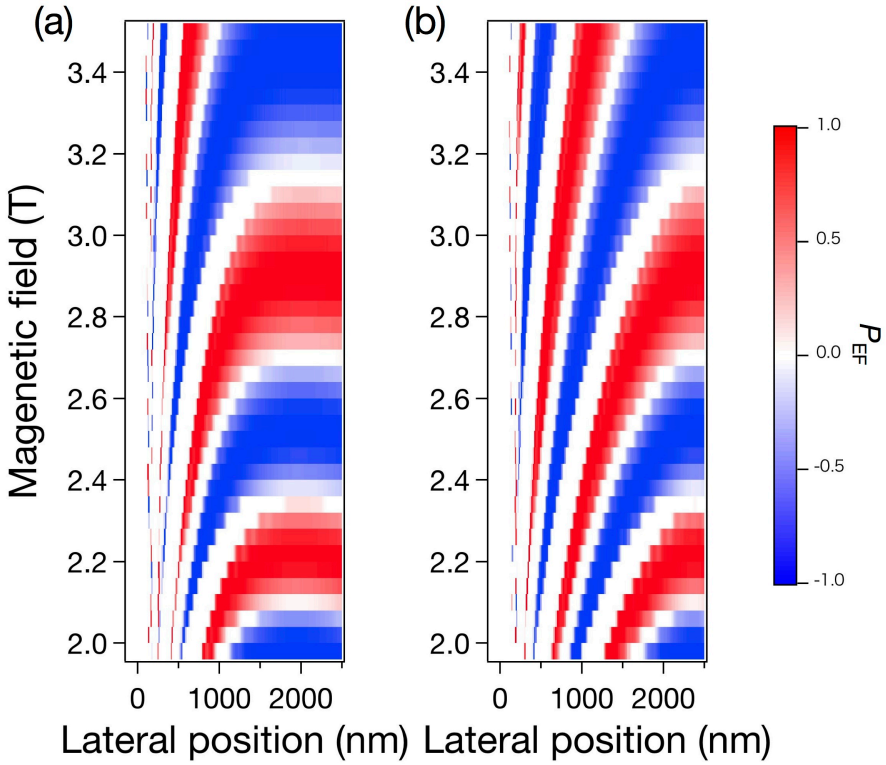


**Figure 2.** Calculated electron occupations near the Fermi level ($P_{EF}$) for (a) fourth-order polynomial and (b) parabolic confinement potentials as functions of lateral position from the edge of the sample and magnetic field. $P_{EF}$=1 (-1) indicates that the electrons at the Fermi level is fully polarized to up- (down-) spin.

# Nuclear Electric Resonance and its Application to Magnetic Resonance Imaging

K. Hashimoto[1], T. Tomimatsu[1*], S. Shirai[1], K. Sato[1], and Y. Hirayama[1,2]

[1]*Graduate School of Science, Tohoku University, Sendai, Miyagi, Japan*
[2] *WPI-AIMR, Tohoku University, Sendai, Miyagi, Japan*
**Present address; The University of Electro-Communications, Chofu, Tokyo, Japan*
*e-mail: hirayama@m.tohoku.ac.jp*

The resistively-detected nuclear magnetic resonance (NMR) has been widely used as a highly sensitive tool to detect electron spin physics and electron-nuclear spins interactions in quantum Hall systems. However, conventional NMR based on a radio-frequency (RF) magnetic field generated by a coil has drawbacks of poor spatial resolution and Joule heating. To overcome these issues, it is desirable to develop nuclear resonance mediated by RF electric field oscillation. Such nuclear electric resonance (NER), which was already reported in bulk GaAs systems [1], are recently extended to the two-dimensional quantum Hall systems [2].

In the experiment, nuclear polarization and detection were carried out by using quantum Hall breakdown at $\nu = 1$. The RF voltage was superimposed on a DC backgate bias for NER. The obtained NER spectra clearly indicates the unique characteristics for the NER caused by electric quadrupole interaction, i.e., a reduction of the central line intensity among the three quadrupolar-split lines of $^{75}$As with $I = 3/2$ and appearance of the resonance at twice the precession frequency.

We measured NER characteristics at various filling factors. Differently from the conventional NMR, the NER signal strongly depends on whether electronic states are localized or extended, suggesting important role of the screening ability of the quantum Hall systems for NER.

The NER using a scanning nanoprobe as a local gate instead of the backgate enables us magnetic resonance imaging (MRI) of the quantum Hall properties. We have succeeded to obtain a two-dimensional plot of the NER signal near $\nu = 1$ quantum Hall breakdown regime [3]. The obtained images provide us a hint to understand the breakdown characteristics and related nuclear polarization.

[1] For example, E. Brun, R. J. Mahler, H. Mahon, and W. L. Pierce, Phys. Rev. 129, 1965 (1963).

[2] T. Tomimatsu, S. Shirai, K. Hashimoto, K. Sato, and Y. Hirayama, AIP Advances **5**, 087156 (2015).

[3] K. Hashimoto, S. Shirai, T. Tomimatsu, S. Taninaka, K. Nagase, K. Sato, and Y. Hirayama, EP2DS/MSS Tu-B3-5 (2015).

# Spotting the elusion Majorana under the microscope

Ali Yazdani

*Department of Physics, Princeton University, Princeton, NJ 08540*
*e-mail: yazdani@princeton.edu*

Topological superconductors are a distinct form of matter that is predicted to host boundary Majorana fermions. The search for Majorana quasi-particles in condensed matter systems is motivated in part by their potential use as topological qubits to perform fault-tolerant computation aided by their non-Abelian characteristics. Recently, we have proposed a new platform for the realization of Majorana fermions in condensed matter, based on chains of magnetic atoms on the surface of a superconductor. This platform lends itself to measurements with the scanning tunneling microscope (STM) that can be used to directly visualize the Majorana edge modes with both high energy and spatial resolution. Using rather unique STM instrumentation, we have succeeded in creating this platform and have observed the predicted signatures of localized Majorana edge modes. I will describe our Majorana platform, the experiments to date, and the outlook for further experiments on Majorana fermions in our platform.

[1] S. Nadj-Perge, I. Drosdov, A. Bernevig, A. Yazdani, Physical Review B, Rapid Communication, 88, 020407 (2013).

[2] S. Nadj-Perge, I. K. Drozdov, J. Li, H. Chen, S. Jeon, J. Seo, A. H. MacDonald, B. A. Bernevig, A. Yazdani, Science 346, 6209 (2014).

{3] J. Li, H. Chen, I. K. Drozdov, A. Yazdani, B. A. Bernevig, A. H. MacDonald, Physical Review B 90, 235433 (2014).

# Probing Spin-Orbit Coupling in Superconducting Junctions: From Spintronics to Majorana Fermions

Igor Žutić[1], Petra Hoegl[2], Alex Matos-Abiague[1,2], and Jaroslav Fabian[1]

[1] *Department of Physics, University at Buffalo, State University of New York, Buffalo, NY 14260, USA*

[2]*Institute for Theoretical Physics, University of Regensburg, 93040 Regensburg, Germany*

*e-mail: zigor@buffalo.edu*

Spin-orbit coupling (SOC) is a key interaction in spintronics [1-3], allowing an electrical control of magnetization and, vice versa, a magnetic control of electrical current. Such SOC determines the timescales and lengthscales over which spin information is preserved. In systems lacking space inversion symmetry (bulk, hybrid structures, or junctions) SOC induces spin-orbit fields [1, 2]. These fields are responsible for many intriguing phenomena, not existent or fragile in the bulk, such as the tunneling magnetoresistance (TAMR), interfacial spin-orbit torque, skyrmions, and Majorna fermions. In ferromagnet/superconductor (F/S) junctions we investigate the interplay of magnetism and spin-orbit fields [4]. We show that this interplay leads to marked anisotropies in the junction conductance with respect to the orientation of magnetization. We examine the influence of SOC and crystalline anisotropy on the process of Andreev reflection (AR) in which the reflected particle carries the information about both the phase of the incident particle and the macroscopic phase of the superconductor to which a Cooper pair is being transferred [1,3]. While the main interest in AR is currently the proximity effect coupled with SOC, inducing Majorana states, in spintronics AR is used to probe the spin polarization in F/S junctions [1,3]. We reveal that AR can also be a sensitive probe of interfacial spin-orbit fields [4]. We predict a giant magnetoanisotropy of the junction conductance, even orders of magnitude larger than its normal state counterpart –TAMR. If the F is highly spin-polarized the magnetoanisotropic AR (MAAR) depends universally on the spin-orbit fields only [4]. The predicted magnetization control of the AR suggests a similar control of the superconducting proximity effect and Majorana states.

[1] I. Žutić, J. Fabian, and S. Das Sarma, Rev. Mod. Phys. **76**, 323 (2004).

[2] J. Fabian, A. Matos-Abiague, C. Ertler, P. Stano, and I. Žutić, Acta Phys. Slov. **57**, 565 (2007).

[3] E. Y. Tsymbal and I. Žutić, eds., *Handbook of Spin Transport and Magnetism* (CRC Press, New York, 2011).

[4] P. Hoegl, A. Matos-Abiague, I. Žutić, and J. Fabian, Phys. Rev. Lett. (in press), arXiv:1502.08022

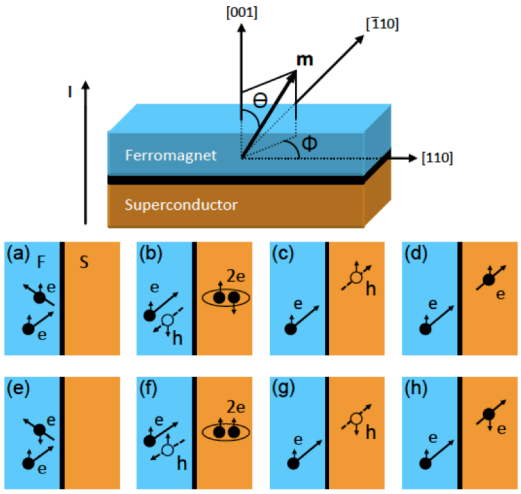


Top: F/S junction. Magnetization vector **m** is given by the polar angle Θ and azimuthal angle Φ. Current, **I**, flows perpendicular to the interface. To specify spin-orbit fields we use principal crystallographic orientations. Bottom: Scattering processes at the F/S interface with SOC. Electrons (holes) are depicted by full (empty) circles. Vertical arrows denote the spin. The processes for a spin up incoming electron: (a) Specular reflection, (b) AR, (c) hole-like transmission, and (d) electron-like transmission. (e)-(h) Corresponding spin-flip counterparts. Spin-flip AR is in (f).

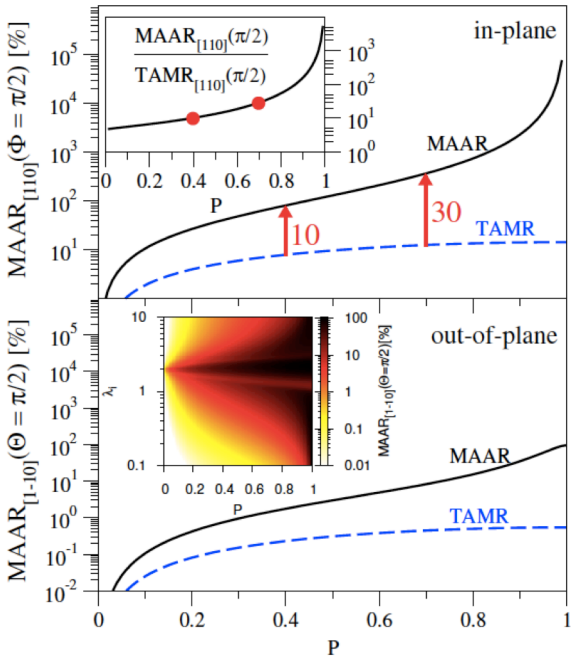


Calculated in-plane (top) and out-of- plane (bottom) magnetoanisotropic AR (MAAR) and tunneling magnetoresistance (TAMR) as a function of spin polarization P for a moderate barrier (Z = 1) and bias V = 0. The in-plane case is calculated with $\lambda\alpha = \lambda\beta = 1$, while for out-of-plane we have included Rashba SOC $\lambda\alpha = 0.5$ only. The top inset shows the ratio of MAAR and TAMR for the in-plane case, while the bottom inset shows the color map of out-of plane MAAR as a function of P and Rashba (or Dresselhaus) SOC $\lambda i$ (where i could be either $\alpha$ or $\beta$).

# Stability and Properties of Disordered Weyl Semimetal Phases

Hassan Shapourian[1], and Taylor L. Hughes[1]

[1] Department *of Physics and Institute for Condensed Matter Theory, University of Illinois at Urbana-Champaign, Urbana, Illinois 61801, USA*
*e-mail: hughest@illinois.edu*

Weyl semimetals are gapless topological materials with a set of isolated nodal points forming their Fermi surface. They manifest their topological character in a set of electromagnetic responses including the anomalous Hall effect, and through the existence of surface-state Fermi-arcs. Here we study the effect of disorder on Weyl semimetals while monitoring both their semi-metallic and topological response properties. We compute the longitudinal and Hall conductivities, as well as other diagnostic quantities in order to determine the stability and phase diagrams of Weyl semimetals. To this end we have examined three different models that realize a Weyl semimetal in part of their phase diagrams. Surprisingly, we find that there are regions of the phase diagrams where disorder enhances the properties of the Weyl semimetal phase, as well as regions where the phase is weakened and finally destroyed. We discuss the underlying reasons for this varied behavior, and indicate future directions for investigation.

# Surface States or Electron Fractionalization in Bismuth

Philip Phillips

*University of Illinois at Urbana-Champaign*

Electrons in a metal subject to magnetic fields commonly exhibit oscillatory motion with a period set by the area of the quantized electron orbits. Several years ago, Behnia and colleagues[1] observed oscillations in Bi up to 9T that did not follow the simple dependence and interpreted their results as evidence for electron fractionalization in a bulk 3D material. If this is true, this would be the first instance of electron fractionalization in bulk 3D material. I will critique in this talk the surface state theory[2] we constructed to explain the experimental observations as well as highlight the recent experiments that have been done to settle the debate between bulk oscillations and surface state quantization in elemental Bismuth. The recent experiments[3] indicate that while surface states of Bi can dominate the transport for Bi bilayers as thick as 64Å, bulk transport ensues beyond this limit. The experiments of Behnia and colleagues are reinterpreted in light of this recent crossover.

## References

[1] K. Behnia, L. Balicas, and Y. Kopelevich, Science **31**, 1729 (2007).

[2] B. Seradjeh, J. Wu and P. Phillips, Phys. Rev. LEtt. **103**, 136803 (2009).

[3] M. Aitani, T. Hirahara, S. Ichinokura, M. Hanaduka, D. Shin, and S. Hasegawa, Phys. Rev. Lett. **11**, 206802(2014).

# Non-uniform magnetic structures and anisotropic spin wave dispersion in Dirac semimetals

Yasufumi Araki[1,2], Kentaro Nomura[1]

[1] *Institute for Materials Research, Tohoku University, Sendai 980-8577, Japan*
[2] *Frontier Research Institute for Interdisciplinary Sciences, Tohoku University, Sendai 980-8578, Japan*
*e-mail: araki@imr.tohoku.ac.jp*

Recent realizations of Dirac semimetallic states in three dimensions have opened a new way to access various nontrivial magnetoelectric and transport properties characterized by the quantum anomaly of the Dirac nodes [1]. Control of the magnetism by the spin-momentum locked Dirac carriers is one of the important questions in Dirac semimetals for spintronic applications.

We study the behavior of background magnetic structure formed by localized magnetic moments in three-dimensional Dirac semimetals, in terms of the effective field theory of the local magnetization [2]. The effective Hamiltonian, derived by integrating out the carrier degrees of freedom, has an anisotropic structure correlating the real and spin spaces to each other, reflecting the spin-momentum locking nature in the Dirac Hamiltonian. Such an anisotropy becomes stronger around the vanishing density of states (Dirac nodes), preferring not only the uniform ferromagnetism but also topologically nontrivial vortex-free structures, like the “hedgehog” and “coaxial” ones, as the ground state (see Fig.1).

We further investigate the characteristics of spin waves in the ferromagnetic state. We find the spin wave less dispersed in the direction perpendicular to the magnetization than that in the longitudinal direction. This anisotropic spin wave dispersion implies that the ferromagnetic structure is rather flexible against the transverse bending in Weyl semimetals (see Fig.2), which is a straightforward consequence from the structure of the effective field theory. We discuss the stability of the magnetic structure and the possibility of magnetic phase transitions in this system.

[1] Z. K. Liu *et al.*, Science **343**, 864 (2014); Z. K. Liu *et al.*, Nat. Mater. **13**, 677 (2014); M. Neupane *et al.*, Nat. Commun. **5**, 3786 (2014); S. Borisenko *et al.*, Phys. Rev. Lett. **113**, 027603 (2014).
[2] Y. Araki and K. Nomura, *paper in preparation*.

Figures:

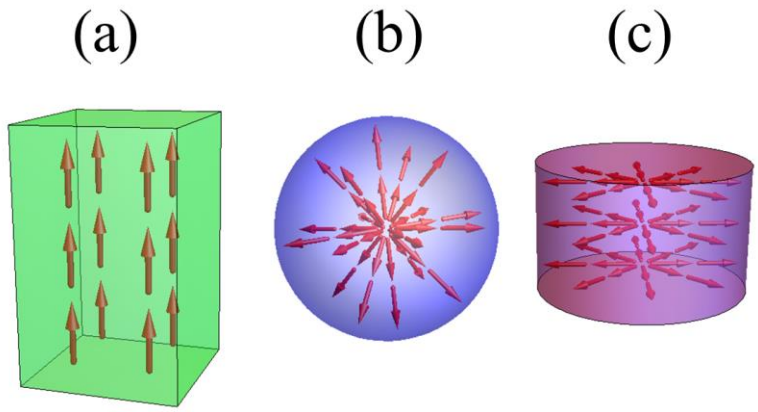


Fig.1: Possible magnetic structure under the effective Hamiltonian derived in this work: (a) ferromagnetic, (b) “hedgehog”, and (c) “coaxial” structures.

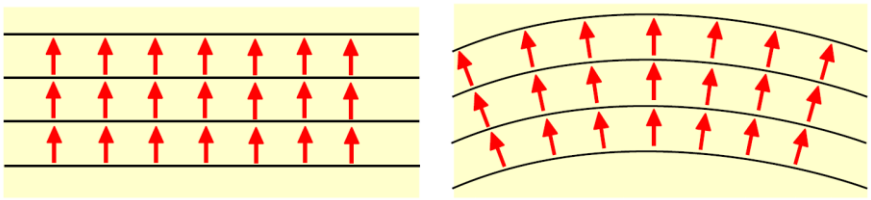

Fig.2: Ferromagnetic structure (left) and that slightly bent in the transverse direction (right). The ferromagnetic structure in Weyl semimetals is rather flexible against the transverse bending.

# Writing superconductivity in bismuth selenide by controlled local doping

J. T. Mlack[1,2], Atikur Rahman[1,3], Natalia Drichko[1] and Nina Markovic[1,4]

[1] *Department of Physics and Astronomy, Johns Hopkins University, Baltimore, MD, USA*
[2] *Department of Physics and Astronomy, University of Pennsylvania, Philadelphia, PA, USA*
[3] *Brookhaven National Laboratory, NY, USA*
[4] *Department of Physics and Astronomy, Goucher College, Towson, MD, USA*

*e-mail: nina@pha.jhu.edu*

Bismuth selenide is a topological insulator with topologically protected metallic surface states that exhibit a spin texture and a Dirac-like dispersion. The unique properties of these states offer possibilities for creating a variety of novel nanoscale spintronic and electronic devices. Of particular interest is the creation and manipulation of Majorana fermions, which has the potential to revolutionize quantum information applications. While bismuth selenide is a promising platform for these applications, the required high-quality interfaces with superconductors are not trivial to obtain. I will describe our recent experiments on controllable local doping of bismuth selenide by palladium atoms. We find that superconductivity can be "written" directly into the bismuth selenide, with the resolution limit set by electron beam lithography. Measurements of resistance as a function of temperature and magnetic field in Pd-doped bismuth selenide, combined with Raman spectroscopy, indicate that superconductivity is localized in the targeted areas. Depending on the level of doping, we observe either partial or full superconducting transition, with an unusual subgap structure. I will discuss the origin and the nature of superconductivity in this doped topological insulator and the possible applications in novel devices.

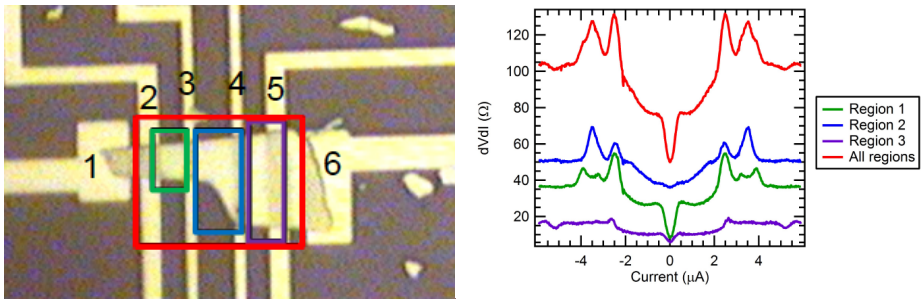

# Transport in Topological Insulators and Topological Superconductors: In Search of Majorana Fermions

Ewelina M. Hankiewicz

*Institute for Theoretical Physics, Wurzburg University,*
*Am Hubland, Wurzburg 97074, Germany.*

Topological insulators (TIs) have a bulk energy gap that separates the highest occupied band from the lowest unoccupied band while gapless energy electronic states that are protected by time reversal symmetry live at the edge (2D TIs) or surface (3D TIs) [1]. Similarly, topological superconductors have gapless zero energy states protected by the particle-hole symmetry, which in some cases form Majorana bound states. In this talk, we focus on the proximity-induced superconductivity in Tis [2,3] as well as on unusual properties of topological superconductors [4] showing that they both can pave a road to find a Majorana state.

Concerning proximity-induced superconductivity in TIs, we describe a novel superconducting quantum spin-Hall effect (quantum spin Hall system in the proximity to the s-wave superconductor and in the orbital in-plane magnetic field), which is protected against elastic backscattering by combined time-reversal and particle-hole symmetry [2]. This effect is characterized by spin-polarized edge states, which can be manipulated in weak magnetic fields due to a giant effective orbital g-factor, allowing the generation of spin currents. The phenomenon provides a novel solution to the outstanding challenge of detecting and generating the spin-polarization of the edge states. We discuss unusual transport properties of superconducting quantum Hall effect and possible Majorana detection schemes through a non-monotonic excess current and a zero-bias conductance splitting.

Finally, we discuss new systems like topological superconductors on the hexagonal lattices. We develop combined microscopic and macroscopic description of these materials that predicts realistic scanning tunnelling microscopy signal in these superconductors [4]. Is there a way to measure Majorana state in these systems?

[1] G. Tkachov and E. M. Hankiewicz, topical review in *Phys. Status Solidi B* **250**, 215 (2013).
[2] R. Reinthaler, G. Tkachov and E.M. Hankiewicz, arXiv:1502.07521 (2015) , accepted to *Rapid Comm.*
[3] I. Sochnikov, L. Maier, C. A. Watson, J. R. Kirtley, C. Gould, G. Tkachov, E. M. Hankiewicz, C. Brüne, H. Buhmann, L. W. Molenkamp, and K. A. Moler, *Phys. Rev. Lett.* **114**, 066801 (2015).
[4] L. Elster, C. Platt, R. Thomale, W. Hanke, and E. M. Hankiewicz, *Nature Comm.* **6**, 8232 (2015).

# Nanoscale optical studies of band potential fluctuations and lateral carrier diffusion in semipolar InGaN/GaN quantum wells

Saulius Marcinkevičius[1], Mounir Mensi,[2] Ruslan Ivanov,[1] Daniel L. Becerra,[2] Shuji Nakamura,[2] Steven P. DenBaars,[2] and James S. Speck[2]

[1] *KTH Royal Institute of Technology, Department of Materials and Nanophysics, Electrum 229, 16440 Kista, Sweden*

[2] *Materials Department, University of California, Santa Barbara, California 93106, USA*

*e-mail: sm@kth.se*

A common feature for ternary nitride semiconductors are band potential fluctuations, which are typically assigned to spatial variations of alloy composition, quantum well (QW) width, strain and defects. Such fluctuations may have different consequences on nitride device performance. In some cases, carrier localization at band potential fluctuations separates carriers from extended defects reducing the nonradiative recombination, in other - the localization occurs at domain boundaries with a larger defect concentration. Carrier localization also broadens the emission spectrum reducing the modal gain. Thus, detailed understanding of the origin of potential fluctuations, their manifestation in single and multiple QW structures and their relation to properties of material growth and defects is important for the development of efficient light emitting devices. Since fluctuations occur on the nanoscale, optical techniques with resolution overcoming the diffraction should be used. Photoluminescence (PL) measurements using scanning near-field optical microscopy is a suitable technique for such material characterization.

In this work, scanning near-field PL spectroscopy has been applied to study semipolar (20-21) plane $In_xGa_{1-x}N$/GaN quantum wells that are promising for applications in green semiconductor lasers and LEDs. Single and multiple QWs and wells of different widths were explored. The investigations have shown that optical properties of individual wells in multiple QW structures are very similar and band potential fluctuations are uncorrelated between the wells. Measurements on QWs of different widths allowed distinguishing the primary origin of the inhomogeneous broadening between alloy composition and well width variations induced by non-planarity of QW interfaces [1]. Experiments with simultaneous measurement of PL signal through the exciting probe and in the far-field allowed evaluating parameters of the lateral carrier diffusion. Such dual detection measurements are quite unique and might be useful for studies of carrier transport in other inhomogeneous systems.

[1] Y. Zhao et al., Appl. Phys. Express **7**, 025503 (2014).

# Designing a Binary Random Phase Array to Improve the Light Extraction Efficiency of White Organic Light-Emitting Devices

Akira Hashiya, Yasuhisa Inada, and Taku Hirasawa

*Advanced Research Division, Panasonic Corporation, 1006 Kadoma, Kadoma City, Osaka 571-8501, Japan*
*e-mail: hashiya.akira@jp.panasonic.com*

White organic light-emitting devices (WOLEDs) have attracted much attention due to their thin, flat shape and flexibility. Many studies have demonstrated the high internal quantum efficiencies of electroluminescence; however, the light extraction efficiencies of conventional WOLEDs with flat surfaces are low, since the emitted light is confined to the organic layer and the substrate due to total reflection. We have developed a binary random phase array (BRPA) that can control the divergence angle of light scattering by adjusting its dimensions to improve the extraction efficiency of WOLEDs [1].

In this presentation, we describe how we designed the geometry of a random array to optimize the extraction efficiency of WOLEDs. Our design method was based on tuning the spatial frequency spectrum to control the direction of scattering. We calculated the relationship between the scattering angle and the extraction efficiency and discovered that low-angle scattering makes little contribution to enhancing the extraction efficiency. The new BRPA pattern was designed to contain fewer low-frequency components and, therefore, it generates directional scattering. Figure 1 shows images of conventional and the new BRPA patterns (Fig. 1(a, b)) with spatial frequency spectrum (Fourier transformation) shown (Fig. 1 (c, d)). We confirmed that the WOLED with the developed BRPA showed higher extraction efficiency.

[1] Y. Inada *et al.*, Appl. Phys. Lett, **104**, 063301 (2014).

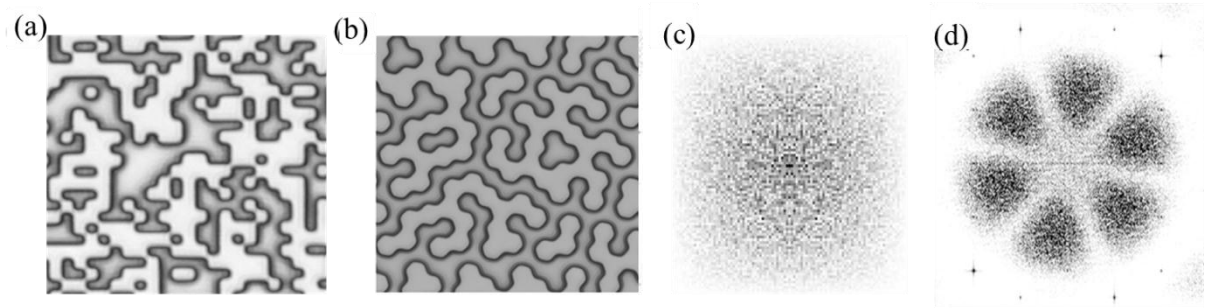


**Figure 1**. Microscope images of (a) conventional and (b) new BRPA,
the 2D spatial frequency spectrum of (c) a conventional and (d) new BRPA

# Quantum processes of exciton dissociation at organic solar-cell interfaces; Effects of interface disorder, hot exciton, and polaron

Takashi Nakayama, Hideyuki Iizuka, and Yoshimitsu Masugata

*Department of Physics, Chiba University, Inage, Chiba 263-8522, Japan*
*e-mail: nakayama@physics.s.chiba-u.ac.jp*

Exciton dissociation at donor/acceptor-molecule interfaces is one of key processes to generate electron and hole carriers in various organic solar-cell systems. Recent experiments showed that the control of interface roughness and higher-energy excitation (hot exciton) is important to increase the energy-conversion efficiency [1,2]. Moreover, the polaron (carrier-vibration) interaction is recognized essential to understand the carrier behavior in organic systems [3]. However, most of previous theoretical studies do not consider these features. In this work, we study the quantum processes of exciton dissociation at organic hetero-interfaces, by using one/two-dimensional tight-binding models (Fig.inset) [4] and calculating time-evolution of electron-hole-pair wave packet, and clarify how the interface-disorder, hot-exciton, and polaron effects change the fundamental process of exciton dissociation.

Main results are summarized as follows; (1) When the structural disorders exist at the interface, the dissociation probability is significantly enhanced (See Figure), being in agreement with experiments [1,2]. This occurs due to the remarkable increase of interface area ratio caused by the nm-scale disorders. (2) When the spatial scale of disorders becomes less than the exciton radius, the dissociation decreases again reflecting the localization of exciton around the interface; the electron and hole carriers are pinned at the disordered interface potentials and are difficult to escape from the Coulomb binding. (3) The dissociation probability becomes large for the hot excitons compared to the ground-state exciton due to their small binding energies and large cross section. (4) When the carrier-vibration polaron interaction increases, the dissociation increases because the interaction incessantly deforms the interface potential profile into a gentle slope and decreases the interface carrier reflection. These results are discussed in details, together with comparing to the experiments.

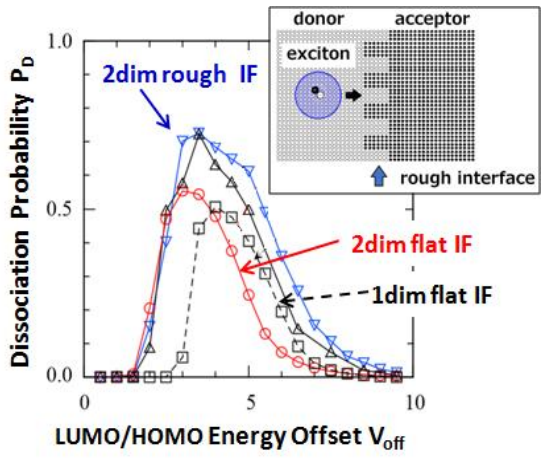


Figure: Dissociation probability of exciton at flat & rough interfaces, as a function of band offset.

[1] W. L. Rance et al., ACS Nano, **5**, 5635 (2011).
[2] J. You et al., Nat. Commun., **4**, 1446 (2013).
[3] H. Ishii et al., Phys. Rev. B**85**, 245206 (2012).
[4] H. Ishii et al., Phys. Rev. B**69**, 085325 (2004).

# Smart stacked heterogeneous multijunction solar cells fabricated by advanced bonding using metal nanoparticle arrays

Takeyoshi Sugaya[1], Kikuo Makita[1], Hidenori Mizuno[1], Toru Mochizuki[1, 2], Ryuji Oshima[1], Jiro Nishinaga[1], Yoshinobu Okano[2], and Koji Matsubara[1]

[1] *National Institute of Advanced Industrial Science and Technology (AIST), 1-1-1 Umezono, Tsukuba, Ibaraki 305-8568, Japan*

[2] *Tokyo City University, 1-28-1 Tamazutsumi Setagaya-ku, Tokyo 158-8557, Japan*

*e-mail: t.sugaya@aist.go.jp*

Cost reduction and improved conversion efficiency are the most important issues facing the wide-scale deployment of solar photovoltaic systems. Although multijunction solar cells have the highest reported efficiencies and have been commercialized for space and concentrator applications, their use has not become widespread due to their high cost. Our objective is to develop advanced multijunction technologies with extremely low cost and high conversion efficiency.

Multijunction solar cells enable ultra high efficiencies due to the effective utilization of a solar spectrum by interconnecting different kinds of solar cells. A traditional fabrication method is a monolithic epitaxial growth technique, which is very difficult and limits the choice of materials and cell combinations. We have developed a novel semiconductor bonding technology (smart stacking technology) to stack different kinds of solar cells with high flexibility.

We have proposed a novel semiconductor bonding technology for mechanically stacked multijunction solar cells by using conductive nanoparticle alignment with low bonding resistances and minimal optical absorption losses as shown in Fig. 1 [1, 2]. This technique is very attractive for interconnecting different kinds of solar cells. We have demonstrated an InGaP(Eg-1.89eV)/GaAs(Eg-1.42 eV)/InGaAsP(Eg-1.05 eV)/InGaAs(Eg-0.75 eV) 4-junction solar cell with a high efficiency of 31.6% under AM1.5. We also demonstrated an InGaP/GaAs/CIGS 3-junction solar cell with an efficiency of 24.2% for the first time. These results suggest that our stacking method is highly useful to realize the ultra-high efficiency multijunction solar cells and various heterogeneous cell combinations, such as III-V, Si, and chalcogenide semiconductors. Moreover, the cost reduction can be expected because we can use inexpensive substrates for high efficiency III-V solar cells.

[1] H. Mizuno, K. Makita, and K. Matsubara, Appl. Phys. Lett. **101**, 191111 (2012).

[2] K. Makita et al., Proc. 29th European Photovoltaic Solar Energy Conf. Exhib., 2014, p. 1427.

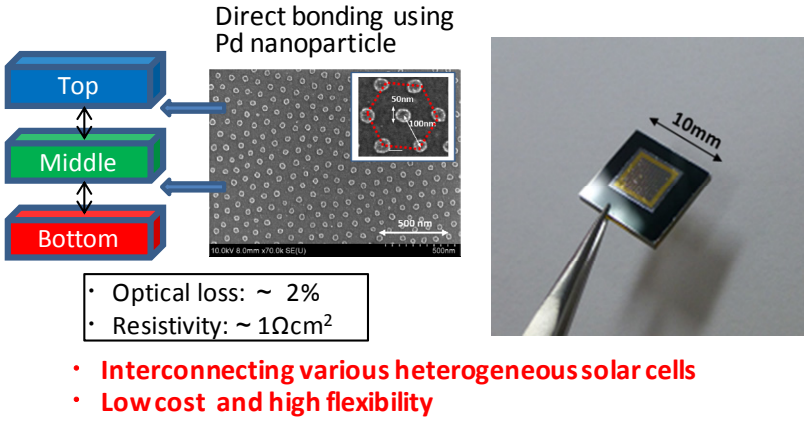


Fig. 1 Schematic drawing of a stacking structure and a photograph of the stacked cell.

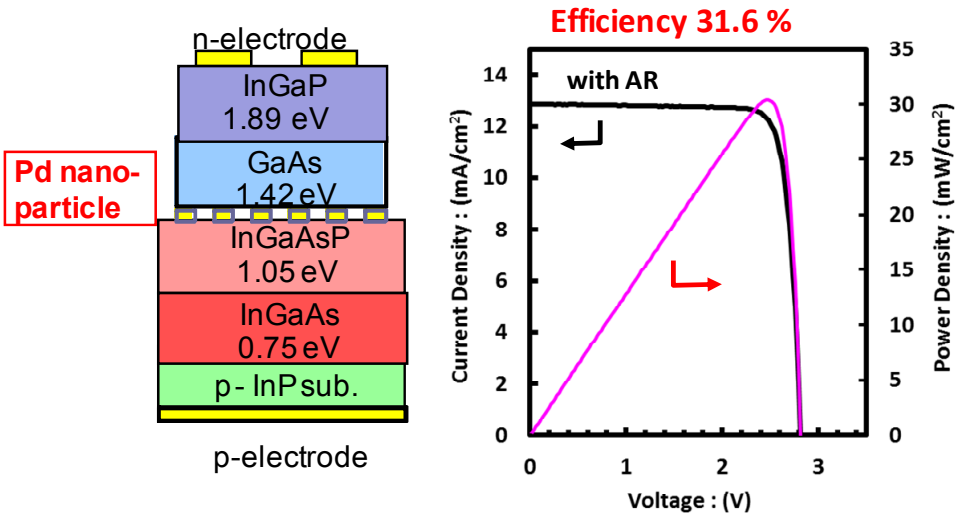


Fig. 2 Schematic layer structure of a 4-junction solar cell and its I-V characteristics.

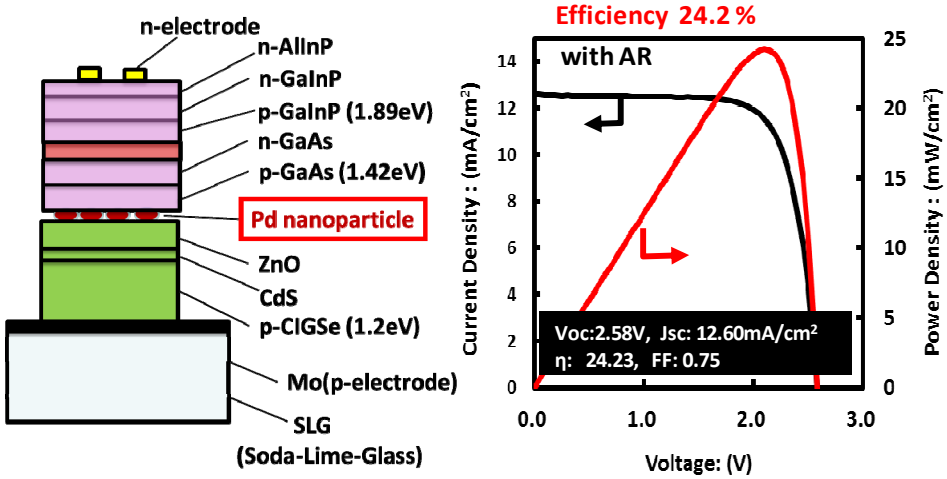


Fig. 3 Schematic layer structure of a CIGS-based 3-junction solar cell and its I-V characteristics.

# III-V dilute nitride solar cells with record open circuit voltages enabled by nanoscale engineering

G.K. Vijaya [1], W. Wang [1], A. Mehrotra [1], D. Tang [2], A. Freundlich[1] , D. J. Smith [2]

[1] *Center for Advanced Materials, University of Houston, Houston TX-USA*
[2] *Physics Department Arizona State University, Tempe AZ-USA*
*e-mail: afreundlich@uh.edu*

Tandem devices based on III-V semiconductors have shown promise for boosting solar cell conversion efficiencies. In particular the use of a bottom subcell made with dilute nitrogen alloys of GaAs has already shown practical conversion efficiencies in the range of 44%. However thus far access to higher efficiencies has suffered from the relatively poor open-circuit voltages associated with these lower bandgap solar cells.

Here we report the demonstration of 1.05 eV- 1.25 eV solar cells with open circuit voltages that exceed significantly the prior art. To make this breakthrough possible we have designed devices that incorporate sets of carefully crafted ultra-thin resonantly coupled multi-quantum wells of dilute nitrides [1]. These devices were fabricated by nitrogen-plasma-assisted molecular beam epitaxy following an optimization of the nitrogen delivery system [2]. Devices fabricated with appropriate carrier extraction design and under optimal growth conditions, exhibit near ideal carrier collection efficiency (QE ~1). Another remarkable feature of these devices is their open circuit voltage that approaches the radiative limit of Eg-0.4eV and suggests potential for boosting the practical efficiency of triple junction solar cells to beyond 49%.

[1] A. Freundlich and A. Alemu, “Thermo-tunneling design for quantum well photovoltaic converter”, United States Patent Application US 13/740,726, publication #20130186458 A1, July 2013

[2] G.K. Vijaya, A. Freundlich, D. Tang, D.J. Smith, “MBE growth of sharp interfaces in dilute-nitride quantum wells with improved nitrogen-plasma design”, J. Vac. Sci. Technol. B 33, #031209, 2015

# Simulation of Carrier Dynamics and Conversion Efficiency of III-V Nanowire Photovoltaic Devices

Raghuraj Hathwar[1], Pietro Luppina[2], Dan Popescu[2], Paolo Lugli[2], and Stephen Goodnick[1,2]

[1] *School of Electrical Computer and Energy Engineering, Arizona State University, Tempe AZ 85287, USA*

[2] *Institute for Advanced Studies and the Institute for Nanoelectronics, the Technical University of Munich, 80333 Munich, Germany*

*e-mail: stephen.goodnick@asu.edu*

Nanowire (NW) based solar cells have emerged in recent years as a promising candidate for next-generation solar cells [1,2]. Some of the potential advantages include the flexibility in materials due to relaxed growth constraints, optical light trapping due to the NWs, and the potential for realizing advanced concepts such as multi-excitation generation (MEG) for exceeding the single gap limits for photovoltaic devices. Here we investigate the short time carrier dynamics in III-V NW devices under varying photoexcitation conditions using full band Cellular Monte Carlo (CMC) simulation as well as drift-diffusion based device simulation based on the 3D geometry of the devices, in to understand the limiting factors affecting solar cell performance. The CMC code is used to simulate the dynamics of photoexcited electrons in the quantum confined states III-V nanowire systems using an atomistic tight binding representation of the nanowires, including scattering processes due to optical and acoustic phonons. Decreased carrier cooling is found due to the reduced density of states and phonon bottleneck effects in very narrow wires, which is advantageous for observing MEG effects. Simulation of the performance of core-shell InGaAs/InP NWs shows reduced open circuit voltage due to the geometry, in agreement with experimental results. Simulations of different doping profiles were performed to examine how they influence the short-circuit current and open circuit voltage. Also different layer thicknesses are simulated and the same figures of merit are calculated. In a final step we place the best nanowire solar cell design in a small array and study the influence of light reflection on the cell performance.

[1] C. Colombo et al., Appl. Phys. Lett., **94**, 173108 (2009).

[2] T. J. Kempa et al., J. American Chem. Soc., **135**, 18354 (2013).

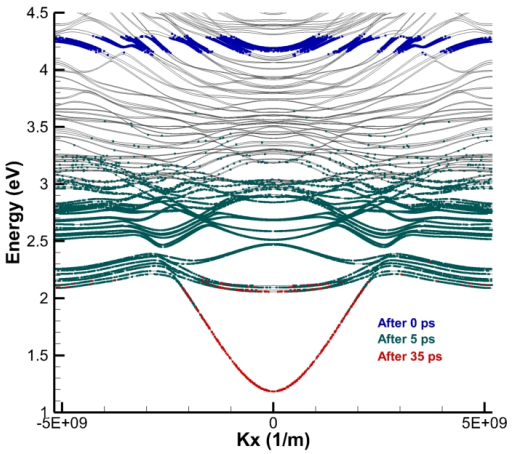


Fig. 1 Carrier relaxation in a 2nm x 2nm InGaAs nanowire at various times after a Gaussian pulse at t=0.

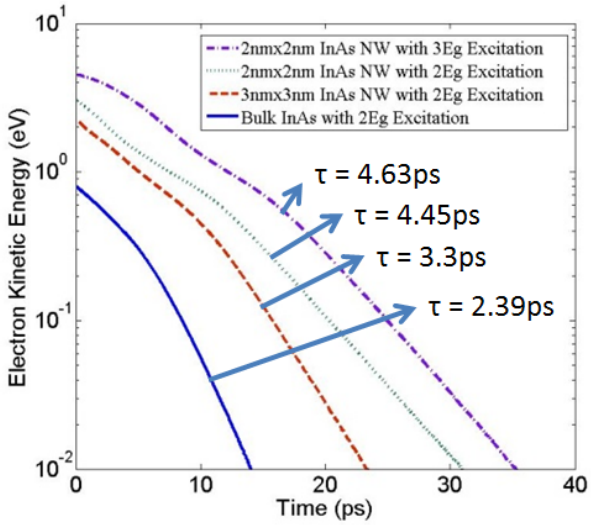


Fig. 2 Energy relaxation rates for several different NW widths and bulk.

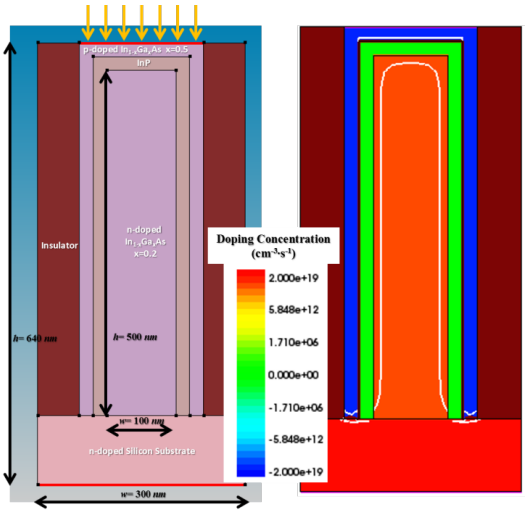


Fig. 3 (Left) Schematic of the simulated core-shell nanowire and (Right) doping profile of the same structure (the n-doping in red, p-doping in blue).

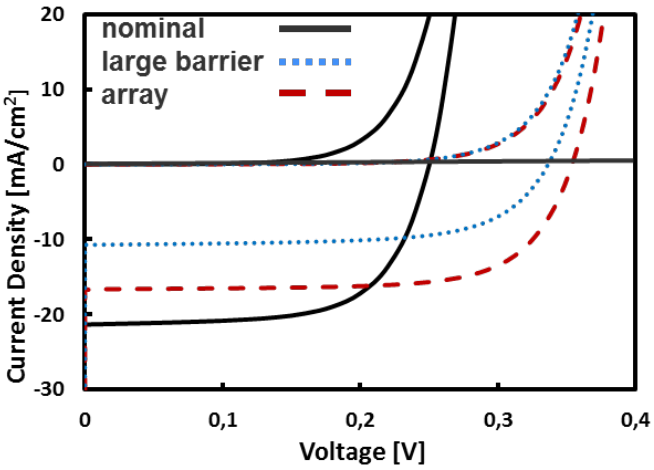


Fig. 4 Comparison between the nominal nanowire structure the one with increased barrier and finally the solar cells with increased barrier inside a 3 solar cell array.

# Optically and electrically pumped graphene bilayer lasers: Dramatic enhancement of terahertz gain by remote doping

Victor Ryzhii[1], Taiichi Otsuji[1], Maxim Ryzhii[2],
Vladimir Mitin[3], and Michael S. Shur[4]

[1] *Research Institute of Electrical Communication, Tohoku University, Sendai 980-8577, Japan*
[2] *Department of Computer Science and Engineering, University of Aizu, Aizu-Wakamatsu 965-8580, Japan*
[3] *Department of Electrical Engineering, University at Buffalo, SUNY, Buffalo, New York 1460-1920, USA*
[5] *Department of Electrical, Electronics, and Systems Engineering, Rensselaer Polytechnic Institute, Troy, New York 12180, USA*
*e-mail: v-ryzhii@riec.tohoku.ac.jp*

The gapless energy band spectra of graphene layers (GLs) and graphene bilayers (GBLs) enable the negative dynamic conductivity in the terahertz (THz) range of frequencies [1,2] under optical or electrical (injection) pumping due to the interband population inversion. Therefore GL- and GBL-based heterostructures can be used as the active media in the THz lasers. Several research groups have already reported the manifestation of of the THz gain in the pumped GLs paving the way to the demonstration of the graphene THz lasers. An increase in the THz gain in pumped GL-heterostructures could help reaching this goal. One of the pertinent options is to use GBL-heterostructures with a remote impurity layer (RIL) layer shown in Fig. 1 [3]. The carrier scattering on long-range potential created by the RIL enhances the indirect interband radiative transitions that can prevail over the indirect intraband radiative transitions [4] (responsible for the Drude absorption), see Fig. 2 showing the different types of the radiative transitions. As a result, the net dynamic conductivity Re $\sigma$ can become negative in a wide range of the THz frequencies overcompensating the Drude absorption. Its absolute value can substantially exceed that associated with the direct interband transitions $\max|\mathrm{Re}\ \sigma_d| = 2\sigma_Q = 2(e^2/4\hbar)$, where Re $\sigma_d < 0$, $e$ is the electron charge, and $\hbar$ is the reduced Planck constant (see Fig.3).

This work was supported by the Japan Society for Promotion of Science (Grant-in-Aid for Specially Promoting Research, #23000008), Japan. The works at UB and RPI were supported by the US AF award FA9550-10-1-391 and by the US ARL Cooperative Research Agreement, respectively.

[1] V. Ryzhii, M. Ryzhii, and T. Otsuji, J. Appl. Phys. **101**, 083114 (2007).

[2] M. Ryzhii and V. Ryzhii, Jpn. J. Appl. Phys. **46**, L151 (2007).

[3] V. Ryzhii, M. Ryzhii, V. Mitin, M. S. Shur, and T. Otsuji (unpublished).

[4] D. Svintsov, T. Otsuji, V. Mitin, M. S. Shur, and V. Ryzhii, Appl. Phys. Lett. **106**, 113501 (2015),

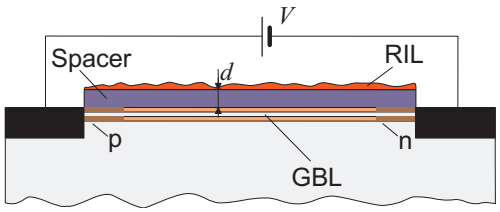


Figure 1: Schematic view of a GBL-RIL heterostructure for an injection laser with a RIL doped with both donors and acceptors.

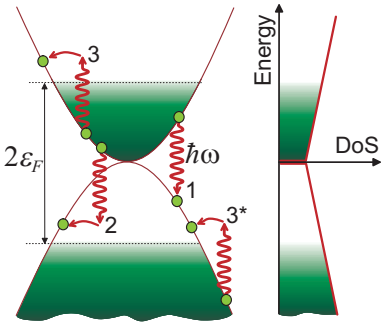


Figure 2: Energy band diagram of a pumped GBL (left panel) and energy dependence of its density of state DoS (right panel). Arrows correspond to direct and indirect interband transitions with the emission of photons with energy $\hbar\omega$ ($\varepsilon_F$ is the quasi-Fermi energies of both electrons and holes in GBL) as well as to indirect intraband transitions with the photon absorption in the conduction and valence bands.

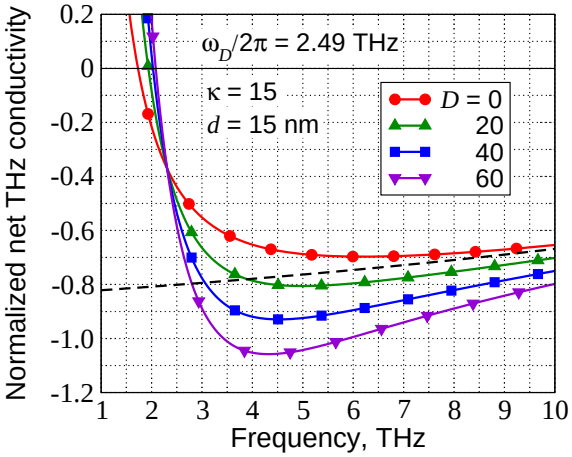


Figure 3: Frequency dependence of the normalized net THz conductivity Re $\sigma/2\sigma_Q$of GBL-RIL heterostructures for different structural parameters ($\kappa$ is the effective dielectric contant of the substrate and the spacer, $d$ is the thickness of the latter, $\omega_D$ and $D$ are the Drude characteristic frequency (proportional to the carrier scattering time in a GBL without a RIL and the Drude parameter proportional to the density of impurities in the RIL, respectively). THe quasi-Fermi energy $\varepsilon_F = 60$ meV. The curve marked by circles ($D = 0$) corresponds to a GBL without a RIL. Dashed line corresponds to normalize THz conductivity due to solely direct interband transitions.

# Inducing Strain to Encapsulated Graphene

Hikari Tomori[1, 2], Rineka Hiraide[1], Youiti Ootuka[1], Kenji Watanabe[3], Hisashi Taniguchi[3], Akinobu Kanda[1]

[1] *Division of Physics and TIMS, Faculty of Pure and Applied Sciences, University of Tsukuba 1-1-1 Tennodai, Tsukuba, Ibaraki 305-8571, Japan*

[2] *PRESTO-JST, Kawaguchi, Saitama 332-0012, Japan*

[3] *National Institute for Materials Science (NIMS), Tsukuba, Ibaraki 305-0047, Japan*

*e-mail: tomori@lt.px.tsukuba.ac.jp*

Due to the characteristic lattice structure, lattice strain in graphene corresponds to an effective gauge field. Theories tell that by controlling spatial variation of lattice strain, one can tailor the electronic state and transport properties of graphene. For example [1], under uniaxial local strain, graphene exhibits a transport gap at low energies, which is attractive for a graphene application to field effect devices.

In this study, we develop a method for encapsulating a strained graphene film in hexagonal boron-nitride (hBN). It is known that the graphene carrier mobility is significantly improved by the encapsulation of graphene in hBN.[2], which has never been applied to strained graphene.

Graphene is encapsulated in hBN using the so-called van der Waals assembly method.[3] Strain is induced by sandwiching a graphene film between patterned hBN sheets. An example is shown in Fig. 1, in which circle-shaped hBN with diameter of 6.5 μm is placed inside a hole (diameter: 10 μm) in another hBN, and a graphene film is sandwiched between them. The strain calculated from the geometry is ~ 0.6%, and the spatial variation of strain is confirmed with micro Raman spectroscopy. Transport measurement of encapsulated strained graphene is in progress.

[1] V. M. Pereira and A. H. Castro Neto, Phys. Rev. Lett. 103, 046801 (2009). [2] C. R. Dean et al., Nat. Nanotechnol. 5, 722 (2010). [3] L. Wang et al. Science 342, 614 (2013).

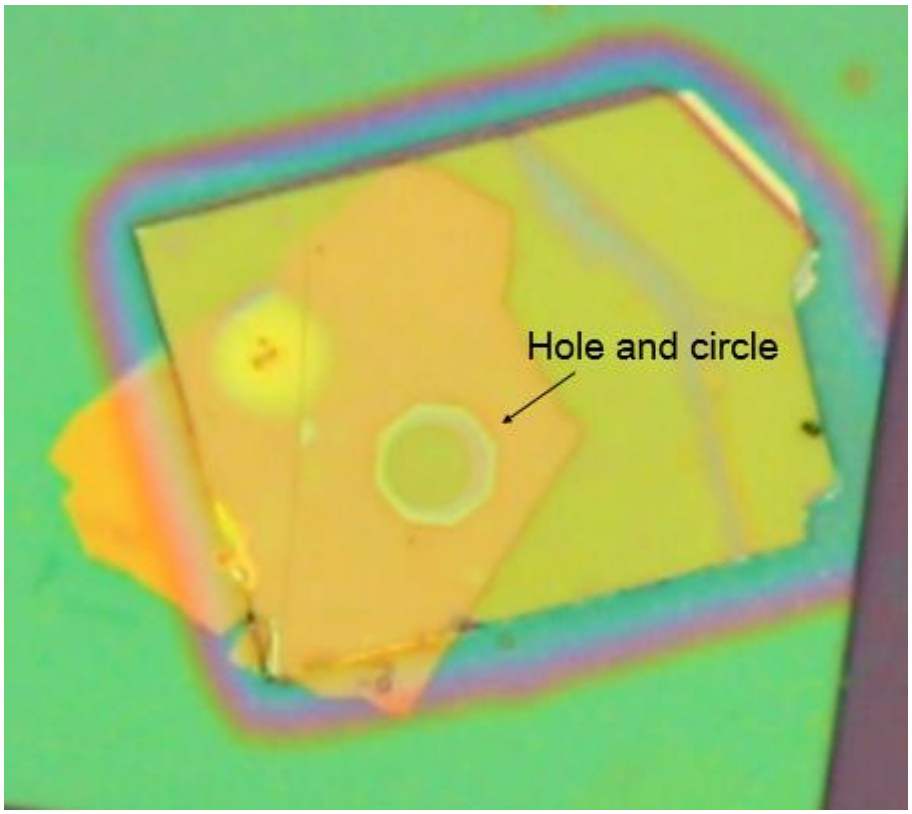


Figure 1: Optical image of a sample.

# Tuning Graphene via Engineered Strain Arrays

Nadya Mason

*Department of Physics and Materials Research Laboratory, University of Illinois at Urbana-Champaign, Urbana IL 61801 USA*
*e-mail: nadya@illiois.edu*

Strain-engineering of graphene has received significant attention as a method of enabling desirable electronic behavior, such as band gaps and 1D channels. Non-uniform strains on graphene are particularly interesting, as they can be described by local scalar and vector potentials that generate pseudomagnetic fields; in particular, strains having triangular symmetry (e.g., pyramid features) can generate nearly uniform field profiles. In this talk, I will discuss experiments probing the response of monolayer graphene deposited on substrates patterned with arrays of mesoscale triangular pyramids[1]. We systematically study the morphology of graphene for pyramid arrays having different spacing, symmetry, and surface rigidity by atomic force microscopy (AFM) and Raman spectroscopy. We show that the adhesion of graphene to the substrate—and hence the strain experienced by the graphene—can be controlled by changing the array aspect ratio and/or topological arrangement of pyramids in the array. We also demonstrate that the arrays can be used to induce large areas of non-uniform strain in graphene on the order of 1%. From simulations of graphene conformally adhered on pyramids, we show that non-uniform strains form closely around the apex and calculate a pseudomagnetic field profile with intensity as high as 300 T. These results suggest that the control over the morphology and strain of graphene on an engineered surface is a critical and promising step toward attaining strain-engineering of membranes.

[1] S.T. Gill, J.H. Hinnefeld, S. Zhu, W.J. Swanson, T. Li, and N. Mason, "Mechanical Control of Graphene on Engineered Pyramidal Strain Arrays," *ACS Nano* **9**, 5799-5806 (2015).

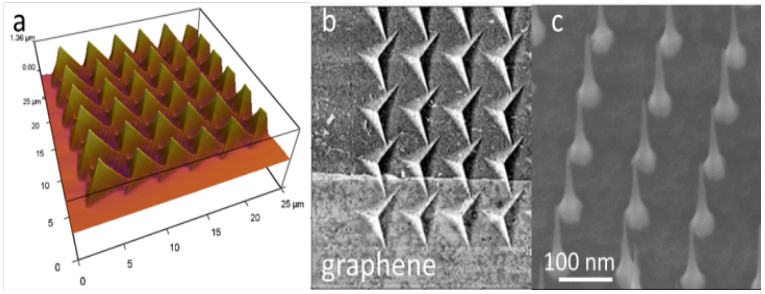


*Fig. 1. a) AFM topograph of pyramid array for inducing strain via substrate engineering. b) Top view of graphene on pyramids, c) Fabrication of narrow, $SiO_2$ pyramids on $SiO_2$/Si*

# Introducing carbon isotopes and isotopic heterojunction into graphene for enhancing graphene-based thermoelectric device performance

Yuki Anno, Kuniharu Takei, Seiji Akita, and Takayuki Arie
*Department of Physics and Electronics, Osaka Prefecture University, Osaka 599-8531, Japan*
*e-mail: anno-4@pe.osakafu-u.ac.jp*

Because the main heat carrier of graphene is phonon, the thermal conductivity of graphene can be easily reduced by introducing carbon isotopes and structural defects. In our previous work, we synthesized artificially controlled isotopic graphene heterojunction which had high thermal resistance without changing its electrical transport [1]. This suggests that the electrical and thermal transports of graphene can be controlled independently by isotopes. High electrical conductivity and low thermal conductivity are suitable for thermoelectric devices. In this study, we investigate the thermoelectric power of graphene containing isotopes as well as isotopic heterojunctions for enhancing thermoelectric device performance and show a guide for practical application of graphene thermoelectric devices.

Isotopically modified graphene samples with various ratios of carbon isotopes, $^{12}C$ and $^{13}C$, and isotopic heterojunctions used in this study were synthesized by low-pressure chemical vapor deposition. From the electrical and thermoelectric measurements of all samples, we found that the values of thermoelectric power of graphene are similar regardless of the carbon isotope fractions and the presence of heterojunctions. The peak values of thermoelectric power of all graphene samples negatively correlate with the electrical conductivity, consistent with those of typical metals and semiconductors. These results strongly support that introducing carbon isotopes and isotopic heterojunctions into graphene structure does not affect the power factor (PF = $S^2\sigma$, $S$: thermoelectric power, $\sigma$: electrical conductivity), and that the thermoelectric figure of merit of graphene devices is only associated with the change in the thermal conductivity. The maximum achievable power factor in graphene samples examined in this study was $6.52\times10^{-3}$ W/mK$^2$ [2]. Based on this value, we conclude that reducing the thermal conductivity down to 1.96 W/mK by using isotopes is a key to realize the practical application (PF/$\kappa$ > 1/$T$, $\kappa$: thermal conductivity, $T$: absolute temperature) of graphene-based thermoelectric devices at room temperature.

**Acknowledgements** This work was partially supported by a grant from The Murata Science Foundation, MEXT KAKENHI Grant Number 15H05869 and JSPS KAKENHI Grant Number 15J12244.

[1] Y. Anno, et al., Phys. Status Solidi RRL 8, 692 (2014).
[2] Y. Anno, et al., Adv. Electron. Mater. in press.

# Influence of Metal Contacts on Graphene Transport Properties and Its Reduction with Nano-carbon Interfacial Layer

Akinobu Kanda[1], Kenta Katakura[1], Yu. Ito[1], Youiti Ootuka[1], Hikari Tomori[2]

[1] *Division of Physics and TIMS, Faculty of Pure and Applied Sciences, University of Tsukuba*
*1-1-1 Tennodai, Tsukuba, Ibaraki 305-8571, Japan*
[2] *PRESTO-JST, Kawaguchi, Saitama 332-0012, Japan*
*e-mail: kanda@lt.px.tsukuba.ac.jp*

Due to high mobility and atomic thickness, graphene is a promising candidate for the next-generation electronic material. While considerable effort has been devoted to achieve higher mobility in graphene films, relatively little attention has been paid to the effect of forming contacts between graphene and metal, which are indispensable to the electric devices. In general, at a graphene/metal interface, mainly due to the difference in work functions, carriers are injected from the metal to graphene. The resulting shift of local Dirac point is not limited at the graphene/metal interface but extends by ~1 micron into the graphene channel. This carrier doping affects more significantly the performance of graphene field effect devices with shorter channel, as well as may conceal Dirac physics at the graphene/metal interface such as the relativistic superconducting proximity effect.

Here, we experimentally investigate the channel length dependence of graphene transport properties and extract the effect of metal contact. Several metal species are investigated and results are compared with numerical models. We reveal that the metal contact causes additional Dirac point in the gate voltage dependence of conductivity, and discuss the effective work function of graphene and the chemical interaction in a graphene/metal interface. Furthermore, we succeed in reducing the influence of metal contact by inserting a thin nano-carbon layer (amorphous carbon or multilayer graphene (MLG)) at the interface.

# Conductance Fluctuations in High-Mobility Bilayer-Graphene/*h*-BN Heterostructures

Masaaki Mineharu[1], Masahiro Matsunaga[1], Yuichi Ochiai[1], Inyeal Lee[2], Gil-Ho Kim[2], Kenji Watanabe[3], Takashi Taniguchi[3], David K. Ferry[4], Jonathan P. Bird[1,5]and Nobuyuki Aoki[1]

[1] *Graduate School of Advanced Integration Science, Chiba University,Chiba, Japan*
[2] *School of Electronic Electrical Engineering and Sungkyunkwan Advanced Institute of Nanotechnology (SAINT), Sungkyunkwan University, Suwon, Korea*
[3] *National Institute for Materials Science, Tsukuba, Japan.*
[4] *School of Electrical, Computer, and Energy Engineering, Arizona State University, Tempe, Arizona, USA*
[5] *Department of Electrical Engineering, University at Buffalo, The State University of New York, Buffalo, USA*
*e-mail: n-aoki@faculty.chiba-u.jp*

Conductance fluctuations in graphene have widely been studied so far however most the studies have been carried out in the diffusive transport regime produced by $SiO_2$/Si substrates [1], in which roughness and charge traps serve as the dominant scattering centers at low temperature. Recently, it has become possible to fabricate much higher mobility samples by using flakes of high-quality *h*-BN as the insulator layers [2], allowing mobility as high as $10^5$ $cm^2/Vs$ to be achieved at room temperature [3]. In such a high quality sample, clear Shubnikov-de Haas oscillations and consequent quantum Hall effect have been observed at low temperature. Nevertheless, conductance fluctuations have also been observed at specific regions, *e.g*. around zero-magnetic field. In this paper, we present our recent results based on the analysis of the conductance fluctuations in a quasi-ballistic *h*-BN/graphene/*h*-BN heterostructure at low temperatures. Four-terminal electrodes (Ti/Au) having a gap of 4 μm in a van-der-Pauw arrangement were fabricated by photo lithography on a flake of *h*-BN on a $SiO_2$/Si substrate. Flakes of bilayer graphene and another *h*-BN for the top passivation were transferred onto the pre-fabricated electrodes by a dry transfer process [2]. The sample was cooled by a $^3$He cryostat to a base temperature of 300 mK. At this temperature, the device shows a very sharp Dirac curve and the highest mobility in *n*- and *p*-type conduction regions are slightly different as $7.1 \times 10^4$ $cm^2/Vs$ and $8.4 \times 10^4$ $cm^2/Vs$, respectively. Conductance fluctuations have been observed in both the transfer curve, and in the magnetoresistance around zero-magnetic field. We discuss on the differences of the characteristics focused on the mobility dependence of the fluctuations compared to results in former low mobility samples.

[1] G. Bohra *et al*., Appl. Phys. Lett. **101**, 093110 (2012).
[2] C. R. Dean *et al.,* Nature Nanotech. **5**, 722 (2010).
[3] L. Wang, *et al.,* Science **342**, 614 (2013).

# Electronic Noise Suppression in the Near-Ballistic BN-Graphene-BN Heterostructure Field-Effect Transistors

Maxim A. Stolyarov[1], Sergey L. Rumyantsev[2,3], Michael Shur[2] and Alexander A. Balandin[1]

[1] *Nano-Device Laboratory, Department of Electrical and Computer Engineering, University of California – Riverside, Riverside, California 92521, U.S.A.*

[2] *Department of Electrical, Computer, and Systems Engineering, Center for Integrated Electronics, Rensselaer Polytechnic Institute, Troy, New York 12180, U.S.A.*

[3] *Ioffe Physical-Technical Institute, St. Petersburg 194021, Russia*

*E-mail: balandin@ece.ucr.edu*

Ballistic electron conduction offers a new possible approach to the development of low-power high-speed logic circuits [1]. Ultra-high mobility of graphene allows achieving the ballistic or near-ballistic transport regime at room temperature (RT) in devices with relatively long channels. In this presentation, we show that the heterostructure field-effect transistors (HFETs) with the graphene channel encapsulated between two layers of hexagonal boron nitride (*h*-BN) combine extremely high electron mobility (~36,000 $cm^2$/Vs) with a strongly reduced 1/*f* noise level (*f* is the frequency) [2]. The low-frequency 1/*f* noise hampers operation of numerous devices and can be a major impediment to development of practical low-power applications of graphene and other 2D materials [6-8]. The prototype *h*-BN-graphene-*h*-BN HFETs were fabricated using the mechanically exfoliated *h*-BN and graphene flakes on $Si/SiO_2$ wafers. A micromanipulator was used for careful positioning of the *h*-BN flakes on the stamp over the graphene flakes. The resulting heterostructure was etched to expose the graphene edges and create one-dimensional Cr/Au (10/100 nm) electrical contacts. Figure 1 presents the schematics and an optical microscopy image of a representative device. Figure 2 shows the current-voltage characteristics of a representative HFET ($\mu$~36,000 $cm^2$/Vs at the carrier concentration of $7\times10^{11}$ $cm^{-2}$), normalized 1/*f* noise spectral density and noise amplitude of this encapsulated device. The channel-area normalized noise spectral density in BN-graphene-BN HFET is factor of ×5 – ×10 smaller than that in typical reference graphene FETs without the channel encapsulation. The observed strong noise reduction can be explained by screening of the traps in $SiO_2$ by the BN barrier and isolation of device channel from ambient.

The work at UC Riverside was supported, in part, by SRC and DARPA through STARnet Center for Function Accelerated nanoMaterial Engineering (FAME)

[1] M. S. Shur and L.F Eastman, IEEE Transactions on Electron Devices, 26 (11), 1677 (1979).

[2] M. A. Stolyarov, G. Liu, S. L. Rumyantsev, M. Shur and A. A. Balandin, Applied Physics Letters, 107, 023106 (2015).

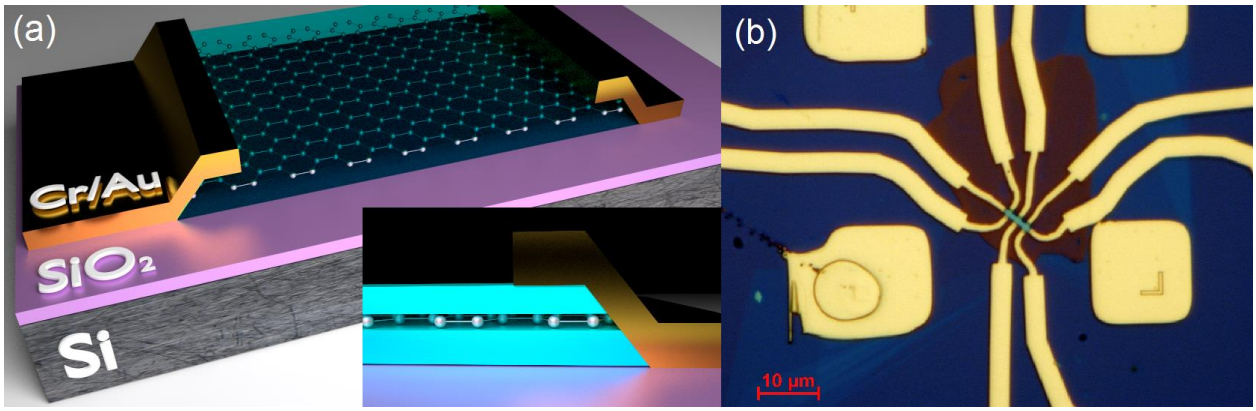


**Figure 1:** Schematics (a) and optical microscopy image (b) of the heterostructure BN-graphene-BN transistor.

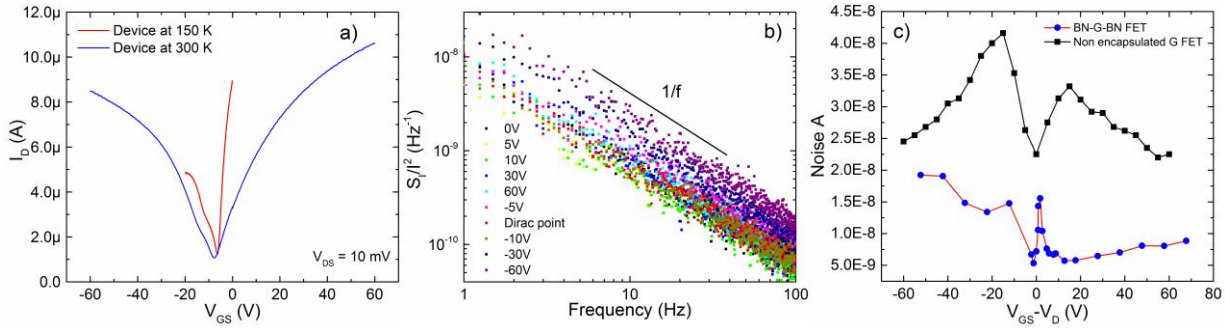


**Figure 2:** (a) Current-voltage transfer characteristics of BN-graphene-BN HFET; (b) Normalized noise spectrum density in *h*-BN-G-*h*-BN HFET as a function of frequency for several values of the back-gate bias $V_G$; (c) Noise amplitude as a function of the gate bias with respect to the Dirac point, $V_{GS}$-$V_D$ for *h*-BN-G-*h*-BN HFET. The data for conventional non-encapsulated graphene FET on Si/$SiO_2$ wafer are also shown for comparison.